Forschungszentrum Karlsruhe

Technik und Umwelt

Wissenschaftliche Berichte

FZKA 6722

Comparison and Interpretation Report of the OECD International Standard Problem No. 45 Exercise (QUENCH-06)

W. Hering, Ch. Homann, J.-S. Lamy *, A. Miassoedov, G. Schanz, L. Sepold, M. Steinbrück

Institut für Reaktorsicherheit

Programm Nukleare Sicherheitsforschung

*delegate from EDF, France

Forschungszentrum Karlsruhe GmbH, Karlsruhe
2002

Impressum der Print-Ausgabe:

Als Manuskript gedruckt

Forschungszentrum Karlsruhe GmbH
Postfach 3640, 76021 Karlsruhe

Mitglied der Hermann von Helmholtz-Gemeinschaft
Deutscher Forschungszentren (HGF)

ISSN 0947-8620

Abstract

The International Standard Problem (ISP) No. 45 is part of the overall ISP program of the OECD/NEA and is dedicated to the behavior of heat-up and delayed reflood of fuel elements in nuclear reactors during a hypothetical accident. ISP-45 is related to the out-of-pile bundle quench experiment QUENCH-06, performed at Forschungszentrum Karlsruhe (FZK), Germany, on December 13, 2000. Special attention was paid to hydrogen production.

To assess the ability of severe accident codes to simulate processes during core heat-up and reflood at temperatures above 2000 K, the behavior of the bundle during the whole experiment should be calculated on the basis of the necessary experimental initial and boundary conditions, but without knowing further experimental details. In this so-called blind phase 21 participants from 15 nations contributed with 8 different code systems (ATHLET-CD, ICARE/CATHARE, IMPACT/SAMPSON, GENFLO, MAAP, MELCOR, SCDAPSIM, SCDAP-3D). Additionally, post-test calculations using the in-house version SCDAP/RELAP5 mod3.2.irs are used for comparison. After the end of the blind phase all measured data were made available and the participants were invited to deliver a second calculation, where this knowledge could be used (so-called open phase). In this report, results of the blind calculations are presented, analyzed, and compared to experimental data.

During heat-up most results do not deviate significantly from one another, except as a consequence of some obvious user errors, so that a definition of a mainstream is justified. For the quench phase the lack of adequate hydraulic modeling becomes obvious: some participants could not match the observed cool-down rates, others had to use very fine meshes to compensate code deficiencies. To overcome this insufficiency some newly developed reflood models were used in MAAP and MELCOR.

In QUENCH-06, oxide layers were thick enough to protect the cladding from melting and failure below 2200 K, so that no massive hydrogen release during reflood was found. This behavior could be simulated by most of the codes with commonly used oxidation models, if no shattering options were used arbitrarily. With respect to calculated hydrogen production the mainstream shows a spreading of ± 15 % prior to reflood initiation and a range of ± 40 % after reflood. However, a group of SCDAPSIM users activated an extreme shattering option, which overestimates the produced hydrogen mass by a factor of 5. In the mainstream, most of the participants calculated correctly that no bundle damage occurred, whereas others calculate slight material relocations, mainly due to overestimation of the cladding temperatures.

However, detailed inspection showed that the codes still have difficulties to predict correctly the bundle initial conditions for reflood. Another surprising finding was that the energy balance has to be checked prior to further interpretation of the results. Lacking user experience and problems to model the QUENCH facility adequately was a main reason for larger deviations.

In the open phase 9 participants delivered results in time, a further participant with some delay; lacking manpower or time was mentioned as main reason for not participating in the open phase. The results show that their codes are able to simulate adequately the QUENCH-06 experiment. Some participants performed successful error corrections as well as code improvements. The spreading of the results, e.g. the spreading of the calculated hydrogen mass was reduced significantly.

Vergleich und Interpretation der Ergebnisse des Internationalen Standard-Problems Nr. 45 der OECD (QUENCH-06)

Zusammenfassung

Das Internationale Standard Problem (ISP) No. 45 ist Teil des allgemeinen ISP Programms der OECD/NEA und bezieht sich auf die Untersuchung des Kernverhaltens in Kernkraftwerken beim Aufheizen und verzögertem Fluten während eines angenommenen Unfalls. Als Basis für ISP-45 wurde am 13. Dezember 2000 Versuch Nr. 6 in der out-of-pile Versuchsanlage QUENCH im Forschungszentrum Karlsruhe durchgeführt. Ein wesentliches Ziel war die Untersuchung des Wasserstoffquellterms.

Um den Stand von Kernschmelzcodes für die Simulation der Kernaufheizung und der Abschreckung mit Wasser (quench) bei Temperaturen oberhalb von 2000 K beurteilen zu können, wurden in der sogenannten blinden Phase nur die notwendigen Anfangs- und Randbedingungen für die Rechnungen vorgegeben, aber keine weiteren experimentellen Einzelheiten. An dieser Phase beteiligten sich 21 Organisationen aus 15 Staaten mit 8 Code-Systemen (ATHLET-CD, ICARE/CATHARE, IMPACT/SAMPSON, GENFLO, MAAP, MELCOR, SCDAPSIM, SCDAP-3D). Außerdem wurden eigene Nachrechnung mit SCDAP/RELAP5 mod3.2.irs gemacht. In diesem Bericht werden die berechneten Ergebnisse dargestellt, analysiert und mit den Messungen verglichen.

Während der Aufheizphase weichen die meisten Ergebnisse nicht wesentlich voneinander ab, außer als Folge von offensichtlichen Benutzer-Fehlern. Dies rechtfertigt die Definition eines sogenannten „Hauptfeldes“. Für die Abschreckphase zeigt sich, dass die Modellierung der Thermohydraulik unzureichend ist: einige Teilnehmer konnten die beobachteten Abkühlraten nicht nachvollziehen, andere mussten ein sehr feines Gitter benutzen, um Unzulänglichkeiten des Rechenprogramms auszugleichen. Um dieses Defizit zu beheben, wurden in MAAP und MELCOR neue Modelle entwickelt und eingesetzt.

Im Versuch QUENCH-06 verhinderte eine hinreichend dicke Oxydschicht ein Versagen der Hüllrohre unterhalb von etwa 2200 K und damit die Freisetzung von metallischer Schmelze. Dieses Verhalten konnte in den meisten Rechenprogrammen mit den normalen Oxidationsmodellen beschrieben werden, wenn nicht willkürlich ein Abplatzen der Oxidschicht angenommen wird. Im „Hauptfeld“ erhöhte sich die Streuung der berechneten freigesetzten H_2-Masse von ca. ±15 % vor dem Fluten auf ca. ±40 % nach dem Fluten. Verschiedene Anwender von SCDAPSIM überschätzten jedoch die freigesetzte Wasserstoffmenge um einen Faktor 5 durch die Annahme einer sehr umfangreicher Entfernung der schützenden Oxydschicht. Im Hauptfeld wurde von den meisten Teilnehmern richtig berechnet, dass keine Zerstörung des Bündels eintritt, während andere Teilnehmer kleinere Schmelzeverlagerungen -Bildung berechnen, meist wegen einer Überschätzung der Hüllrohrtemperaturen.

Eine detaillierte Untersuchung zeigte auch, dass die Codes noch Probleme mit der korrekten Berechnung der Anfangsbedingungen im Bündels zu Beginn des Flutens haben. Eine weitere überraschende Erkenntnis ist, dass die Energiebilanz sorgfältig überprüft werden muss, bevor man an die Interpretation der Ergebnisse gehen kann. Fehlende Erfahrung der Codebenutzer sowie Schwierigkeiten bei der angemessenen Modellierung der QUENCH-Anlage waren die Hauptursache für größere Abweichungen.

In der offenen Phase lieferten 9 Teilnehmer termingerecht Ergebnisse ab, ein weiterer mit Verzögerung; fehlendes Arbeitspotential oder fehlende Zeit wurde von den anderen als Hauptgrund angegeben, nicht an der offenen Phase teilzunehmen. Die Ergebnisse zeigen, dass die Codes das Experiment QUENCH-06 zufriedenstellend analysieren können. Einige Teilnehmer haben Fehler korrigiert oder den Code verbessert. Die Streuung der Ergebnisse, z. B. der H_2—Masse, wurde deutlich reduziert.

Table of Contents

List of Figures

List of Tables

List of Abbreviations

AMM	Accident management measures
ATHLET-CD	Analysis of THermal-hydraulics of LEaks and Transients - Core Degradation, GRS, (AT)
BDBA	Beyond Design Basis Accident
CSNI	Committee on the Safety of Nuclear Installations of the OECD
CNSNS	Commission of Nuclear Safety and Safeguards, Mexico
CORA	Out-of-pile severe fuel damage tests performed at FZK, 1984-1992, http://hikwww4.fzk.de/irs/organisation/IRS1/CORA01.html
DBA	Design Basis Accident
DC	Direct current
DMX	De-multiplexed data format used for RELAP5
ECC	Emergency core cooling
ENEA	Ente per le Nuove Tecnologie l'Energia el'Ambiente, Italy
FP	Fission products
FZK	Forschungszentrum Karlsruhe in der Helmholtz-Gemeinschaft, http://www.fzk.de/
GAMA	OECD/NEA Working Group on Accident Management and Analysis
GENFO	GENeral FLOw code, VTT, (GE)
GRS	Gesellschaft für Anlagen und Reaktorsicherheit, Germany
HR	Heater rod
ICARE/CATHARE	
IMF	Institut für Materialforschung at FZK
IMPACT/SAMPSON	New modular severe accident code developed at NUPEC, (IS)
INEEL	Idaho National Engineering and Environmental Laboratory, Idaho Falls, USA, formerly INEL
IRS	Institut für Reaktorsicherheit, http://hikwww4.fzk.de/irs/
ISP	International Standard Problem of the OECD/NEA
LOCA	Loss Of Coolant Accident
LOFT	Loss Of Fluid Test (Idaho National Engineering Laboratory, Idaho Falls, USA)
LWR	Light Water Reactor
MAAP	Modular Accident Analysis Program, EPRI, (MA)
MELCOR	Integrated code to model the progression of severe accidents in light water reactor nuclear power plants, SANDIA, (ME)
NEA	Nuclear Energy Agency of the OECD: http://www.nea.fr , Issy-les-Moulineaux, France
NUKLEAR	Programm Nukleare Sicherheitsforschung at FZK
NUPEC	Nuclear Power Engineering Company, Tokyo, Japan
NSI	Nuclear Safety Institute, Moscow, Russia
n/a	not available

OECD	Organization for Economic Co-operation and Development
PSF	Projekt Sicherheitsforschung, predecessor of Programm Nukleare Sicherheits-forschung at FZK
PWR	Pressurized Water Reactor
QUENCH	Research program at FZK, focused on investigations on material behavior during LWR reflood conditions: http://imf1-wt-server.fzk.de/quench/
RELAP5	old: Reactor Excursions and Leak Analysis Program, presently: Reactor Leak and Analysis Program, for LWR transients and SBLOCA
RMBK	Light Water Graphite Reactor (Russian abbreviation)
SBLOCA	Small break LOCA
SCD	Severe Core Damage
SCDAP	Severe Core Damage Analysis Package, (USNRC code, developed at INEEL)
SCDAP-3D	SCDAP version coupled with RELAP5-DOE, INEEL, (S3)
SCDAP/RELAP5	Coupled SCDAP and RELAP5 code to simulate reactor conditions up to SFD conditions
SCDAPSIM	SCDAP/RELAP5 improved by ISS, commercial code version (abbr. SI)
SFD	Severe Fuel Damage
t.b.d	to be defined
TC	Thermocouple
USNRC	United States Nuclear Regulatory Commission, http://www.nrc.gov
Zry	Zircaloy

(Remark: URL-Addresses valid March 2002)

TOKENS

CMX	Commission of Nuclear Safety and Safeguards, Mexico City, Mexico
DMM	Dept. of Mechanical, Nuclear and Production Engineering, University of Pisa, Italy
DRS	CEA/DRS/IPSN, Cadarache France
EDF	Electricité de France, Clamart, France
ENE	Ente per le Nuove Tecnologie l'Energia el'Ambiente, Italy
FRA	Framatome-ANP SA, Paris, France
GRS	Gesellschaft für Anlagen- und Reaktorsicherheit, Garching, Germany
IJS	Institute Jožef Stefan, Ljubljana, Slovenia
INL	Idaho National Engineering and Environmental Laboratory, Idaho Falls, USA
ISS	Innovative Software Systems, Idaho Falls, and University of Florida, USA
NEH	Nuclear Engineering University of Hacettepe, Turkey
NK[1,2,3]	NSI of RCC Kurchatov Institute, Moscow, Russia
NUP	Nuclear Power Engineering Company, Tokyo, Japan
REZ	Nuclear Research Institute, Prague, Czech Republic

RUB	Ruhr University Bochum, Department for Energy Systems and Energy Economics, Bochum, Germany
SES	Studsvik Eco & Safety, Nyköping, Sweden
SIE	Framatome-ANP GmbH, Erlangen, formerly Siemens Nuclear Power, Erlangen, Germany
SNL	Sandia National Laboratories, Albuquerque, USA
UZA	University of Zagreb, Croatia
VTT	Finish State Research Center, VTT Energy, Finland

DEFINITION OF TERMS

Collapsed water level	total amount of water, represented by its height in the test section
Cool-down rate	average rate of temperature decrease before the "quench point"
Fast water injection	pressure driven water injection into the steam injection line to fill empty volumes and pipes
Flooding rate	average rise of the water level in the test section: $\dot{Z} \approx \frac{\dot{m}(z)}{\rho \cdot A_{bundle}}$
Injection rate	mass flow rate delivered by the quench pump to the quench pipe in QUENCH facility
LM501	measured pressure difference across the whole test section. Under stationary conditions it can be transferred into a collapsed water level
Pre-injection system	fast water injection system
Quench front	movement of quench point in the bundle
Quench point	temperature and time of sharp change in cool-down rate due to partial wetting of the TC or cladding, breakdown of stable film boiling
Quench profile	axial distribution of quench times
Quench rate	fast cool-down of structures due to effective convective heat transfer (transition or nucleate boiling)
TCRC	TC in the centerline of the unheated fuel rod
TFS	thermocouple mounted on cladding surface
TSH	thermocouple mounted on shroud outer surface

Executive summary

When during a postulated accident the overheated core of a nuclear reactor is flooded with water as part of an accident management measure (AMM), hydrogen is released due to oxidation of the Zry cladding by steam, if the core temperature exceeds 1000 K. In spite of great efforts, knowledge is still too limited to predict this hydrogen release rate sufficiently well with computer programs. The International Standard Problem No. 45 (ISP-45) of the OECD/NEA is initiated to extend the database for such situations, to identify key phenomena and to encourage an extended code validation so that the accuracy and reliability of the codes can be assessed and improved.

ISP-45 is based on the out-of-pile experiment QUENCH-06, performed at Forschungszentrum Karlsruhe (FZK), Germany, on December 13, 2000. The main objective of QUENCH-06 is to investigate fuel rod bundle behavior up to and during reflood/quench conditions without severe fuel rod damage prior to reflood initiation. In particular, the conditions of a Design Basis Accident (DBA) plus an additional failure, leading to a delayed activation of the emergency core cooling (ECC) system, were investigated up to total reflood of the heated section of the bundle with water, starting with conditions representative for normal reactor operation.

After heating the bundle to about 1500 K a pre-oxidation phase was used to establish a reactor specific oxide layer thickness. In the following transient phase electrical heating and chemical power release due to oxidation led to a maximum cladding temperature to app. 2200 K; higher temperatures would have caused dissolution of the pellets by liquid Zr with subsequent melt relocation prior to reflood and would hence have led to conditions as simulated in QUENCH-02 and QUENCH -03, and ISP-31 (CORA-13 at FZK). Water reflood was initiated at that temperature, and most of the measured temperatures dropped nearly immediately to 400 K due to fast steam cooling caused by water evaporation. At reflood initiation cladding failure and slightly afterwards shroud failure were detected. About 250 s after reflood initiation the temperatures up to the level of the off-gas pipe decreased to saturation. Prior to reflood app. 32 g of hydrogen were produced and during reflood additional 4 g.

Post-test analysis showed that the bundle remained largely intact. This is mainly due to the fast reflood process and the limited axial extension of the hot zone. Despite the very high temperatures a great deal of reliable information was obtained also for thermal-hydraulics, giving an adequate basis to simulate not only of the experiment up to quench initiation, but also of the reflood phase.

The first task of ISP-45 consisted in blind calculations of the whole test on the basis of general data of the facility and of the specific experimental initial and boundary conditions. About 400 variables were requested; the most informative of them were used for this report, many data for global and detailed comparison are presented in /22/, others were requested to facilitate our interpretation of the results. Afterwards the whole set of experimental data or results were transmitted to the participants, and they were invited to perform open calculations using that information. For the open phase only global data were requested.

ISP-45 started in October 2000 with the preparatory workshop at FZK, the blind exercise lasted from end of January 2001 up to end of June 2001. A Comparison Workshop with discussions of the blind phase was held at December 10-12, 2001, the final workshop with discussions about the open phase and consent of the participants on the contents of this report on March 18, 2002. 21 organizations from 15 nations participated with detailed mechanistic or integral codes (MAAP, MELCOR) in the blind phase, 9 participants delivered open phase results in time and one more participant just before printing of this report. Additionally, FZK post-test analyses were performed with an in-house version of SCDAP/RELAP5 mod3.2, which includes the new reflood model of PSI and FZK improvements (see table).

Participants in ISP-45 blind and open phase

Code	Token	Organization Country	Phase	Code	Token	Organization Country	Phase
ATHLET-CD	GRS	GRS Germany	B	MELCOR Me 1.8.5QZ	IJS	Institut Jožef Stefan Slovenia	B
	RUB	Ruhr-Uni. Bochum, LEE Germany	1		NK2	NSI of RRC Kurchatov Inst. Russia	1
GENFLO	VTT	VTT Energy Finland	B	SCDAP SIM	CMX	Nat. Com. Nuc. Saf. Safg. Mexico	1
ICARE/ CATHARE	DRS	IPSN/DRS/SEMAR/LECTA France	B		DMM	University of Pisa, Italy	1
	ENE	ENEA Italy	B		ISS	ISS & Uni. of Florida USA	1
	NK3	NSI of RRC Kurchatov Inst. Russia	2		NEH	Nuc. Eng., Uni. Hacettepe Turkey	B
IMPACT/ SAMPSON	NUP	NUPEC Japan	B		NK1	NSI of RRC Kurchatov Inst. Russia	1
MAAP 4.04	EDF	Electricité de France (EDF) France	1		SIE	Framatome-ANP, Erlangen Germany	1
	FRA	Framatome-ANP, Paris France	1		UZA	University of Zagreb Croatia	B
MELCOR Me 1.8.5RB *incl. reflood*	REZ	Nuc. Res. Inst., Rez Czech Republic	1	SCDAP-3D	INL	INEEL USA	1
	SES	Studsvik ECO & Safety AB Sweden	1	S/R5.irs	FZK	FZK Germany	
	SNL	Sandia Nat. Labs USA	B	Remark: 1: blind phase, 2: open phase; B: both			

Evaluation of the delivered blind phase data showed that it was a difficult task for most of the participants to simulate adequately the non-reactor specific features of the QUENCH facility, above all the axial power distribution in the electrically heated rods and the radiative heat transfer in the gap between shroud and cooling jacket in the upper electrode zone. However, this is a prerequisite for an adequate code-to-data comparison and hence for a reliable code assessment, as has been seen in previous ISPs (e.g. ISP-31, ISP-36).

Despite these difficulties nearly all participants calculated the thermal-hydraulic conditions prior to reflood fairly well. For the end of the pre-oxidation phase 8 participants delivered results for the total hydrogen mass in the range of ± 15 % around the experimental value. A small group of participants calculated ballooning with subsequent clad failure early in the pre-oxidation phase. It was, however, found that even at the end of the pre-oxidation phase, where a quasi steady

state is reached in the bundle, the energy balance seems not to be fulfilled in each of the calculations, giving a variation by a factor of 3 compared to experimental values and FZK post-test analyses. Even with the same code version to rather different results were obtained. Therefore the energy balance of the different code systems should be checked carefully and improvements should be made where necessary.

Participants, who calculated the reflood process fairly well, are within an error band of app. 40 % for hydrogen production compared to the experimental data. Some participants calculated too much hydrogen release by arbitrarily removing the protective oxide scales (shattering). In addition the participants calculated axial positions of the quench front (breakdown of stable film boiling) above as well as below the collapsed water level (total amount of water, represented by its height in the test section), while the experiment shows clearly that the quench front is above. One participant calculated fuel rod damage and blockage formation during reflood phase. In the open phase the results for the whole test were generally improved with respect to the blind calculations, mainly by input modifications.

Participants also found - and this is strongly supported by the organizers' experience - that for a reasonable modeling, the maximum axial mesh length should not exceed app. 0.07 m. However, such a mesh length may cause problems for reactor applications. Therefore, as a minimum requirement for realistic calculations, some code developers suggest an automated mesh refinement strategy at least for calculations of reflood situations.

The codes still suffer from inadequate simulation of thermal-hydraulics in the reflood phase. Several codes have no dedicated reflood models, others have models which are not yet validated sufficiently using reflood experiments simulating design basis accidents. The ICARE/CATHARE code only used the simplified built-in thermal-hydraulics model of ICARE2V3; therefore the involved participants are invited to repeat the exercise with the extended capabilities of the combined code. EDF and SNL improved MAAP and MELCOR, respectively. The models are still in a preliminary state, but may reduce the previous shortcomings. Thermal-hydraulic packages developed for design basis accidents behave somewhat better (ATHLET-CD, SCDAPSIM, GENFLO), but they have still difficulties at high surface temperatures, though the GENFLO code was improved.

However, the codes can be used to assess the reflood of an intact fuel rod bundle roughly, but in most cases they cannot simulate the processes in a quality as required for DBA investigations or licensing purposes. Hence, a wider code qualification and code improvement with respect to reflood / quench simulation are recommended. Further improvements may be desirable with respect to the oxidation correlations and the clad failure criteria, which is still a user parameter. So thermal shock triggered clad failure as observed in QUENCH-06 cannot be described. Moreover the significant additional hydrogen release during reflood has to be considered adequately for higher rod temperatures as measured in other reflood experiments.

It turned out that two groups joined the ISP-45 exercise: More experienced participants including code developers were able to analyze the case correctly and deliver mostly results within the mainstream, but they tended to over-predict the hydrogen production during reflood. Less experienced participants including those who just started with analyses of severe accidents or

of out-of-pile experiments also had to gain experience during the performance of these analyses. For this reason their results were evaluated separately.

This constellation sheds light on the need to transfer knowledge for the sake of continuity of work and spread of experience e. g. to younger scientists and engineers and to organizations who up to now were less involved in problems as addressed in ISP-45. Participation in this exercise has maintained or even improved the expertise of participants, not only of those in the second group. Furthermore it has enhanced transfer of knowledge between participants, as can be deduced from the comparison of blind and open phase results. The participants also became aware of the difficulties of such investigations and learnt about modeling the combined problem of thermal-hydraulics and fuel rod behavior under fast transient conditions.

Despite some large discrepancies between some measured and calculated results, especially during the quench phase, a blind exercise like ISP-45 has turned out to be very valuable. The participants of such blind exercises are forced to assess the code capabilities in a more profound way than simply to modify input parameters to fit the code predictions to known experimental results. However, blind exercises should always be followed by an open phase for a more sophisticated evaluation and a more extended verification of code or facility models as well as for deepening user experience.

The present results indicate not only differences in the mechanistic treatment of phenomena but an inadequate balancing between them, even in this experiment without significant bundle damage. It is most important for the simulation of severe situations not only to consider all pertinent phenomena, but also their inter-dependencies. A reasonably revised ranking of the relevant phenomena will help to limit the necessary analytical effort also for more severely damaged bundles. It is emphasized that this ranking must be done carefully to avoid inappropriate model development. As an example the large over-prediction of hydrogen release in ISP-45 was mainly caused by application of the shattering models, originally developed to explain the measured hydrogen source term of ISP-31.

ISP-45 may be considered to be a first step for further code validation concerning reflood phenomena as addressed in the ongoing QUENCH program. Future tests are intended to enlarge, to verify or to precise the findings drawn from the past tests, including the influence of absorber components.

1 INTRODUCTION

An International Standard Problem (ISP) is defined as a broad comparison between experimental and analytical results derived from various computer codes. Especially in the field of beyond design basis accidents (BDBA), the reliability of code prediction has to be assessed for predictions of different phases of an accident and, moreover, for consequences occurring after operator interactions such as valve and/or emergency core cooling activation.

In the past Forschungszentrum Karlsruhe (FZK) has contributed several times to OECD/NEA international standard problems dedicated to fuel rod bundle behavior under various conditions. Two of them were devoted to reflood problems, namely the fuel rod bundle test in the REBEKA facility (ISP-14) and the PWR test in the CORA-facility (CORA-13, ISP-31). The experiment CORA-W2, ISP-36, was devoted to core degradation of a VVER type fuel rod bundle. The fourth one was a test on melt-concrete interaction, performed in the BETA facility (BETA V5.1, ISP-30).

The present International Standard Problem, ISP-45 (see Table 1.1), is based on the out-of-pile experiment QUENCH-06 performed at Forschungszentrum Karlsruhe, Germany, on December 13, 2000. The main objective of this experiment is to investigate fuel rod bundle behavior up to and during reflood/quench conditions without severe fuel rod damage prior to reflood initiation. In particular the conditions of a Design Basis Accident (DBA) plus an additional failure, leading to a delayed activation of ECC, were investigated up to total reflood of the bundle, starting with conditions representative for normal reactor operation.

The task of ISP-45 consisted in blind calculations of the whole test on the basis of general data of the facility like geometry, and of the specific experimental initial and boundary conditions, but further experimental data or results were not transmitted to the participants before these calculations were finished.

The results delivered by the participants were checked and the global data were presented in a draft overview /9/ data which was sent to all participants in August 2001. Some participants could not deliver all results in time due to serious reasons. They were accepted after a brief check before the release of the experimental data. All participants were invited to perform open calculations and to present their results at ISP-45 Comparison workshop. In doing that they were asked to deliver a list of modifications as well as global results for comparison. Some participants sent us comments and error corrections after the release of that draft overview. Such comments are listed in the appendix; the original text and figures have not been changed.

It is a pleasure that we could realize our intention to keep as many participants as possible within the exercise. Finally 21 participants from 15 nations delivered their results. Together with posttest analyses based on calculations at Forschungszentrum Karlsruhe (FZK) with in-house version of SCDAP/ RELAP5 mod 3.2 (S/R5irs) and the experimental results this sums up to 23. In the open phase exercise 9 participants delivered results in time (Table 1.1), another one not before end of March so that we only could include her comments in the appendix.

During ISP-45 some delays occurred which are listed in Table 1.1. Nevertheless we could reach our aim to mainly end ISP-45 in time for those who wanted to participate or who organized ISP-46, the THENPHEBISP project.

The general intention of this report is to present results for the blind and the open phase, delivered by the participants, and to compare most significant data to allow each participant to check and validate her or his code, input model, and the parameters used for the blind phase calculations. A list of recommendations to future ISP-organizers and to OECD is added in this report.

Table 1.1 Initial and actual time schedule for ISP-45

Initial time frame	Schedule / Meeting	Final time frame
Oct 13, 2000	Preparatory workshop: Definition of procedure, time schedule, participants, deliverable input (FZK) and results of calculations (participants)	Dec 13, 2000
End of Oct.	Official confirmation of participation to OECD	Nov. 2000
End Nov	**QUENCH-06 test conduct at FZK**	**Dec 13, 2001**
End Jan 2001	Delivery of the experimental data by FZK to OECD	End Jan 2001
	Plus: updated **ISP-45 Specification report** due to unexpected experimental conditions	April 2001
May 2001	Delivery of blind phase results by the participants to FZK Last contribution received	June 22, 2001 July 2, 2001
	Draft overview of global data delivered by FZK	**August 1, 2001**
	Delivery of QUENCH-06 experimental data, begin of the open phase	August 8, 2001
End Sep 2001	Delivery of FZK preliminary comparison report to OECD	Nov 12, 2001
	Delivery of the list of modifications for blind/open phase comparison to FZK	Nov 26, 2001
Oct 18-19, 01	ISP-45 Comparison workshop at FZK	Dec 10-11, 2001
Oct 16-18, 01	7th International QUENCH workshop at FZK	Dec 12-14, 2001
	Final comparison report of blind phase (FZKA-6677)	March 2002
Feb 2002	Final workshop together with informal ISP-46 meeting in Petten, NL	March 18, 2002
	Deadline for last changes of the final OECD report	March 31, 2002
	Presentation of OECD report at GAMA meeting	September 2002

2 THE QUENCH FACILITY

For the description of the ISP conditions the QUENCH facility can be split into two sections: the facility with all external devices and the test section itself. The overall description of the QUENCH facility is documented in several FZK Reports describing the commissioning tests /1/, experiment QUENCH-01 /2/, and the two experiments QUENCH-02 and QUENCH-03 /3/.

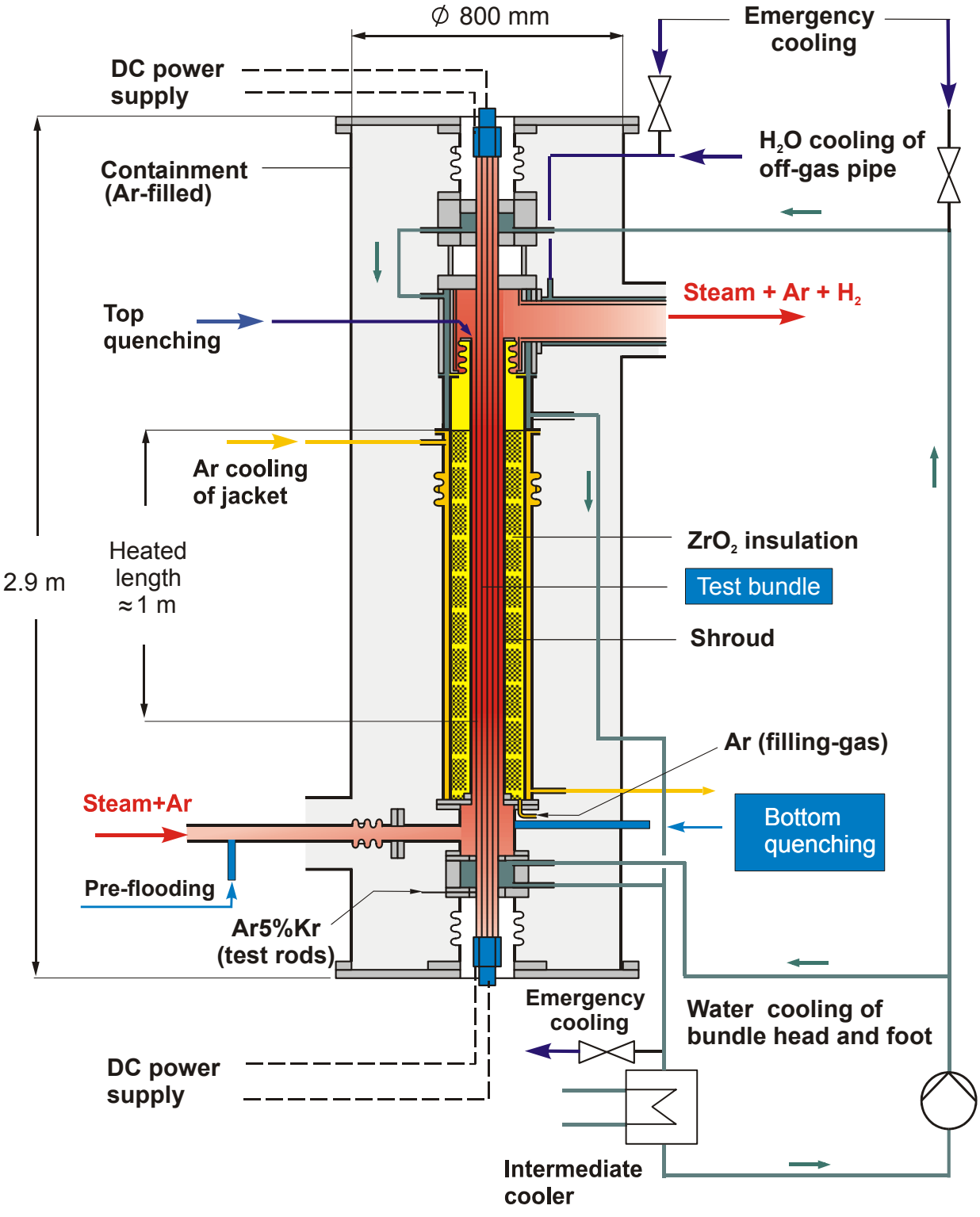

Figure 2.1 Main flow paths in the QUENCH facility.

In this report some additional information is given, including errata concerning the above-mentioned reports. Some of this information is added for the sake of completeness, but not absolutely necessary for this ISP. The schematics shown in Figure 2.1 give an overview of flow paths, entrance and boundary conditions.

2.1 Bundle Test Section

The geometry of the inlet volumes at the lower end of the test section is presented in Figure 2.2. The inlet pipe has an inner diameter of 0.054 m and a total length of 0.905 m between the valve and the wall of the lower plenum. The axial position of the inlet pipe centerline is at -0.412 m. The lower plenum has an inner diameter of 0.1053 m and contains a tube (outer diameter 0.0889 m, wall thickness 0.0025 m) with a number of holes to get a reasonable flow velocity profile in the bundle.

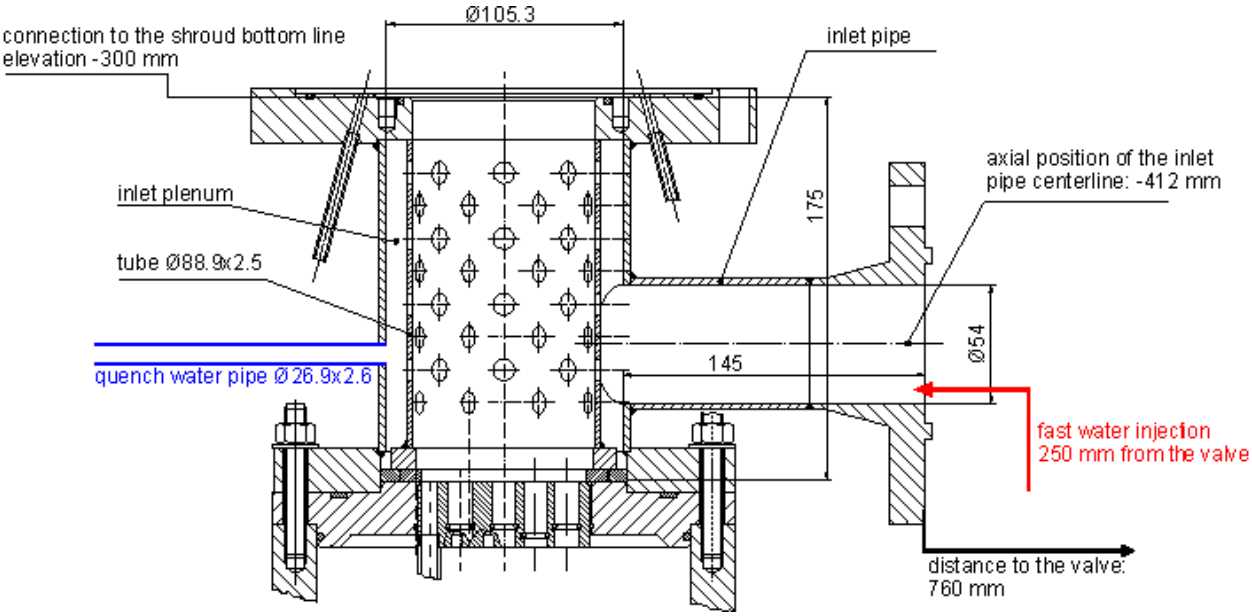

Figure 2.2 Detailed schematics of the lower plenum with fluid inlet pipe, fast water injection system (right), and quench water pipe (left).

In radial direction the QUENCH fuel rod bundle (Figure 2.1 center) is composed of an unheated rod (Figure 2.4 left side) at center position, an inner ring of eight heater rods (Figure 2.4 right side) connected to one electric power supply, an outer ring of 12 heater rods connected to a second power supply system, and a set of four corner rods at the vacant rod positions of the bundle. The 21 fuel rod simulators are filled with a mixture of 95 vol% argon and 5 vol% krypton at a pressure slightly above fluid pressure in the bundle and connected to a compensating volume at room temperature. More information on the internal structure of the heater rods as well as the unheated rod are given in /1/, /2/, and /3/. Details of the electric heating systems are summarized in /4/.

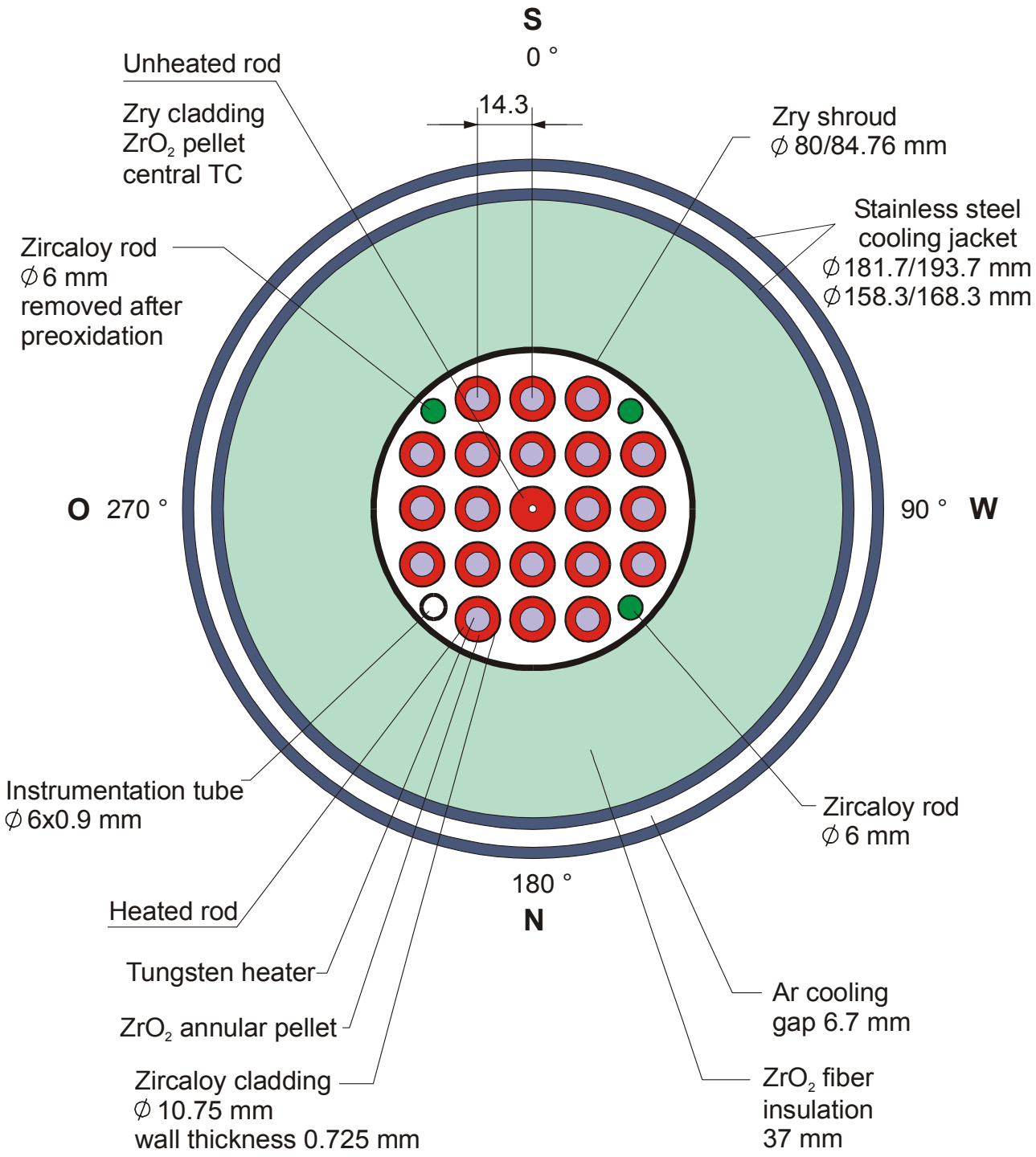

Figure 2.3 Bundle cross section and characteristic dimensions.

The bundle is enclosed in the shroud (Figure 2.3), which is composed of the Zircaloy liner (2.38 mm thick), a ZrO_2 fiber insulation and the inner cooling jacket, made of stainless steel. The thickness of the ZrO_2 fiber insulation was changed from 0.035 m in QUENCH-01 (/2/, Fig. 6) to 0.037 m for all subsequent tests. Bottom of the insulation is located at –0.3 m. Location of the upper end of the insulation is at +1.024 m. Properties and characteristics of the insulation provided by the manufacturer are taken from /6/. The region between the shroud and the inner cooling jacket, i.e. the ZrO_2 fiber insulation and the empty space above this insulation are flooded with argon before the test, the pressure being about 2 bar. In the fiber insulation convection may be inhibited due to the friction losses. In the empty space above, the main contribution of the radial heat losses is due to radiation, but natural convection may contribute to a cer-

tain extend. However, no information is available whether this argon remains stagnant during the whole test or whether a natural convection develops.

The bundle outlet geometry is sketched in Figure 2.1. Detailed drawings are published in /8/. Since nearly no participant simulated this section in detail, we refer to the description in /2/, /3/, or /7/.

The off-gas pipe mainly consists of a water-cooled inner pipe for the fluid leaving the bundle. This water-cooling is a countercurrent flow within the cooling jackets with a flow rate of app. 500 g/s at 300 K inlet temperature. Mass spectrometer sampling position is located at the distance of 2.660 m from the beginning of the off-gas pipe (intersection with the QUENCH test section).

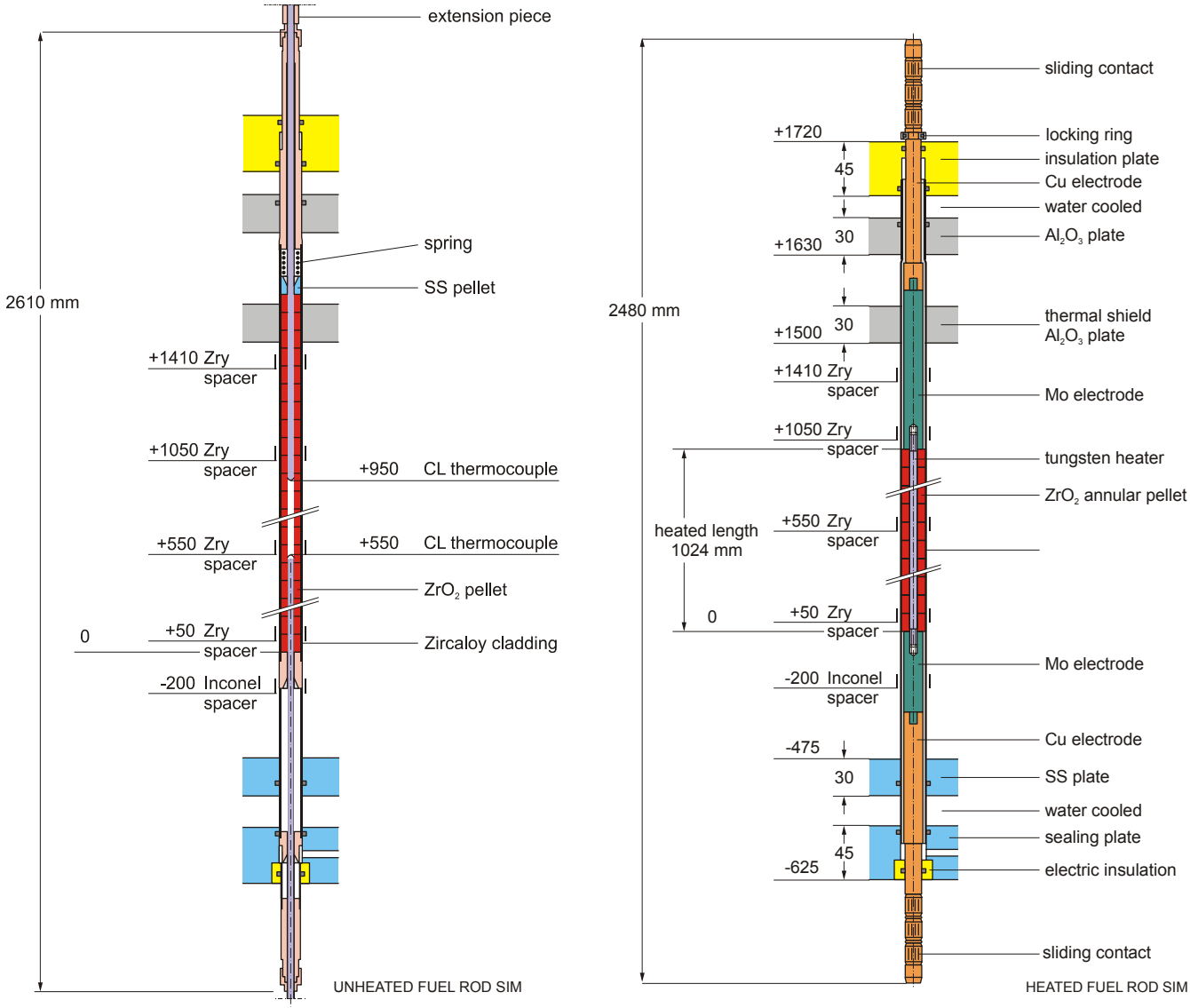

Figure 2.4 Detailed schematics of the QUENCH fuel rod simulators: unheated fuel rod (left) and heated fuel rod (right).

2.2 Electrical heating system

Indirect heating of the heater rods using tungsten and in the electrode zones molybdenum wires simulates the decay heat. The DC voltage measured in the facility includes the voltage drop at the sliding contacts at both ends of the rods, at wires, which lead from the sliding contacts to the power supply, and at screws that fix the wires at their ends. This has to be taken into account to correctly model the input of electrical power into the bundle.

FZK has done the calculational analysis for all tests performed up to now and demonstrated that it is possible to reasonably well reproduce the temperatures and hydrogen production in all five tests, using one fixed value of this constant additional resistance. This value was estimated on the basis of calculations for QUENCH-01 /2/ and was fixed for all other code runs. This value is about 4 mΩ for S/R5irs and might be different for other codes or other calculational domains.

2.3 Experimental measurements and accuracy

The fuel rod bundle and the shroud are equipped with high temperature TCs at various elevations and lateral positions based on the experience gained in the CORA program /12/, /13/. The details of mounting and internal structure can be found in /2/, /3/.

The general accuracy is app. ± 50 K, the individual mounting as well as the fluid environment have to be taken into account: In gaseous atmosphere the temperatures measured by surface mounted high temperature TCs show an app. 50 K lower value than the corresponding cladding temperature. In two-phase flow environment, however, the 2 mm thick TC blocks the flow cross-section substantially as an obstacle in the path of the water droplets. In that case the TC indicates liquid temperature without much delay. The droplet at a TC can evaporate before the water bulk arrives, so that the TC shows more elevated values afterwards, but probably below rod surface temperature. If that fin effect becomes dominant, the real temperature may vary between saturation (wetted TC) and the temperature measured in vapor atmosphere. Inner TCs do not suffer from such difficulties, but they show a delay due to thermal inertia of the surroundings. Temperatures measured by wall TC such as TSH should be used preferentially for two-phase flow conditions. If possible, both TC types should be used for comparison at a given elevation. Fluid mass flow rates of argon and steam are imposed by the pump whose make-up rate is calibrated. In case of steam, the delay due to evaporation is negligible here.

The quadrupole mass spectrometer (QMS) is used to detect the concentrations of several gas species in the off-gas pipe. Its accuracy is 5 %, the minimum detectable value for H_2O and H_2 is given to 20 ppm, that for non-condensable gases app. 1 ppm. In the beginning of the experiment steam measurements are subjected to local steam condensation at cold off-gas pipe structures.

The time delay of the temperature and mass flow rate measurements is negligible. The time delay of the QMS and CALDOS has been determined from a series of calibration tests with several bundle flows and gas injections at the 700 mm level. A first series was performed at room pressure and temperature with 3 and 6 g/s argon flow in the bundle and hydrogen as injection gas. A second series was performed at 1000 K maximum rod surface temperature with a mixture of 3 g/s argon and 3 and 50 g/s steam flow in the bundle at a system pressure of 0.2 MPa and with helium as injection gas. The time delay for the QMS was found to be approx. 5 s, that of the CALDOS analyzer to be 20 s as a minimum, depending on the fluid velocity in the off-gas

pipe and hence on the total mass flow rate. Moreover, the signal shapes are different for the two systems, i.e. the CALDOS analyzer gives a broader peak due to the diffusion of the hydrogen in the fluid.

3 THE QUENCH-06 EXPERIMENT

The QUENCH-06 test results are documented in detail in /7/, so that only a brief description will be given in this section, including the data specified as input data for the blind phase exercise.

3.1 Test Conduct

The ISP-45 experiment QUENCH-06 was successfully performed at FZK on December 13, 2000 /5/. In Table 3.1 the times (in seconds) of the various events and phases are listed.

As in the previous QUENCH experiments, the bundle was heated by a series of stepwise increases of electrical power from room temperature to ~600 °C in an atmosphere of flowing argon (3 g/s) and steam (3 g/s). The bundle was stabilized at this temperature for about two hours, the electrical power being about 4 kW. During this time the operation of the various systems was checked. Shortly before the end of this phase data acquisition was started.

At the end of the stabilization period the bundle was ramped by stepwise increases in power up to about 11 kW to reach an appropriate temperature for pre-oxidation. The temperature level was maintained for about 1 hr by control of the electrical power to reach the desired oxide layer thickness.

Table 3.1 Events and phases of QUENCH-06

Time	Event	Phase
0	Start of data acquisition	
30	Heat up to about 1500 K	Pre-oxidation
1965	Pre-oxidation at about 1500 K	
6010	Initiation of power transient	Power transient
6620	Initiation of pull-out of corner rod (B)	
7179	Quench phase initiation	Reflood
	Shut down of steam supply	
	Onset of fast water injection	
	Start of quench water pump	
	Detection of clad failure	
	First temperature drop at TFS 2/1	
7181	Steam mass flow rate zero	Quench
7205	Onset of electric power reduction	
7221	Decay heat level reached	
7430	Onset of final power reduction	
7431	Shut down of quench water injection	Post-reflood
7431	Electric power < 0.5 kW	
7435	Quench water mass flow zero	
11420	End of data acquisition	

At 6000 s, after the pre-oxidation phase, the electrical power was ramped at 0.3 W/s per rod to start the transient phase in the same way as in QUENCH-05. At 6620 s a corner rod was withdrawn during the transient to check the amount of oxidation at that time. The quench phase was initiated when pre-defined criteria similarly to QUENCH-05 were reached; therefore the cooling initiation conditions for these two tests are virtually identical.

Within 5 s app. 4 kg of water were injected to rapidly fill the lower parts of the set-up (fast water injection system). At the same time the quench pump was started to inject water from the bottom of the test section at a rate of ~40 g/s. About 20 s later the electrical power was reduced to 4 kW within 15 s to simulate decay heat level. Quenching of the test section was completed within ~250 s; the steam and electrical power were then shut off, terminating the experiment. During the quench phase argon injection was switched to the upper plenum to continue to provide carrier gas for quantitative hydrogen detection. From the pressure histories at least one rod and the shroud were detected to fail shortly after the initiation of the quench phase. The lowest position of that hole is at 0.87 m bundle elevation.

3.2 Data evaluation

Quench progression

As found in the previous QUENCH experiments without fast water injection the main cooling phase is characterized by (a) a relatively moderate cool-down mainly due to steam and two-phase flow cooling and then (b) a rapid cooling period with a drastic improvement in heat transfer (transition boiling). As described in /7/ the beginning of the first period is called “onset of cooling”, the beginning of the latter period is called “onset of quenching”, the related temperature being called “quench temperature”. In the upward direction this onset of quenching is delayed due to higher fuel rod temperatures and water losses by evaporation.

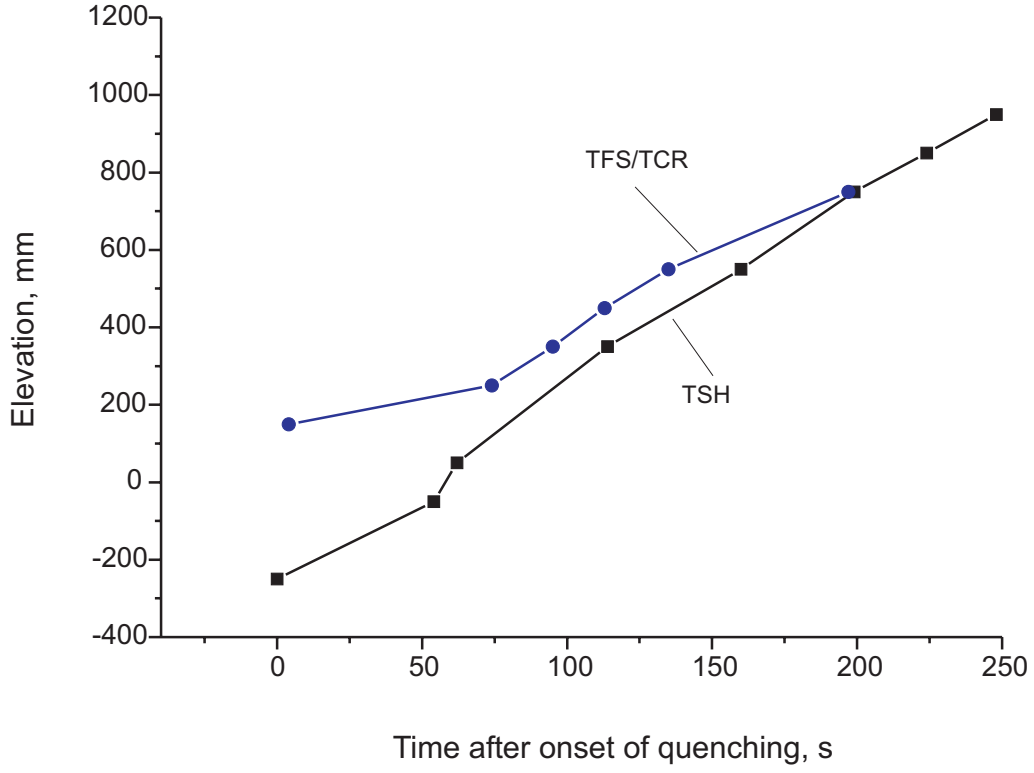

Figure 3.1 Quench positions relative to reflood initiation at 7179 s.

Based on the thermocouple temperature measurements information about the quench front progression can be evaluated. In Figure 3.1 two quench front progression curves are shown based on cladding thermocouples (types TFS and TCR) and on the shroud thermocouple readings (TSH). Particularly the shroud data show a linear behavior with a velocity of app. 5 mm/s in the heated section.

To compare quench front progression with water level rise, the data from pressure difference measurement (LM 501) and results of FZK post-test analyses with S/R5irs, as described later, are given in Figure 3.2 together with quench positions from thermocouple wetting data. To eliminate the noise of LM 501, low-pass filtering was performed leading to the curve. "ISP-45: Lm501". The cladding thermocouple readings reflect the rapid cooling due to the two-phase flow caused by the fast water injection. Above 0.2 m the slopes are comparable. For comparison, the injection rate, which is defined by the quench pump injection rate, delivers a net water level rise in the bundle of app. 14 mm/s, if evaporation in the various pipes is ignored.

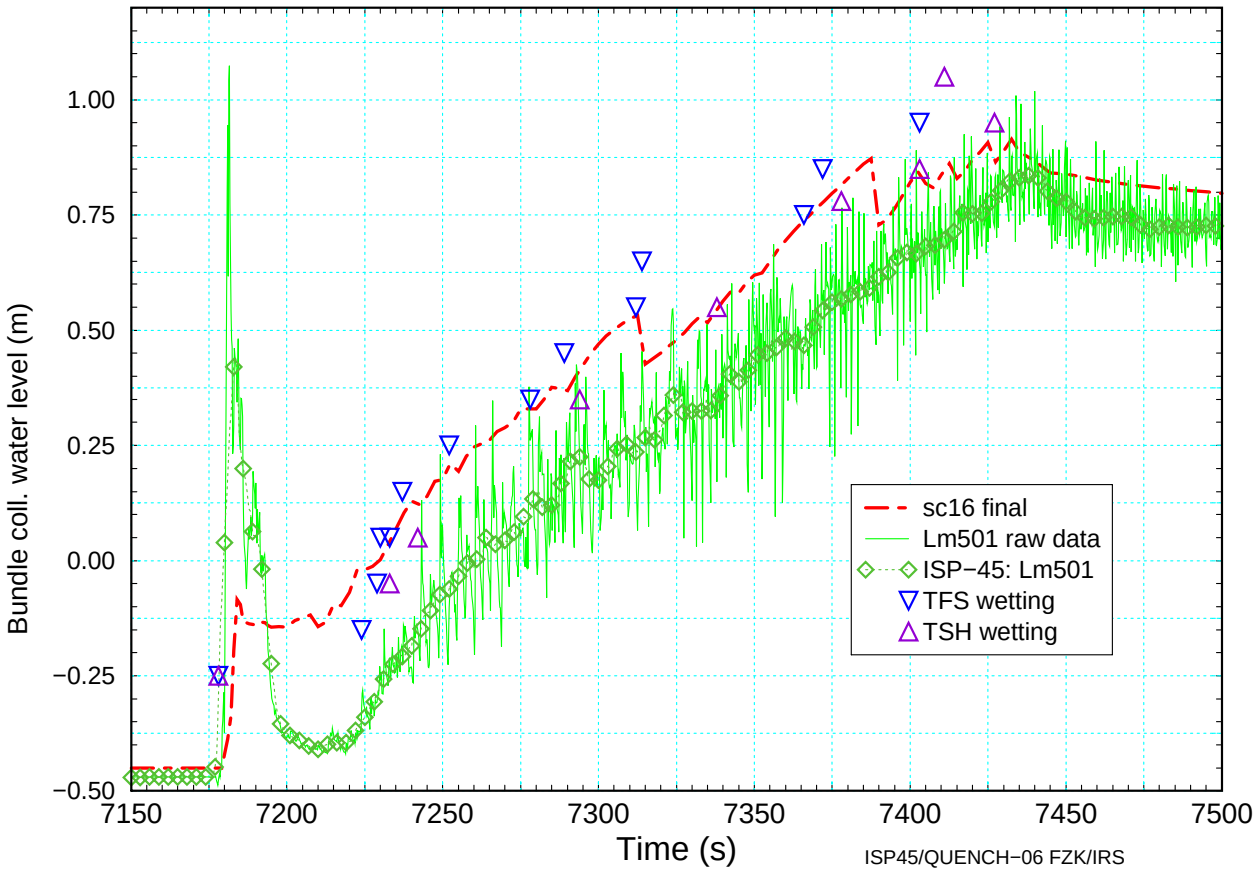

Figure 3.2 Water level increase from experimental data and thermocouple readings compared with S/R5irs calculation.

Quench water mass balance

To evaluate the evaporation that results from the quench water injection into the hot test bundle as a mass flow rate versus time, data from three independent instruments were evaluated: mass spectrometer (MS) data, F 601 orifice data, and L 701 condensate collector data /7/.

In Figure 3.3 the three different data sources used to determine the steam/water mass balance independently are compared, to each other and to the quench water input F 104. The mass flow

rate data F601 are derived from pressure difference measurements (standard orifice plate) assuming that the fluid density composed of steam, hydrogen, and some water rather small droplets can be approximated by the density of steam at the measured temperature. In addition, an average of the three curves by a coarse approximation (thick line in the diagram) is presented as mean steam mass flow rate. These mean data indicate that from the 40 g/s of water injected approx. 30 g/s steam was generated at the beginning of the cool-down phase decreasing to a more or less constant steam flow rate of 15 g/s from 70 – 80 s after quench initiation. So, the ratio of steam produced/water injected seems to change mainly during the first period of the quenching phase. For the quenching phase the total mass of steam measured by the mass spectrometer is app. 3.4 kg, that of the derivative of L 701, is app. 3.5 kg, (app. 7.8 kg is the value for the entire test), and app 4.7 kg is the integrated value of the F 601 standard orifice plate.

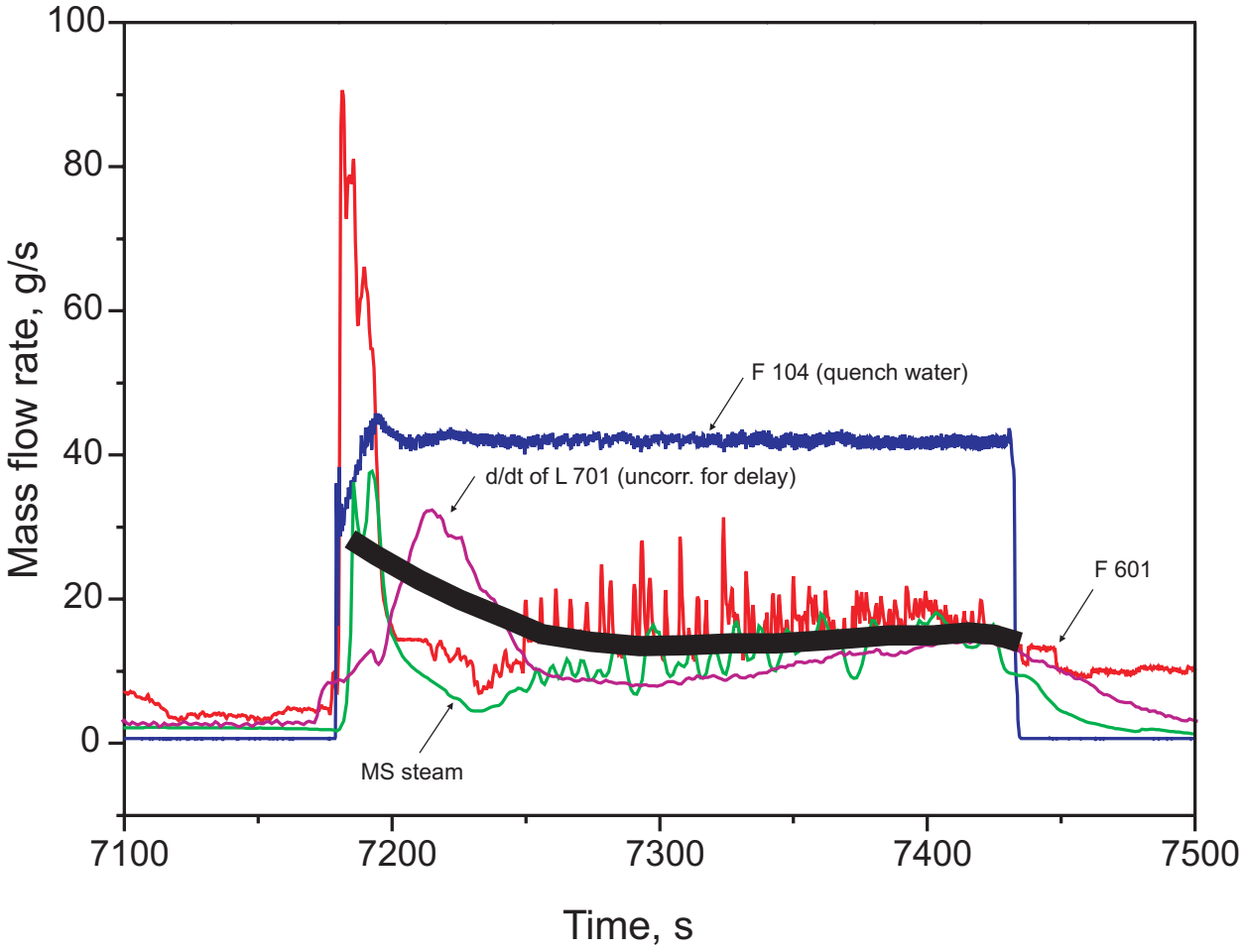

Figure 3.3 Steam flow measurements in the off-gas pipe (MS steam, F 601), in the condensate collector (d/dt (L 701)), and mean steam flow data (thick line) compared to quench water input (F 104).

3.3 Post test examinations

3.3.1 General state of the bundle

Figure 3.4 Shroud failure location above 0.85 m.

After the experiment the QUENCH-06 bundle in total and the Zircaloy rod cladding appeared nearly intact up to ~0.85 m elevation. Neither significant melt formation, nor melt relocation or blockage formation could be detected during post-test analyses from the cross sections, so that the bundle remained intact, except for cladding failure and oxidation.

Up to 0.86 m the Zircaloy shroud was only slightly oxidized, whereas a failure region of the shroud between app. 0.87 m and 1.01 m and between 270° and 0° orientation was detected. In this region the shroud exhibited a localized molten zone together with some breaching as shown in Figure 3.4. The upper end of the damage zone coincides with that of the shroud fiber insulation. The time of melting may coincide with the detected failure shortly after the initiation of the quench phase.

The bundle was cut axially into sections to allow detail analysis of the cross sections and to derive an axial distribution of the oxide layer thickness as discussed in section 3.3.3.

3.3.2 Bundle cross section

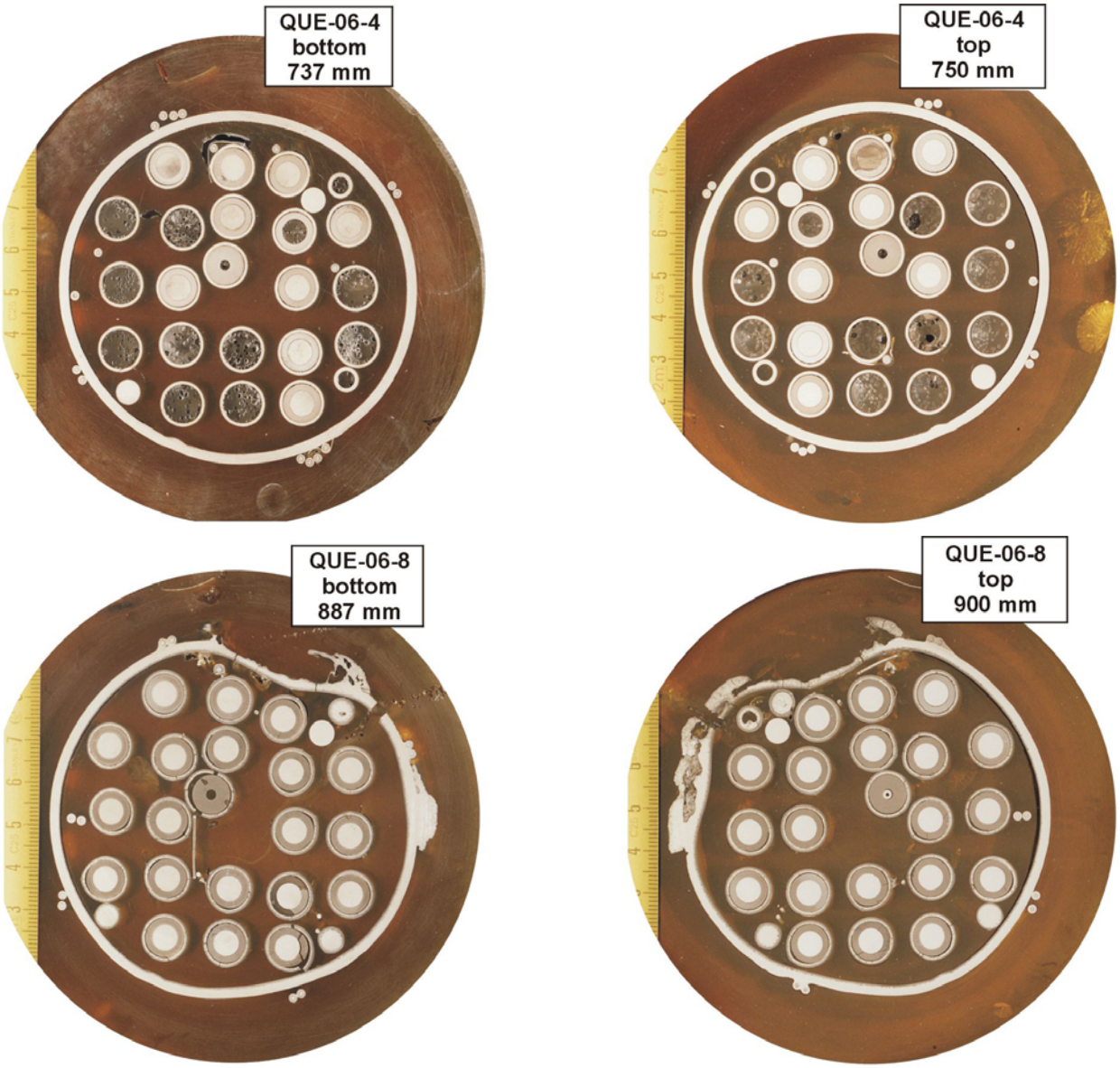

Figure 3.5 Bundle cross sections: top: at 0.737 m and 0.75 m, and bottom 0.887 m and 0.9 m.

Figure 3.5 and Figure 3.6 show bundle cross sections photographed from each side. Therefore the respective elevations differ by the slice thickness (app. 0.013 m). The cross sections show rod bending between the two grid spacers, at 0.592 m and 1.050 m as can bee seen in Figure 3.5 for the elevations 0.737 m and 0.750 m. Missing pellets (Figure 3.5 top) and heater wire materials were lost during handling after cutting of the cross section slabs. They fell off, because the cladding, which is fixed by epoxy, did not support them; evidently the ZrO_2 pellets had neither reacted with the Zircaloy cladding nor with the tungsten heater wire at that elevation. Corner rod B had been removed from the bundle during the transient test phase and is hence missing in the figures. The shroud deformation can clearly be seen in Figure 3.5 at 0.887 and 0.9 m. At 0.887 m and 0.9 m the fragmentation of corner rod A is obvious as well, and a spacer grid fragment is found. Shroud melting and melt agglomeration at the external side is pronounced, but restricted to the azimuthal range given above.

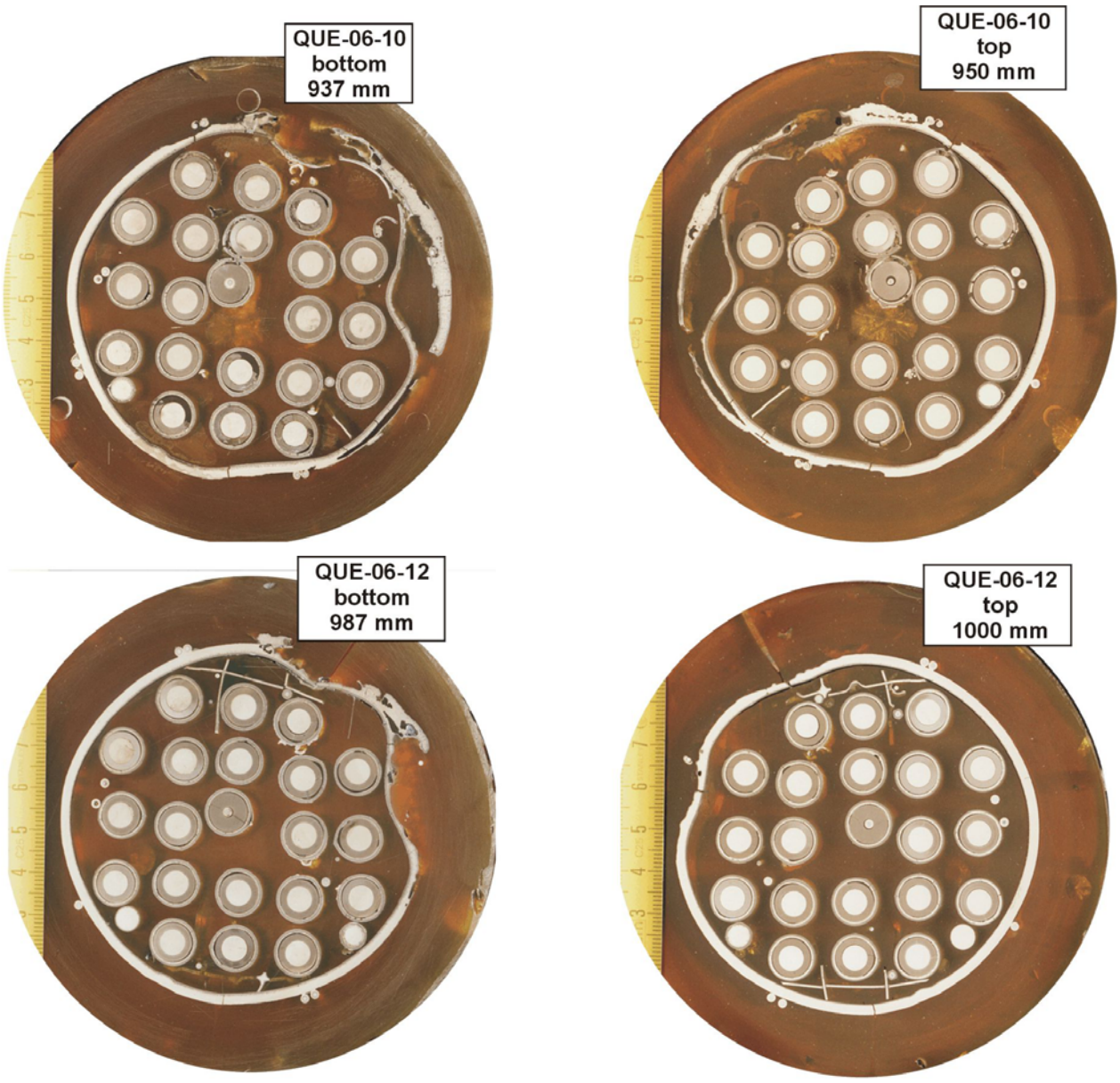

Figure 3.6 Bundle cross sections: top: at 0.937 m and 0.95 m, and bottom 0.987 m and 1.0 m.

At 0.937 m and 0.95 m the damaged shroud region is split into an internal and an external part of residual metallic material, both supported by the corresponding scale. Few amounts of re-solidified shroud melt remained, stronger bending of the residual rod and shroud structures occurred under scale growth stress. Fragmentation and downward movement of corner rods are confirmed by their partial or total absence. The observed types of cladding damage are described in section 3.3.4. At 0.987 m and 1.0 m the spacer grid survived only partly, confirming the rubble relocation at 0.887 m as mentioned before. At 1.137 and 1.15 m, i.e. within the upper electrode zone, corner rod A is missing as below. No evidence about the destruction of the spacer grid was found, one explanation may be that it collapsed due to thermal shock during reflood.

3.3.3 Axial oxide layer profile

The oxide scale thickness of the 21 individual rods was determined at the different axial levels by microscopic measurement at four azimuthal orientations. The results are shown in Figure 3.7 and discussed in detail in /7/.

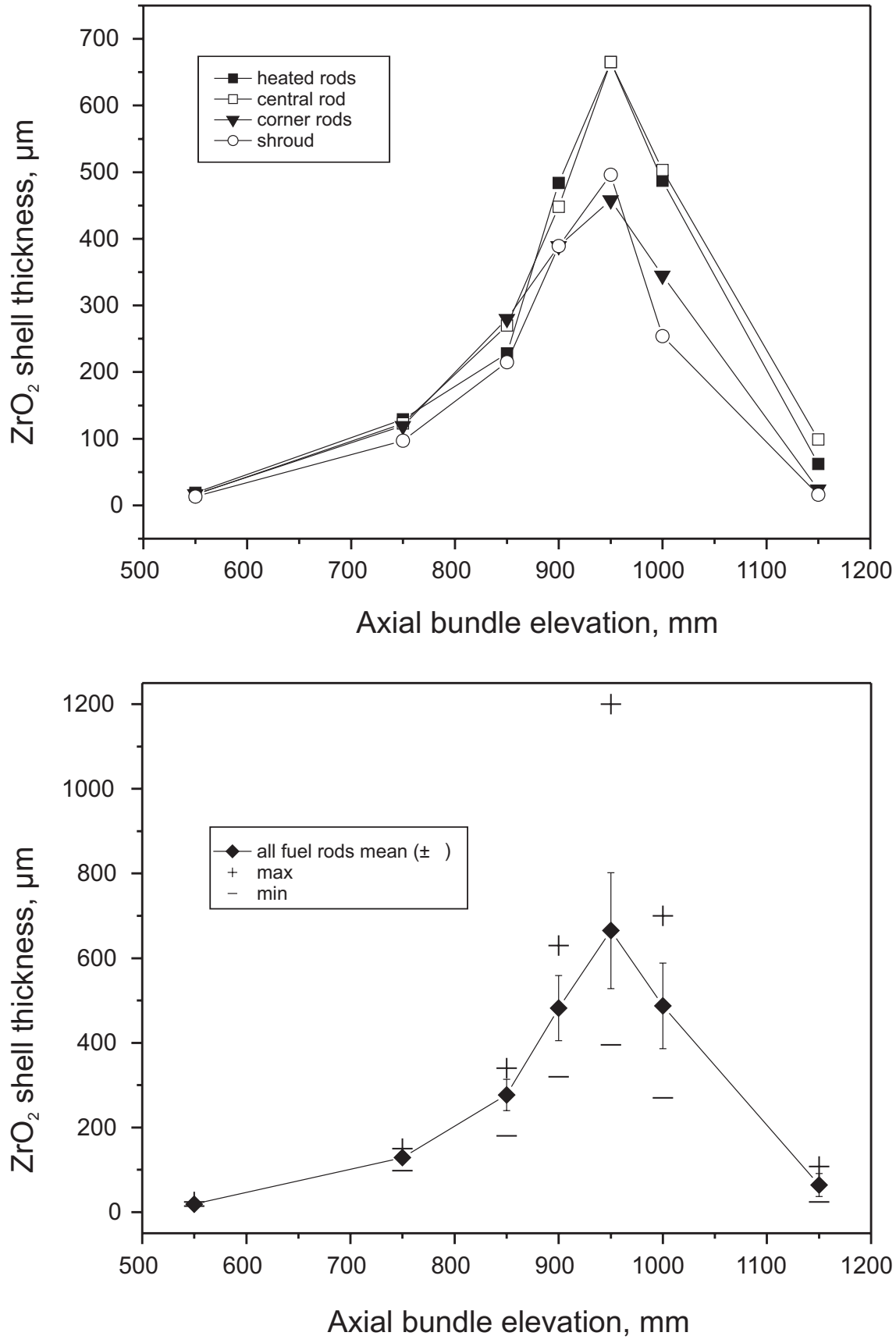

Figure 3.7 Top: Measured axial oxide layer thickness for the unheated rod, fuel rods, corner rods, and the shroud and bottom: averaged curve with standard variation at relevant axial elevations.

From this database the axial distribution of the oxide layer thickness is derived as shown in top of Figure 3.7 for the various rod types and the shroud. As can be seen the oxide layer thickness is smaller than 30 µm below axial elevation 0.5 m and increases to app. 100 µm at 0.75 m and reaches its maximum at 0.95 m. Between 0.9 m and 1.0 m the slopes of the unheated and heated fuel rods are approximately the same. The maximum ZrO_2 layer thickness at 0.95 m amounts to app. 1200 µm, the average value at that level to app. 660 µm (Figure 3.7 bottom). The standard deviation (± σ) ranges from 520 to 800 µm, corresponding to app. ± 20 %. The double of this value (40 %) as well as a slightly reduced one (15 %) were used to assess the accuracy of the calculated results.

3.3.4 Physico-chemical behavior of the bundle

Referring to cross section shown in Figure 3.8 the status of the unheated fuel rod and the heated fuel rods (simulator) at 0.95 m, the peak temperature elevation, is described in more detail. Apart from local deviations the lateral distribution of the cladding oxidation is remarkably flat, due to a correspondingly flat temperature profile.

Even at this elevation every rod has retained some metallic cladding below the thick external scale. In general, the scale remained protective until the formation of through-wall cracks or cladding fragmentation during the cool-down phase of the test. Locally observed clad bulging away from the pellet, due to oxidation-related circumferential elongation had no important influence on the oxidation kinetics, and even clad splitting had only localized consequences: The extent of internal steam oxidation can be estimated to have been of the order of one percent of the external contribution, due to the limited steam access towards the cladding interior and its local consumption. Internal oxygen transfer from the pellet to the cladding, which takes place in pronounced temperature dependence and is restricted to areas of mutual solid-state contact, is identified by the observed α-Zr(O) layers. Their “crucible effect” influenced the rod-internal melt re-distribution: In competition with the oxidation melting began within the cladding matrix and tended to spread during the transient towards the oxygen-enriched surrounding metallic phase.

This behavior was clearly reflected in the final bundle status: Voids, formed by melt relocation and melt accumulation at other positions were observed within some rods. However, in the coolant channel around the rods only a few small isolated melt droplets and some melt on a few rods have been found. No corresponding rod perforation failure position could be identified. It is deduced that the final bundle oxidation status was reached under essentially intact bundle geometry by one-sided steam oxidation as dominating mechanism.

Locally inhomogeneous lateral temperature distribution, triggering rod bending, in turn responsible for rod-to-rod contact and hot-spot formation, resulted in variations of the above-described behavior for different rods and cladding positions. The more pronounced melting phenomena observed for corner rods and shroud are seen in relation to the originally less advanced oxidation and the availability of more metallic mass for continuing steam oxidation later on.

It can be assumed that temperature escalation at the hot spot of the shroud has been supported by violent external steam oxidation after shroud perforation and steam leakage through the breach opening. Melt formation and external melt pool expansion by interaction with the adjacent volume of ZrO_2 fiber material is understood to have followed.

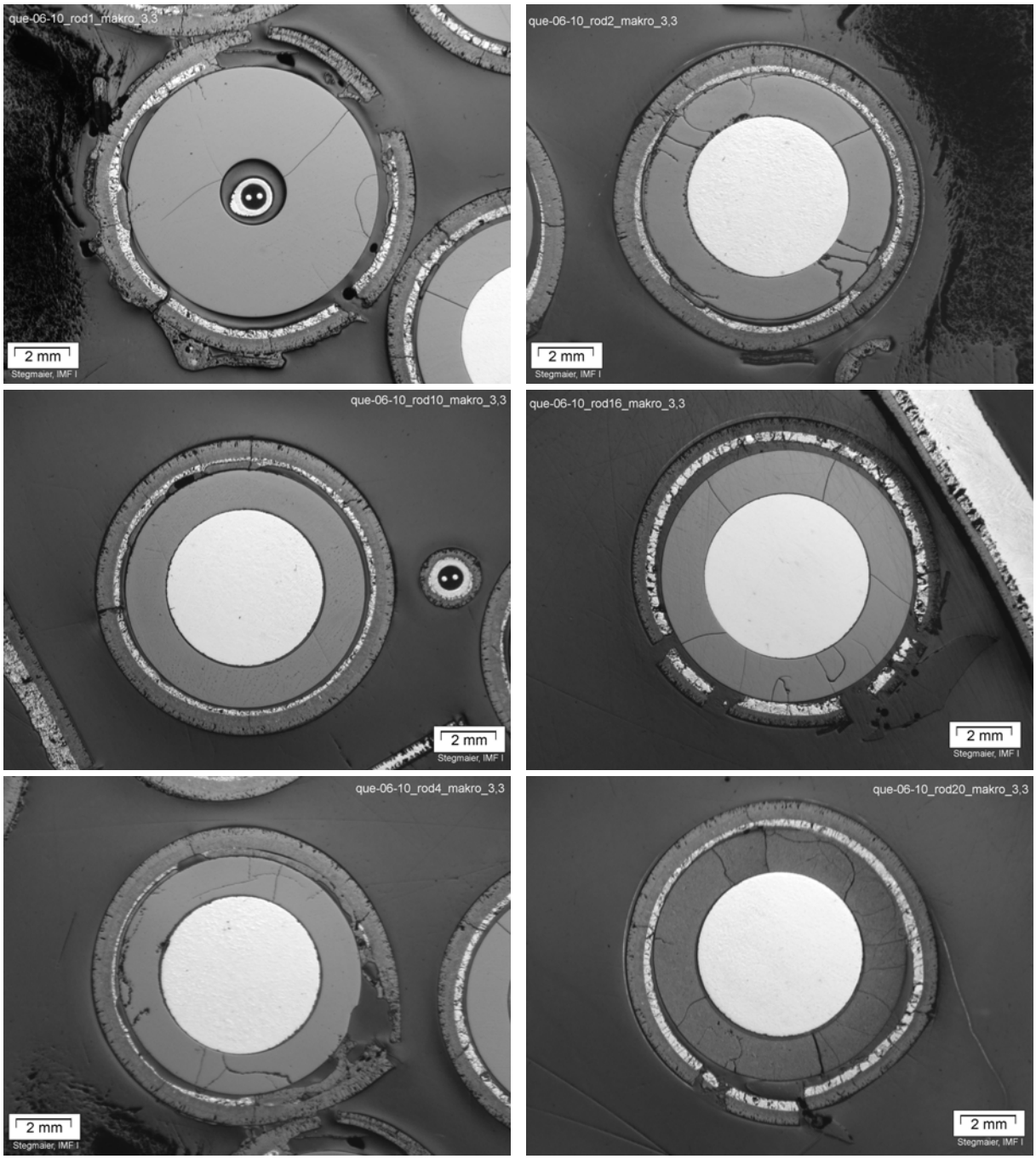

Figure 3.8 Individual cross sections of the unheated rod (top left) and some heated fuel rods including a shroud segment (center) at 0.95 m elevation.

3.4 FZK Calculations

Within FZK institutional R&D activities calculations are made to define experimental parameters of the QUENCH experiments and to interpret the experimental results after the experiment had been performed, using the in-house version of SCDAP/RELAP5mod 3.2, S/R5irs. It contains an improved model for heat transfer in the transition boiling region /15/, an adaptation of the CORA heater rod model to the conditions of the QUENCH facility, and the material property data for ZrO_2 instead of those for UO_2 to model the pellets. The various calculations also rely on the experience gained from calculations, done up to then. Especially the adjustment of the electrical resistance of the circuit outside the electrical heater rods, performed on the basis of test QUENCH-01 /2/, was kept.

Modeling of the QUENCH facility

For the results presented in this report, if not stated otherwise, a 16 nodes facility model is used as defined hereafter. In the radial direction the whole facility including the containment is modeled, because the radial heat losses out of the bundle depend ultimately on the ambient room temperature. This modeling is mandatory for all work performed before experimental data are available, and it is desirable for all post-test analyses, because the calculated data are more detailed than the experimental ones.

Axially the heated part is modeled with ten 0.1 m long meshes. In the lower and upper electrode zones 0.45 and 0.6 m, respectively, of the test section are considered, each by three meshes, assuming molybdenum as electrode material and giving 16 axial nodes in sum. The unheated rod, the two rows of rods to be heated independently, the four Zircaloy corner rods, the inner and outer cooling jacket, and the containment are modeled as separate SCDAP components. In this way two-dimensional heat conduction within the structures and radiation between adjacent structures are taken into account. The temperature at the end of the rods is set to 300 K. For the electrical resistance of the circuit outside the electrical heater rods the same value of 4.2 mΩ per rod was used as for test QUENCH-01 /2/. The ZrO_2 fiber insulation is modeled to end at the upper end of the heated zone. With this exception all structures must be modeled to have the same length because of limitations in the code. Therefore the upper and lower head cannot be modeled in all details.

The bundle flow and the gas atmospheres outside the outer cooling jacket, i.e. in the containment and the laboratory, are represented by a single channel each. Besides the gas atmospheres outside the outer cooling jacket are assumed to be stagnant, thus neglecting natural convection in these regions. Because of restrictions in the code, where only a limited number of materials can be specified, these atmospheres are modeled to consist of argon.

The off-gas pipe is taken into account with its whole length of 3 m, including the orifice at the position where the gas sample for the mass spectrometer is taken and the orifice at the outlet of the off-gas pipe. The mass flows in the off-gas pipe and the adjacent cooling jacket are modeled to be one-dimensional; the structures are modeled as RELAP heat structures, thus taking into account radial heat transfer within the structures.

In addition a 32 nodes bundle model has been created as a fast running approximate solution, where all axial mesh lengths in the heater and the electrode zones are halved. All heated rods are simulated as a single SCDAP component; the corner rods are not modeled. The facility outside the cooling flows is not considered Therefore the flow area for the argon flow is changed on the basis of the 16 nodes facility model to result in realistic radial heat losses out of the bundle. The lower plenum (Figure 2.2), the inlet pipes and the fast water injection system (Figure 3.9) were modeled in much more detail and with finer mesh lengths than in the 16 nodes facility model.

Meanwhile a 32 nodes facility model is available, where the whole facility is modeled as in the 16 nodes facility model, but all axial mesh lengths in the heated zone and the electrode zones are halved and the lower plenum, the inlet pipes and the fast water injection system are modeled as in the 32 nodes bundle model. Besides the radial discretization of the fuel simulator rods has been refined.

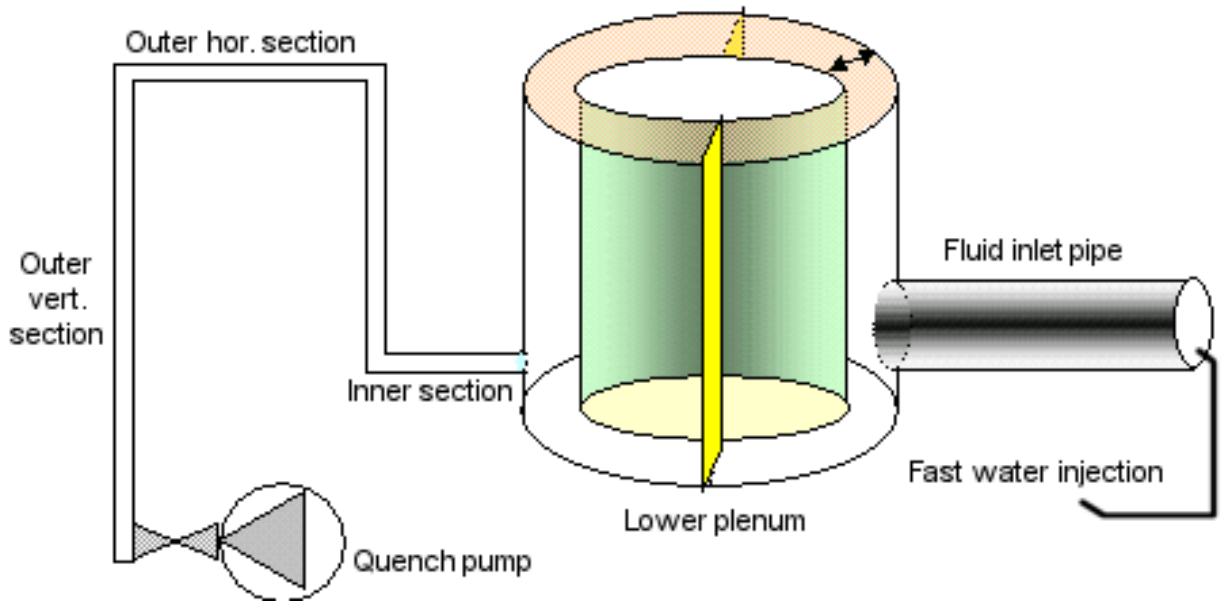

Figure 3.9 Detailed schematics of the inlet volumes including coaxial lower plenum with fluid inlet pipe, fast water injection system (right), and quench water pipe with realistic elevation changes (left) as used for FZK modeling.

Due to a code error the mass balance in the bundle may be wrong for reflood calculations, and the resulting mass error may be so large that the results become incredible for longer calculations. Therefore FZK calculations have been stopped at 7435 s for both the 16 and the 32 nodes bundle version.

Initial reflood conditions

During the post-test analyses of QUENCH-06 the comparison between measured data and those obtained by post-test calculations with S/R5irs revealed some inconsistencies with respect to the reflood initiation, as mentioned in the ISP-45 specification report /8/. An unexpected time delay was found between calculated water level and that deduced from measured temperatures and differential pressure. To identify the origin of this delay, a series of calculations with the 32 nodes bundle model and a profound comparison with experimental data as well as a detailed inspection of the facility revealed the reason for this delay.

Due to an undetected leakage of a check-valve at the quench pump the quench inlet pipe must have drained out partially before quench initiation and before adding to the fast quench water injection system, the quench water had to refill the voided pipe, thus giving the time delay mentioned above. Consequently, the specified mass flow rate is only relevant at the position of the quench pump, where it is measured, and not at the entrance into the lower plenum, where it is needed. On the basis of these investigations the mass flow rate in the lower plenum, to be used for the calculations, could be specified and made available to the participants of ISP-45.

In Figure 3.2 the calculated collapsed water level (sc16 final) as a measure for water level rise is shown in addition to the experimental values. The sharp peak of the pressure difference sensor (Lm501) at 7180 s indicates the violent water injection and cannot be interpreted as a water level. The result of the S/R5irs posttest analysis is in the vicinity of the detected wetting signals derived from different types of thermocouples. In this context the shroud outer surface thermocouples (TSH) are more relevant, because they are not influenced by dispersed droplet flow.

4 DATA BASE

4.1 Delivered Data

A large variety of data sets in different conditions were delivered from the 21 participants listed in Table 4.1. IJS joined after the preparatory workshop and perhaps misunderstood information and had less contact with other participants. Token ISS is retained for technical reasons, though Honaiser, University of Florida, did most of the work.

Table 4.1 Final list of participants and their organizations for ISP-45 blind phase calculations

Token	*Analyst(s)*	*Organisation*	*Address*	
CMX	Nunez-Carrera A.	Nat. Commission of Nuclear Safety and Safeguards (CNSNS)	Dr. Barragan 779, Col Narvarte; 03020, MEXICO D.F.	MX
DMM	Leonardi M.	University of Pisa	Via Diotisalvi, 2 - I-56126 Pisa	I
DRS	Mélis S. Zabiego, M.	IPSN/DRS/SEMAR/LECTA	Cadarache Bat 700; 13108 St Paul Lez Durance	F
EDF	Lacour V., Pineau D.	Electricité de France (EDF)	1 avenue du Général de Gaulle; 92141 Clamart	F
ENE	Bandini G.	ENEA	Via Martiri di Monte Sole 4; 40129 Bologna	I
FRA	Caillaux A.	Framatome-ANP, Paris	TOUR FRAMATOME; 92084 Paris La Defense	F
GRS	Erdmann W.	Gesellschaft für Anlagen- und Reaktorsicherheit (GRS)	Schwertnergasse 1; 50667 Köln	G
IJS	Stanojevic M. Leskovar, M.	Institut Jožef Stefan	Ljubljana, Slovenia	SI
INL	Coryell E.	Idaho National Engineering and Environmental Lab.	Idaho Falls, ID	USA
ISS	Allison C. Honaiser, E.	Innovative Systems Software University of Florida, Tampa	1284 South Woodruff; 83404 Idaho Falls, ID	USA
NEH	Niyazi Sokmen C.	Nuclear Engineering, University Hacettepe	Beytepe, Ankara, 06532	TR
NK1	Pylev S.	NSI of RRC "Kurchatov Institute"	123182 Kurchatov sq.1; Moscow, Russia	RU
NK2	Tomachik D.	NSI of RRC "Kurchatov Institute"	123182 Kurchatov sq.1; Moscow, Russia	RU
NUP	Ikeda T.	NUPEC (Nuclear Power Engineering Corporation)	17-1, 3-chome Toranomon; Minato-ku, Tokyo, 105-0001	JP
REZ	Duspiva J.	Nuclear Research Institute, Rez	250 68 Rez near Prague	CZ
RUB	Reinke N.	Ruhr-University Bochum; Institute for Energy Systems and Energy Economics	Building IB 4/126; 44780 Bochum	G
SES	Sponton L.	Studsvik ECO & Safety AB	SE 611 82 Nyköping	S
SIE	Plank H.	Framatome-ANP, Erlangen	Freyeslebenstr. 1; 91058 Erlangen	G
SNL	Cole R.	Sandia National Laboratories	PO Box 5800-0739; Albuquerque, NM 87185-0739	USA
UZA	Debrecin N.	University of Zagreb	Unska 3; 10000 Zagreb	CR
VTT	Hämäläinen A.	VTT Energy	PO box 1604; 02044 VTT	FIN
FZK	Homann Ch.	Forschungszentrum Karlsruhe, Institute for Reactor Safety	PO Box 3640; 76021 Karlsruhe	G

Since we wanted to keep as many participants as possible in ISP-45 we did not refuse bad data formats and/or miss-aligned data. Besides the specified ASCII tables and the DMX files we got RELAP 5 strip files and MELCOR printout and even one complete "restart plot-file". We corrected typing and other obvious errors. Surprisingly some participants did not match the speci-

fied time vector, causing additional efforts and increased the data storage. We tried to use the inappropriate time vectors if they were in ascending order.

4.2 Codes

In the blind phase of ISP-45 the 21 participants used 8 different codes as shown in Table 4.2. They can be grouped into two families:

- Integral code systems (I), designed for complete reactor analyses and
- Detailed codes (D), as often used to assist and analyze integral experiments.

Table 4.2 List of codes and code options used for ISP-45 blind phase calculations

Code	*Type*	*Token*	*Analyst(s)*	Thermohydraulics general	Thermohydraulics reflood	Clad failure temp.[K]	Oxidation low / high	Remarks
ATHLET-CD	**D**	**GRS**	Erdmann	2p, 1D, 5eq.	Inv. annul. flow	2400 K	C / UH	based on Q-01
		RUB	Reinke	"	"	2400 K	C / UH	based on Q-01
GENFLO	**D**	**VTT**	Hämäläinen	2p, 2D, 5eq.	qft	n/a	UH	UH mod * 0.2
ICARE/	**D**	**DRS**	Zabiego	2p, 1D, 6eq.	Inv. annul. flow	2300	UH	
CATHARE		**ENE**	Bandini	"	"	2300	UH	simpl. crack op.
IMPACT/ SAMPSON	**D**	**NUP**	Ikeda	3p, 2D, multi-field	n/a	n/a	C / UH	
MAAP 4.04	**I**	**EDF**	Pineau	1p+1p, 1D	simpl.qft	2500	C / UH	MAAP4.04c
		FRA	Caillaux	"	mixture level	2500	C / BJ	
MELCOR	**I**	**IJS**	Stanojevic	2p, 1D, 6eq.	no	2500	C / UH	*decay power*
Me 1.8.5QZ		**NK2**	Tomachik	"	no	2250	C / UH	
Me 1.8.5RB		**REZ**	Duspiva	"	simplified qft	deactivated	C / UH	new HR model
		SES	Sponton	"	"	2500	C / UH	"
		SNL	Cole	"	"	2500	C / UH	"
SCDAPSIM	**D**	**CMX**	Nunez-Carrera	2p,1*D,6eq	n/a	n/a	C / UH	*FZKA 6566*
		DMM	Leonardi	"	"	2200	C / UH	"
		ISS	Honaiser	"	"	2500	C / UH	"
		NEH	Sokmen	"	"	2500	C / UH	"
		NK1	Pylev	"	"	2500	C / UH	"
		SIE	Plank	"	"	2200	C / UH	"
		UZA	Debrecin	"	"	2500	C / UH	"
SCDAP-3D	**D**	**INL**	Coryell	2p,1*D,6eq	n/a	n/a	Diff.Model (Olander)	"
S/R5.irs	**D**	**FZK**	Homann/ Hering	2p,1*D,6eq	PSI / FZK	2350	C / UH	FZKA 6566

Oxidation correlation: ***BJ: Baker/Just*** ***C: Cathcart*** ***UH: Urbanic/Heidrick***

Thermal-hydraulics: p: phase D: dimension eq: equations

1*D: 1D + cross-flow capability

n/a: no sufficient information given qft: quench front tracking

Me 1.8.5RB Melcor code version with qf tracking and beta HR model

Me 1.8.5QZ Melcor original version without explicit reflood model and HR model

MAAP4.04c EDF MAAP4.04 code version with qf tracking, C/UH oxidation correlation

4.2.1 General code features

For the pre-quench phases only a single-phase 1-dimensional representation of thermal-hydraulics is required. However, in the quench phase the codes require capabilities to simulate two-phase flow and to track the water level. From literature /10/ it is known that a maximum mesh length of 0.07 m should not be exceeded to track the various fluid states sufficiently. In case of larger meshes, averaging of temperatures and heat fluxes smear the very pronounced temperature drop (quenching) leading to reduced cool-down rates.

In essence the thermal-hydraulic capabilities of the codes can be described briefly as follows (Table 4.2):

- ATHLET-CD and GENFLO use a 5-equation representation of two-phase thermal-hydraulics; the single momentum equation is extended by a drift flux correlation coupling both phases. For reflood situations a dedicated quench front tracking model derived and validated from design bases reflood experiments is available.
- ICARE/CATHARE is based on the French thermal-hydraulic code CATHARE, which uses a 6-equation system and mass balances for non-condensables in the vapor and solutes in the liquid phase. The CATHARE code also allows 1-D multi channel flow in the core region.
- IMPACT/SAMPSON is rather a new modular approach started around 1994. Thermal-hydraulics is modeled based on multi-field, multi-component, multi-velocity field in three phases (gas, liquid, plus solid particles) and in two dimensions. Mass conservation is calculated for each species independently.
- The MAAP code originally only handles one fluid in each cell, either fluid or vapor. Some improvements of EDF allow cells with both phases to simulate a rising water level during reflood. The phases are separated depending on the local void fraction.
- The MELCOR code uses a 6-equation representation of two-phase thermal-hydraulics with two independent momentum equations. The major distinction from more detailed codes is in the "flow regime map" for the coupling of the phases by exchange of momentum. MELCOR's "map" is extremely simple, and is intended only to give good results for the limits of counter-current flow and low-velocity entrainment.

Three of the detailed codes (SCDAP-3D, SCDAPSIM, and S/R5irs, the FZK in-house version of SCDAP/ RELAP5 mod 3.2) are based on the thermal-hydraulic code system RELAP5 that uses a 6-equation system and mass balances for non-condensables in the vapor and solutes in the liquid phase. In S/R5irs the PSI/FZK reflood model has been activated, which gives better results for the quench temperatures using the semi-mechanistic Chen transition-boiling model.

4.2.2 Code options selected

Especially the integral codes use a set of default parameters. If participants modified one of these, this should have been specified. In the third and fourth section of Table 4.2 the clad failure criteria and the oxidation correlation are given as far as delivered by the participants.

Clad failure

In all codes the clad failure criterion is a user-defined parameter, which strongly influences the further progress of the bundle damage, because of U-Zr-O melt relocation into colder parts of the core/bundle. From FZK single rod experiments a certain dependency of the clad failure

temperature on the heat-up rate was detected. This may explain the common observation of different clad failure temperatures used in simulation of reactors and integral experiments.

From physics the melting of the α-Zr(O) weaken the ZrO_2 layer since in liquid metallic Zr the oxygen diffusion coefficient is much higher than in solid state. In addition the ZrO_2 stability is rather low above 2700 K. Therefore, a physically sound parameter range is between 2330 K and 2700 K. To avoid melt relocation some participants increased the clad failure temperature allowing for continuous oxidation.

Oxidation correlation

Nearly all participants used the Cathcart (C) correlation for the low temperature regime of Zircaloy oxidation (Table 4.2), except for ICARE/CATHARE and GENFLO, which both use Urbanic-Heidrick (UH). In the high temperature regime mostly the correlation of Urbanic-Heidrick is used which tends to under-predict the oxide layer growth.

Besides, Baker/Just (BJ) is used by the MAAP code. In the temperature range of QUENCH-06, the differences between UH and BJ are not very pronounced for a large part of the experiment, so that the source of exothermal energy should be similar.

In SCDAP-3D an integral diffusion model for oxidation is implemented, which applies Fick's law of diffusion and the phase diagram of the oxidic and metallic portions of the cladding to calculate the rate of oxygen uptake in the cladding. From that Zr-O phase diagram the oxygen concentrations at phase boundaries were derived, the diffusion coefficients were taken from Olander /11/.

4.2.3 Dedicated models for reflood conditions

Some of the codes have powerful thermal-hydraulics package (SCDAP/RELAP5, SCDAPSIM, ICARE/ CATHARE) others use simplified models that work sufficiently well in the SFD range, but have problems with the two-phase flow conditions. In section 5.2.2 some assessment of the code capabilities with respect to reflood simulation is given.

All codes which are based on RELAP5 mod3.2 include a sophisticated reflood model developed at PSI /14/ and extended at FZK /15/. This model, originally developed for DBA analyses has to be activated by a trip and works efficiently on RELAP5 heat structures.

- The MELCOR thermal-hydraulics package is developed at SANDIA national laboratory based on two independent momentum equations. In the ISP-45 exercise, two MELCOR code versions participate. IJS and NK2 used original MELCOR 1.8.5 (QZ) and REZ, SES, and SNL used an improved MELCOR 1.8.5 MELCOR 1.8.5 (RB) version /16/ which includes a simplified water level tracking model (Table 4.2).
- The original MAAP, used by FRA only, allows either water or steam in one mesh. The heat transfer to the fluid is a function of the fuel rod state and the conditions in the fluid. The EDF version of the MAAP code includes a simplified reflood model is based on four two-phase flow regimes. The transition between these regimes is calculated using local state variables, critical heat flux, and minimum film boiling temperature.
- GENFLO also includes a quench front tracking model, which has been assessed against various DBA reflood tests with surface temperatures up to 1000 K.

- The reflood model of the IMPACT/SAMPSON code selects the heat transfer coefficients depending on the flow conditions comparable to the solution in RELAP5.

4.3 Modeling of test section

In previous ISP exercises, such as ISP-31 (CORA-13, /12/) or ISP-36 (CORA-W2, /13/), most of the participants were only able to simulate the heated section of the CORA bundle which extends to 1.0 m, and the number of axial meshes were mostly fixed to ten. The upper electrode zone, which makes about 20% of the total length, could not be simulated.

In ISP-45 all participants were able to simulate the heated section plus the molybdenum electrode zones extending the length of the simulated test section to 1.6 m as can be seen in Table 4.3. Integral experiments such as QUENCH or Phebus FP can be analyzed sufficiently using a 1-D approach, since the length of the test section (1.6 m) is much larger than the radius (0.04 m). Cross flow effects such as occurred in some CORA experiments are not possible. So most of the participants use several rings for the bundle components in one single fluid channel, except for NUP, EDF and FRA, use 3 fluid channels. A large number of participants also include the external cooling channel (Table 4.3) with Argon and water in the upper electrode zone and consider the absence of the fiber insulation in the shroud above 1.0 m.

The detailed code systems generally use 0.1 m mesh lengths in the heated sections and various lengths in the electrode zones, which often include the copper sections too. As sketched in Table 4.3 nearly all participants simulated the bundle using all five components: unheated rod (Un), inner and outer ring of heater rods (He), corner rod (Cr), and shroud (Shr).

- The ATHLET-CD input deck from GRS originally derived from previous CORA calculations was extended for analyses of various QUENCH experiments. RUB increased in the upper electrode zone the convective heat transfer to the shroud artificially (Table 4.3).
- In the GENFLO code the electric power is distributed homogeneously over the heated length of the tungsten since no dedicated heater rod model is available to simulate the temperature driven negative feedback. Due to this fact, the temperatures in the lower part of the bundle are overestimated.
- The ICARE/CATHARE calculation by DRS is based on a fine mesh originated from CEA studies with ICARE2 to achieve a better representation of the axial temperature profiles prior to reflood. Similar experience was obtained with the 32 nodes input deck used at FZK.
- The ICARE/CATHARE input deck of ENE input deck tripled the number of axial meshes so that in the heated section 0.033 m long meshes were achieved. To account for the convection in the gap above 1.0 m the Zry emissivity at the shroud outer surface was adapted (as indicated by Ar+ in Table 4.3).
- IMPACT/SAMPSON model includes three flow channels, 1) center: including the unheated rod, 2) middle: including the inner ring of heated rods, and 3) outer: with outer ring and the shroud.
- The MAAP code users have only limited degree of freedom to design own input decks, since large parts are coded in the program itself. The FRA input deck is based on an EPRI version for CORA experiments.
- MELCOR input deck from REZ has been developed and validated for QUENCH-01 experiment. It serves as basis for the input decks of SNL, which developed the MELCOR reflood

model. However, some problems arise due to the inadequate modeling of axial power release. In MELCOR six thermal-hydraulic cells (CVH, FL package) are used but in the bundle model (COR package) a much finer discretization is used. The thermal-hydraulic boundary conditions for the COR structures are interpolated base on the CVH values. Other MELCOR users (NK2, IJS, SES) developed input decks with a finer CVH nodalization.

- Nearly all participants using SCDAPSIM or SCDAP-3D (except for SIE and DMM) rely on an input deck developed by ISS, which was distributed as part of SCDAPSIM package.

Table 4.3 Modeling of the QUENCH test section by ISP-45 participants

Code	*Token*	Nodalisation axial	Nodalisation radial	Simulated length [m]	Components Un He Cr Shr	Shroud Upper electr.	Shroud outer bound.	Remarks Special features	Remarks Special options
ATHLET-CD	**GRS**	20	4	-0.475 ...1.5	**1 2 0 1**	Ar*	Ar / W	$\lambda_{(ZrO2)}$+50%	Rv=5.0mΩ
	RUB	19	4	-0.475 ...1.5	**1 2 0 1**	Ar*	Ar		Rv=4.2mΩ
GENFLO	**VTT**	17	4	-0.2 ...1.5	**1 2 0 1**	n/a	n/a	no specific HR-model	
ICARE /	**DRS**	66	5	-0.47 ...1.47	**1 2 1 1**	Ar*	prescribed	$\lambda_{(ZrO2)}$+80%	Rv=4.2mΩ
CATHARE	**ENE**	42	5	-0.45 ...1.5	**1 2 1 1**	Ar+	prescribed	1 channel	Rv=4mΩ
IMPACT / SAMPSON	**NUP**	19	5	-0.3 ...1.5	**1 2 $^3/_4$ 1**	Ar	Ar / W	3 channels	Rv=5mΩ
MAAP 4.04	**EDF**	58	4	-0.46 ...1.51	**0 3 0 1**		prescribed	3 channels	no Rv
	FRA	50	4	-0.475 ...1.5	**0 3 1 1**		prescribed		Rv=4mΩ
MELCOR	**IJS**	19	5	-0.475 ...1.5	**1 2 1 1**	Ar	Ar / W		*decay heat*
vers. 1.8.5QZ	**NK2**	18	4	-0.475 ...1.5	**1 2 0 1**	n/a	Ar+steam		
ver. 1.8.5RB	**REZ**	20	5	-0.475 ...1.6	**1 2 1 1**	Ar	prescribed		Rv=2.5mΩ
	SES	16	4	-0.6 ... 1.79	**1 2 0 1**	Ar*	Ar		Rv=4.2mΩ
	SNL	22	5	-0.475 ...1.5	**1 2 1 1**	Ar*	Ar / W	*off-gas pipe*	Rv=3mΩ
SCDAPSIM	**CMX**	16	5	-0.3 ...1.3	**1 2 1 1**	Ar*	Ar / W	*ISS based*	*O-30*
	DMM	16	5	-0.25 ...1.6	**1 2 1 1**	Ar*	Ar / W	$\lambda_{(ZrO2)}$+80%	Rv=4.3mΩ
	ISS	16	5	-0.3 ...1.3	**1 2 1 1**	Ar*	Ar / W	0.86*Po(el)	Rv=2.5mΩ
	NEH	16	5	-0.3 ...1.3	**1 2 1 1**	Ar*	prescribed	*ISS based*	
	NK1	16	5	-0.3 ...1.3	**1 2 1 1**	Ar*	n/a	*ISS based*	
	SIE	19	5	-0.485 .1.52	**1 2 1 1**	Ar *	Ar / W	$2.2 * \lambda_{(ZrO2)}$	
	UZA	16	5	-0.3 ... 1.3	**1 2 1 1**	Ar*	Ar / W	*ISS based*	*O-30*
SCDAP-3D	**INL**	16	5	-0.25 ...1.35	**1 2 1 1**	n/a	n/a	*ISS based*	Rv=4.2mΩ
S/R5.irs	**FZK**	16 32	5 3	-0.45 ...1.6	**1 2 1 1** **1 1 0 1**	Ar & rad	Ar / W W		Rv=4.2mΩ

Argon gap:
- Ar* Argon with modified heat conductivity
- Ar+ Argon with modified radiation (see text)
- O-30 Option 30 used, no radiation in bundle
- prescribed Temperatures given in the specification report used

External cooling:
- Ar / W Argon below 1.0 m, water above
- W Water cooling at shroud outside
- HR electric heater rod
- $^3/_4$ simulation of corner rod removal

5 RESULTS OF BLIND PHASE

This section is a brief summary of section 4 of /22/, it comprises delivered results of various codes, experimental results, and the FZK post test analyses with S/R5irs. In order to establish a broad data basis for a coherent assessment of the code predictions, a large series of calculated data was requested to the participants. In total more than 400 different physical quantities were plotted as post-script graphics.

To avoid confusion and to assess the code capabilities a “mainstream” was defined which covers all results in the vicinity of the experimental data. The width of that mainstream is oriented at the experimental findings and the visible bandwidth of the calculational results. Also the mainstream may vary with time i.e. the initial width of the hydrogen mass mainstream increases from ± 15 % at 6000 s to ± 40 % after reflood.

In the legend of all graphics shown in this section, all participants are listed. Each participant is identified by its token and the curves are characterized by symbol, color, and line style. Experimental results are identified by (-E-) or by opaque symbols. The FZK posttest calculations can be identified by (-C-) symbol. If the participants did not deliver the desired results or the data could not been read, a ".0" was added to the token. This allows unique line properties for each participant. Furthermore an extension ".1" indicates a change of original database by FZK /22/.

Section 5.1 includes various balances as well s a description of the bundle state at 7170 s prior to reflood phase (section 5.2). The final state of the bundle is discussed in section 5.3 and the summary of the blind phase exercise as documented in /22/ is outlined in section 5.4.

5.1 Pre-reflood

The pre-reflood phase comprises various phases as indicated in Table 3.1 up reflood initiation at 7179 s. During the pre-oxidation period nearly quasi-stationary conditions were achieved in the bundle; they were used for data checking. At 7170 s the bundle state was compared to data of the experiment and post-test calculations.

5.1.1 Data checks and global balances

During data assessment of the blind phase various data were checked with respect to reliability and the deviation to experimental or post-test calculations. That assessment is stored in Table 5.1 for the inlet temperature (Tfg.01), the steam mass flow rate at bundle exit (mdst9), the fluid mass balance (mfbal), the energy losses through the shroud (Pshi), the total electric energy input (Pel), two fluid enthalpy differences (dh1, dh2), and the global power balance. Furthermore the hydrogen mass data (mht) at two times are given. If results are within the bounds specified in the last two rows, it was considered to be within the mainstream. Over-predictions were indicated by (++), under-predictions by (--).

Fluid inlet temperature

In the specification report /8/ the inlet temperature was specified by the thermocouple reading of TFS 2/1. Based on our experience with S/R5irs, it was assumed that no or only minor changes were necessary to the inlet temperature. Inlet temperatures varying less than ± 30 K were considered to be in the mainstream, which can be clearly seen in Figure 5.1.

Table 5.1 Check of global data and balances

Partici-pant	*Code*	*Tfg.01*	*mdst9*	*mfbal*	*Pshi*	*Pel*	*dH1*	*dH2*	*Pbal*	*mht*	*mht (end)*
CMX	**SI**	--	++	++	--		++	++	--	**1.32**	**1.68**
DMM	**SI**	--			++					**0.97**	**5.67**
DRS	**IC**									**0.96**	**0.70**
EDF	**MA**								--	**0.86**	**0.77**
ENE	**IC**								++	**1.02**	**1.01**
FRA	**MA**	--							--	**1.08**	**0.98**
GRS	**AT**								++	**1.22**	**1.81**
IJS	**ME**	--	++	++	--	++	--		++	**2.16**	**1.93**
INL	**S3**	--	++	++	++	++		++		**2.83**	**3.27**
ISS	**SI**						--	++	++	**1.31**	**2.63**
NEH	**SI**									**0.83**	**0.77**
NK1	**SI**				--		++	++	--	**2.71**	**3.77**
NK2	**ME**		++	++	--					**1.58**	**1.58**
NUP	**IS**									**0.81**	**0.82**
REZ	**ME**				--		--			**0.75**	**0.70**
RUB	**AT**	--			--			++		**1.01**	**0.93**
SES	**ME**									**0.63**	**0.58**
SIE	**SI**	--			++	++			--	**1.13**	**1.03**
SNL	**ME**									**0.76**	**0.70**
UZA	**SI**									**1.51**	**3.62**
VTT	**GE**	++	--	--	++		--			**2.09**	**1.91**
		± 30 K	*± 10 %*	*± 10 %*	*< 0.5 kW > 6.5 kW*	*< 10 kW*	*< 1 kW > Ptot*	*> Ptot*	*< 0 kW > 4 kW*	*with respect to experiment*	

The tokens for participants and codes are explained in the list of abbreviations

Deviations were observed for DMM and INL whose values decrease constantly with time, and to CMX and IJS whose temperatures drop during first 2000 s to app. 400 K. FRA, RUB, and SIE used lower values, which follow the temperature history of the specified input temperature. The purpose of these deviations is unclear. Except for these participants the fluid temperatures do not vary more than 10 % compared to the experimental value TFS 2/1, so that a rather good adjustment of the input model for the QUENCH facility can be stated.

Maximum bundle temperature

To get a first overview of the results of the blind phase of ISP-45 the maximum temperature in the bundle (Tbp) is shown in Figure 5.2. The values calculated by the participants are compared with the experimental data (legend string TIT A/13; symbol -E-), a thermocouple in a corner rod at 0.95 m, and the results of FZK post-test calculations (fzk; -C-). In the ISP-45 Specification Report /8/ the maximum initial temperature was given in Figure 3.1 to 900 K.

During the pre-oxidation phase the mainstream varies of ± 7 % (± 100 K) around 1450 K. Only a few participants such as NK1 or GRS exceeded this mainstream. The origin of the glitches in the UZA data at 3900 s and 5195 s driving maximum temperature up to 1510 K and 1850 K, respectively, are numerical errors. After 7000 s the width of the mainstream increased so that its definition became useless.

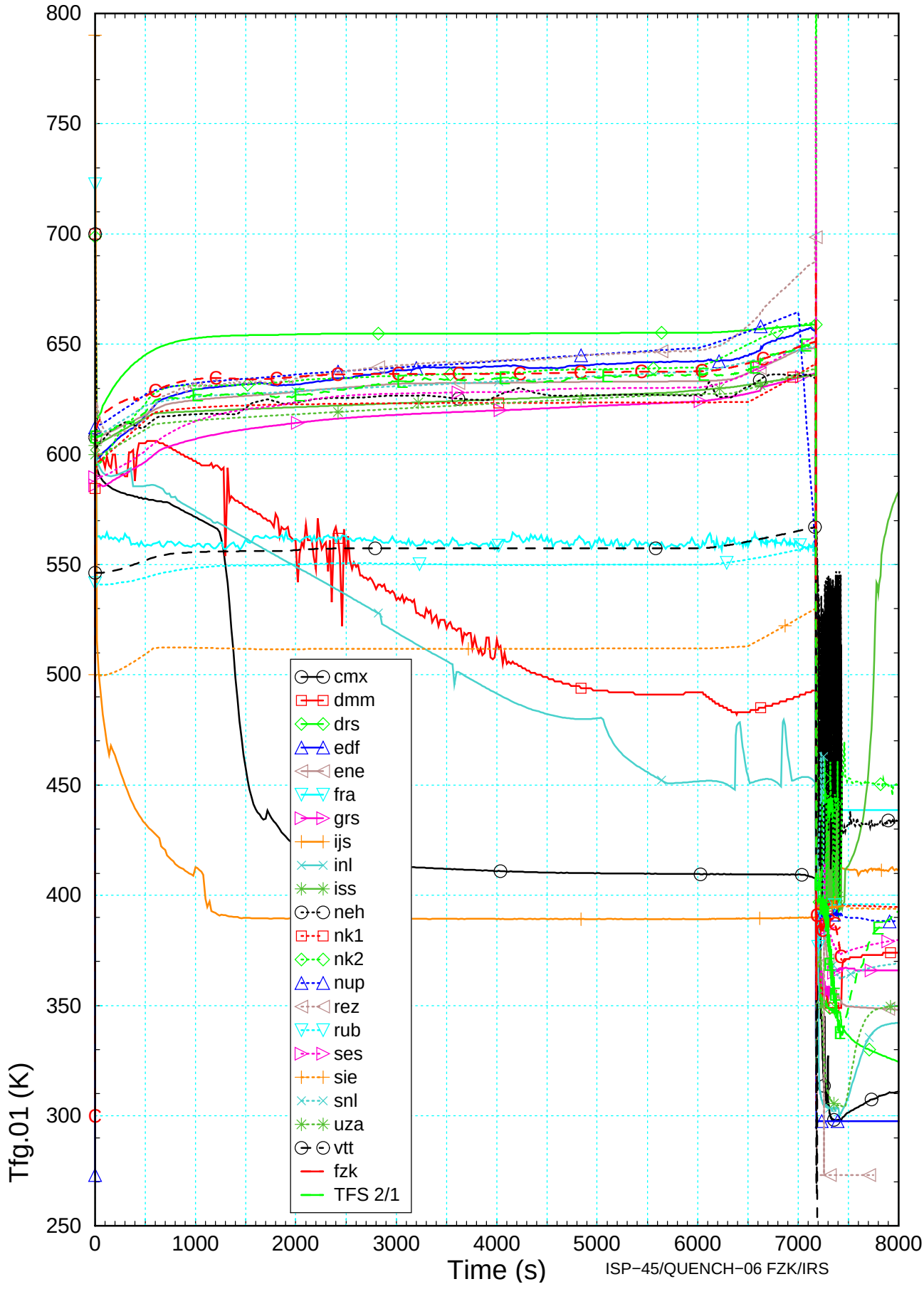

Figure 5.1 Fluid temperature (Tfg.01) at lowest bundle elevation calculated by the participants compared with post-test calculation with S/R5irs (-C-) and delivered fluid temperature derived from TFS 2/1.

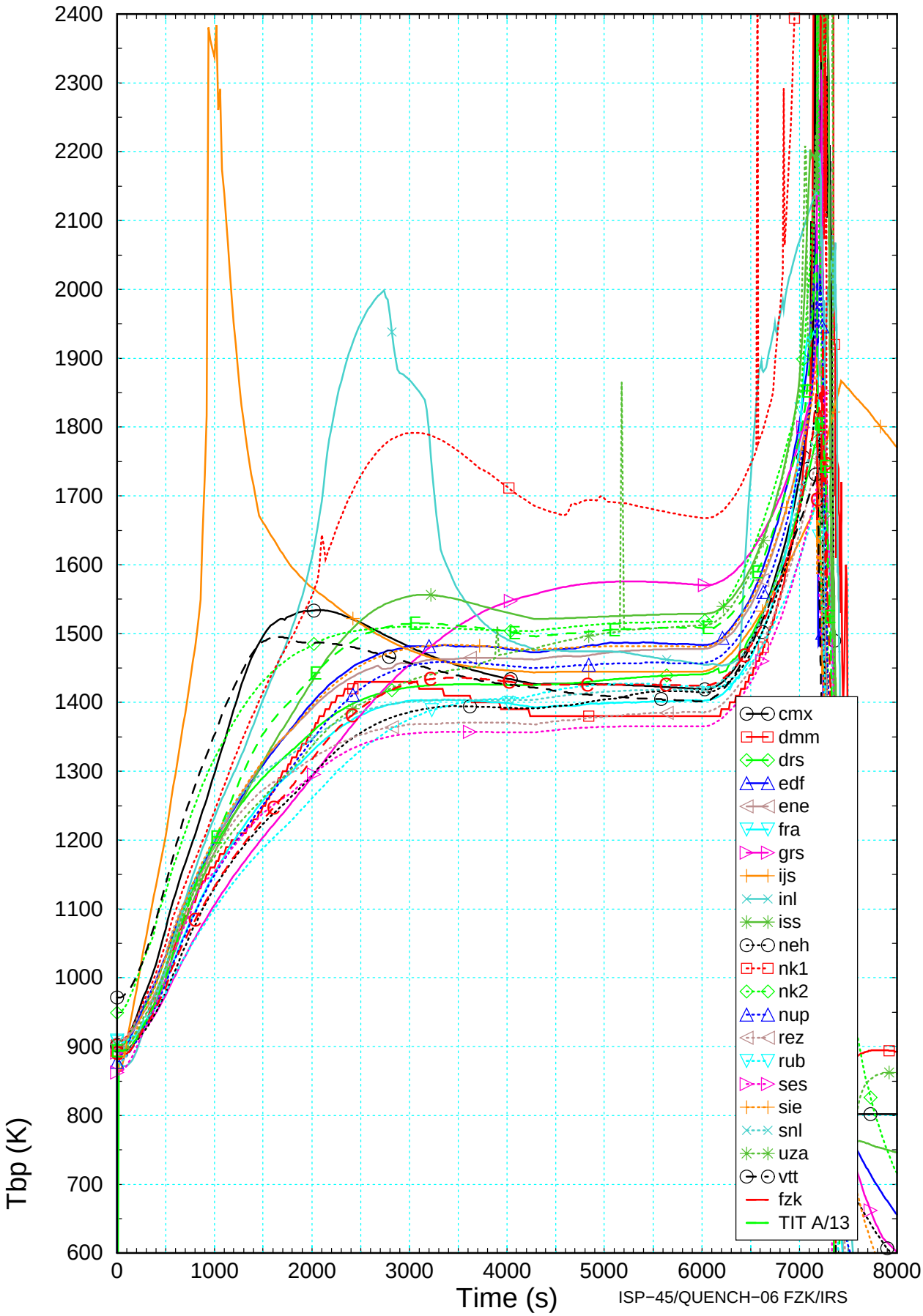

Figure 5.2 Maximum temperature compared to post-test calculations with S/R5irs (-C-), and experimental data using a thermocouple at 0.95 m (TIT A/13, -E-).

Hydrogen mass

The total hydrogen mass is one of the target results of ISP-45. The mass spectrometer data of QUENCH-06 are listed in Table 5.1 and are included in Figure 5.3. They do not include the stored hydrogen, which amounts to additional 3.5 %. The calculated data for the hydrogen source was already shown in /22/ as Poxt, because the exothermal power is strictly proportional to the released hydrogen, but here the magnification is increased so that the spreading becomes more visible.

Generally the temperatures in the test section are too low for significant oxidation before app. 500 s, but not for IJS, where a dramatic increase, starting from the beginning, can be seen. Neglecting the spikes and glitches in Figure 5.3 the spread of the data is very large during first heat-up phase, extending up to 3000 s. Nevertheless, a clear mainstream can be detected which comprises the results of 14 participants. Two others got similar results and 4 participants delivered data that were influenced by either code errors or misinterpreted specification. The initiation of reflood can be seen in the results by very strong variations due to the used shattering models. After 7500 s no hydrogen release was calculated.

Assuming that the Zircaloy oxidation model is implemented correctly, the steep increase in hydrogen release may originate from errors in the energy balance so that the exothermal energy is not released but stored in the cladding leading to the observed temperature excursion. This was attributed to a code error in SCDAPSIM. As discussed before, the Zircaloy oxidation during the steep temperature increase calculated by IJS at 1000 s is caused by uncontrolled oxidation that is only limited by steam starvation at 1064 s. During this short time period nearly all hydrogen is produced. Similar conditions are observed for INL where 0.046 kg hydrogen were calculated up to 3260 s. CMX, NK1, NK2, and VTT also deviate significantly from the experimental data before reflood initiation.

The range of results delivered by the participants is given for four times in Table 5.2. The tendency to over-predict the hydrogen productions is obvious, especially in the quench phase (last column of Table 5.2). The extreme value at 8000 s represents a nearly complete oxidation of the Zircaloy inventory of the bundle.

Table 5.2 Assessment of hydrogen mass and bandwidth at selected times.

Time	**2000 s**	**6000 s**	**7170 s**	**8000 s**
Experiment	4 g	18 g	32 g	36 g
Mainstream Min	2 g -50%	13 g - 30%	20 g - 37%	20 g - 42 %
Mainstream Max	6 g +50%	32 g + 56%	50 g + 67%	134 g + 285 %
Extreme Value	*68 g*	*68 g*	*95 g*	*202 g + 480 %*

The accuracy of the mass spectrometer can be assumed to +/- 5 % (section 2.3).

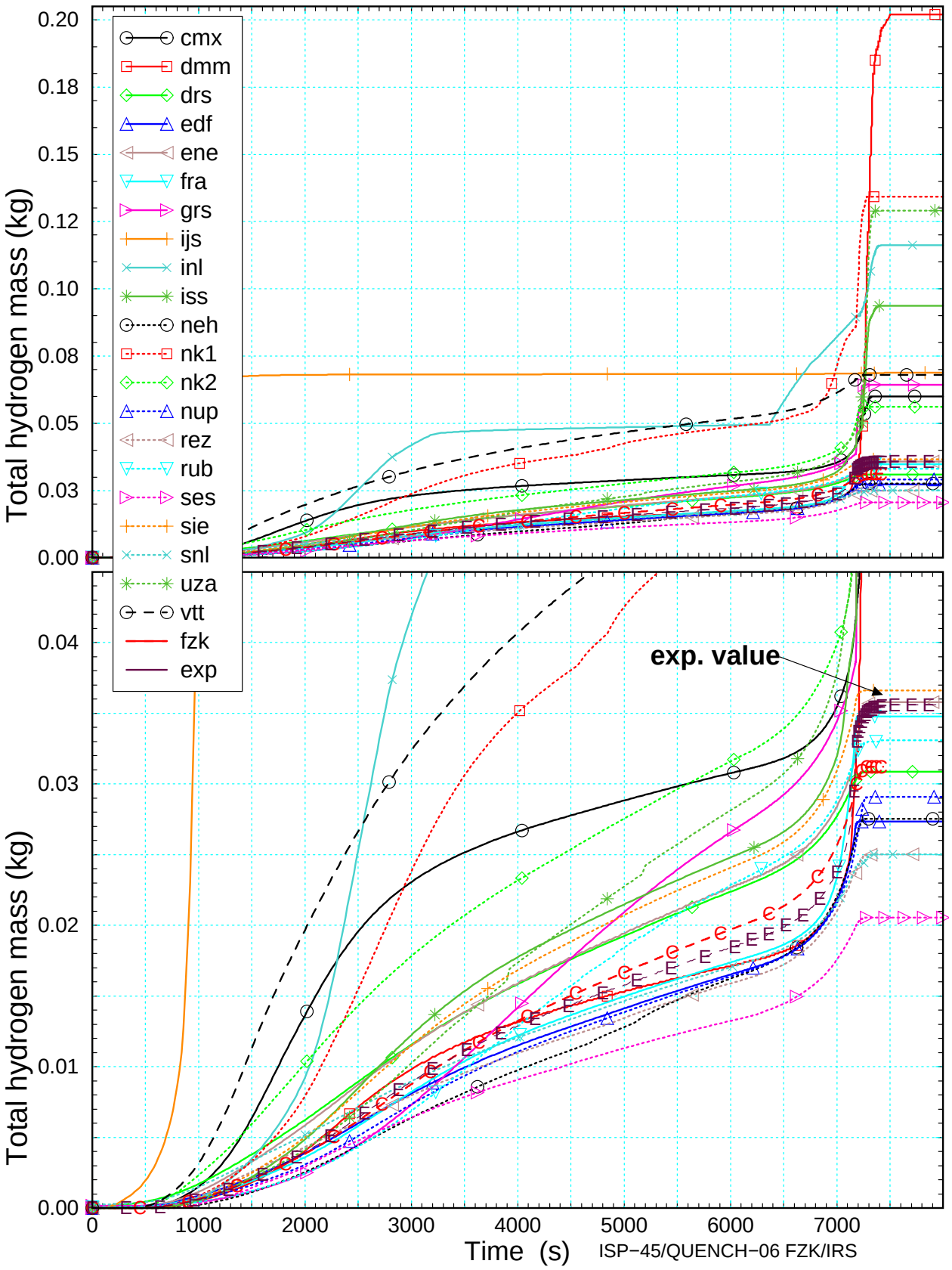

Figure 5.3 Total hydrogen mass calculated compared with measured data (-E-) and post-test calculations with S/R5irs (-C-), top: whole field of participants, and bottom: magnified to show the mainstream.

Fluid mass balances

To check the fluid mass balance in the test section, we used the steam mass flow (mdst9, Figure 5.4) and the hydrogen mass flow rate (mdh9, Figure 5.5) at the bundle outlet to check the mass balance of thermal-hydraulic and oxidation models. In both figures, some strange behavior as strong oscillations or very low hydrogen mass flow can be seen.

If it originates only from oxidation, it should vanish in Figure 5.6, where the steam mass flow at the bundle outlet and the steam consumed due to oxidation are added (variable mbal9). The sum should be equal to the bundle inlet value of about 3 g/s of steam mass flow as specified in /8/. The argon mass flow rate does not need to be considered explicitly, because it should be constant in the bundle. For most of the participants this sum is in fact close to 3 g/s. Two participants delivered the sum of steam and argon mass flow rate at bundle outlet (ISS, NK1) so that the sum is about 6 g/s. Others show a strong drifts (CMX, INL, VTT) during pre-oxidation as discussed earlier. In case of DMM a deviation is observed at app. 2200 s and after 6500 s, indicating mass balance errors caused by steam removal and hydrogen release, probably due to enhanced oxidation. One participant (IJS) calculates very strong oscillations (see Figure 5.4 and Figure 5.6) due to the unintended injection of water into the test section, which causes evaporation and/or condensation problems /21/. The experimental value for mbal9, as derived from measurement with the mass spectrometer, deviates from the steam mass flow rate at bundle inlet due to steam condensation in the off-gas pipe. The condensed water flows to the main steam condenser and is considered in the global water balance.

Fluid enthalpy balances

The heat transferred to the fluid (P_{fluid}) by convection and radiation can be calculated from the given data assuming that all participants used same material properties of steam and argon. The contribution of hydrogen is small, the hydrogen mass flow rate (Figure 5.5) being less than 1 %. Hence P_{fluid} is reduced to H_{diff}, which can be calculated as follows:

$$H_{diff} = \Delta H_{Ar} * \dot{m}_{Ar} + \Delta H_{Steam} * \dot{m}_{Steam} \tag{4.1}$$

with $\Delta H = H_{out} - H_{in}$

H steam or argon enthalpy.

For H_{in} the fluid temperature in the first elevation is used as delivered by the participants (Figure 5.1). At this elevation the fluid inlet temperature is defined in /8/ based on the TFS 2/1 reading and it should be matched by the participants, but evidently is not in all cases. To separate the influences of the uncertainties of facility modeling, especially the modeling of the radiative heat transfer in the upper electrode zone, two fluid enthalpy balance were established, one for the whole bundle, H_diff1 (Figure 5.8, top), using the variable Tfg9 (Figure 5.7) to calculate H_{out}, and one for the heated part of the test section, H_diff2 (Figure 5.8, bottom), using Tfg.13 instead of Tfg9.

Figure 5.4 Steam mass flow rate (mdst9) at the bundle outlet calculated by participants and by FZK post-test analyses.

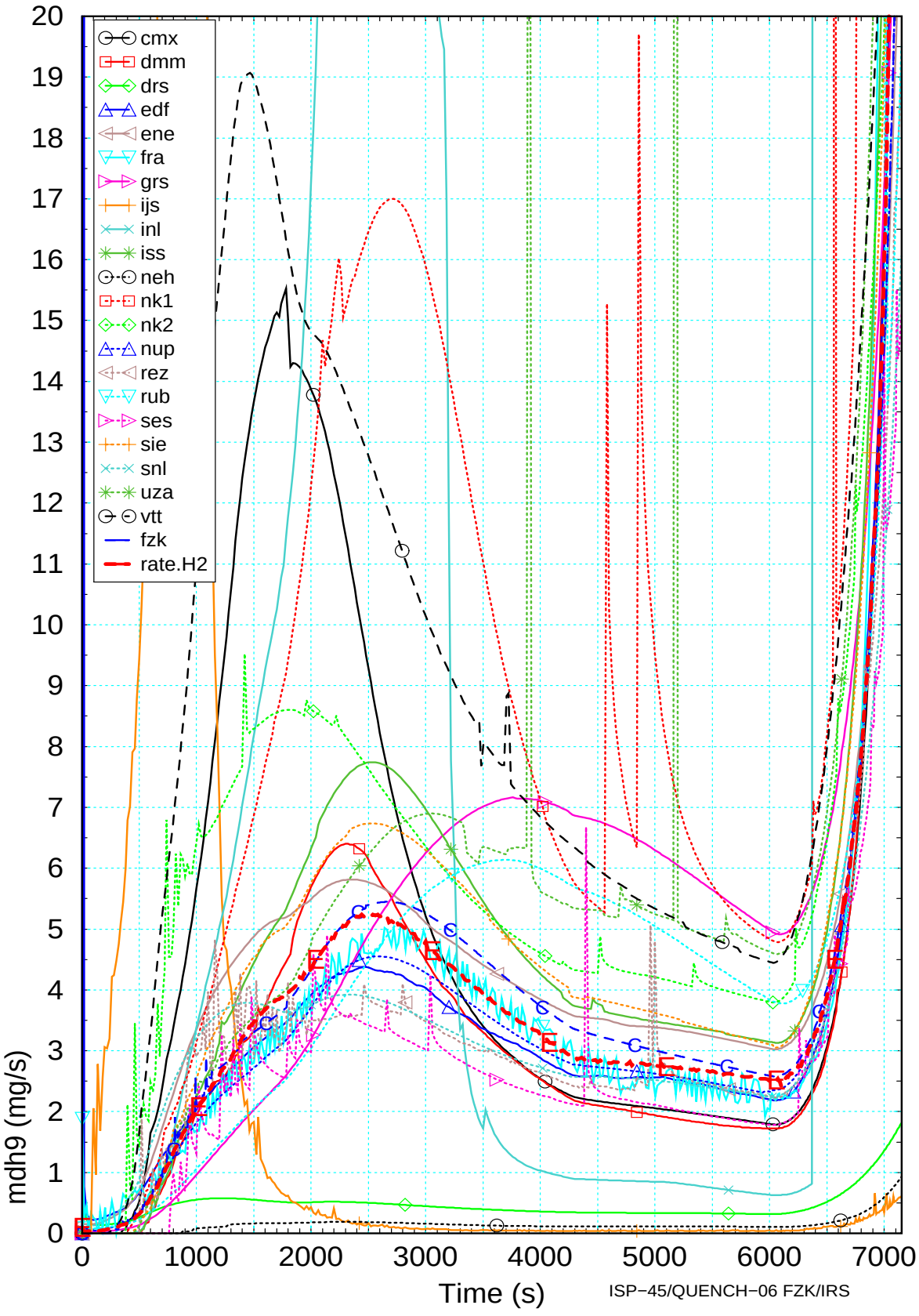

Figure 5.5 Hydrogen source term at bundle outlet (mdh9) calculated by the participants and compared with measured data from experiment (-E-) and post-test calculations with S/R5irs (-C-).

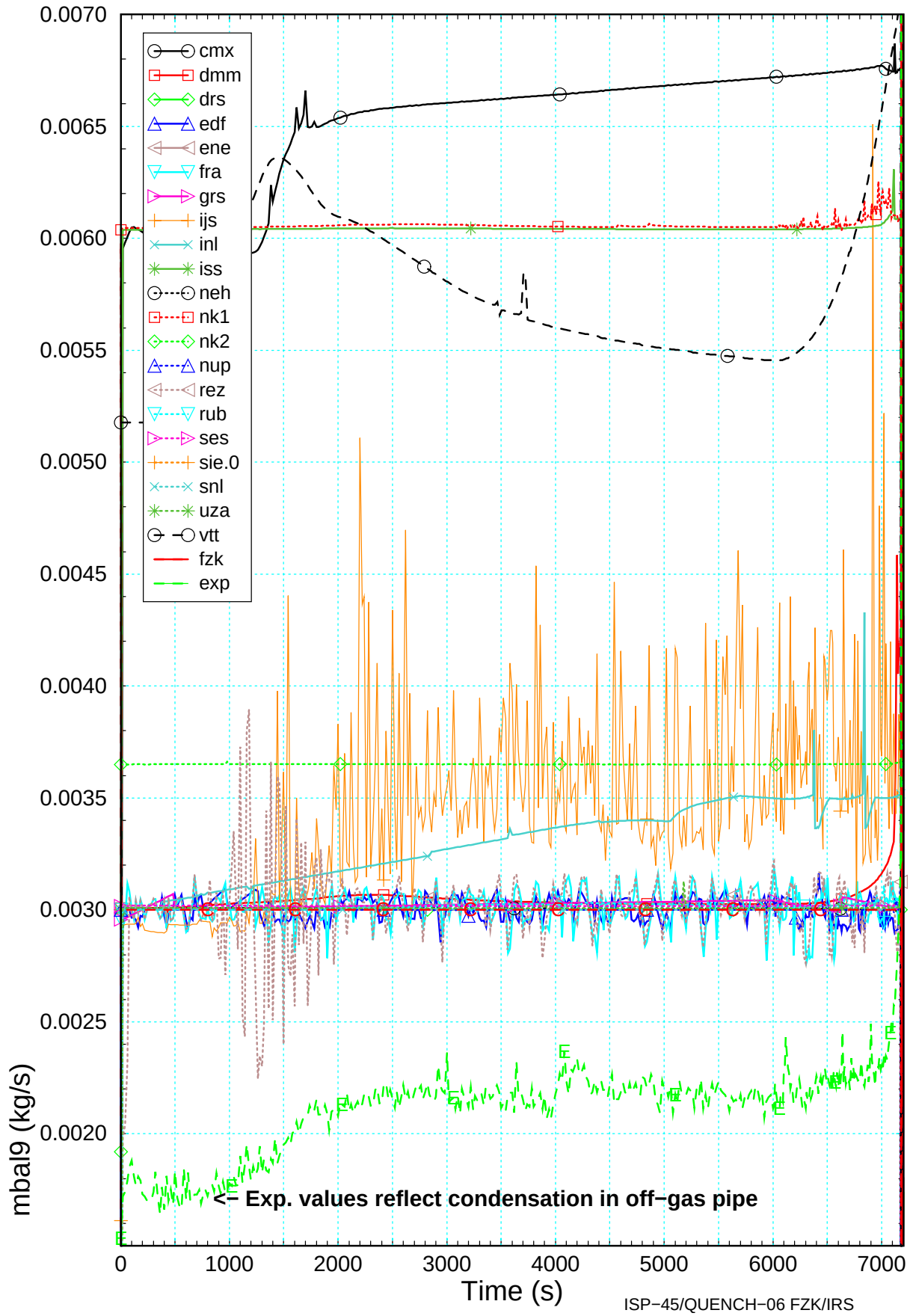

Figure 5.6 Fluid mass balance (mdst9 + 9*mdh9) compared with measured data from experiment (-E-) and post-test calculations with S/R5irs (-C-).

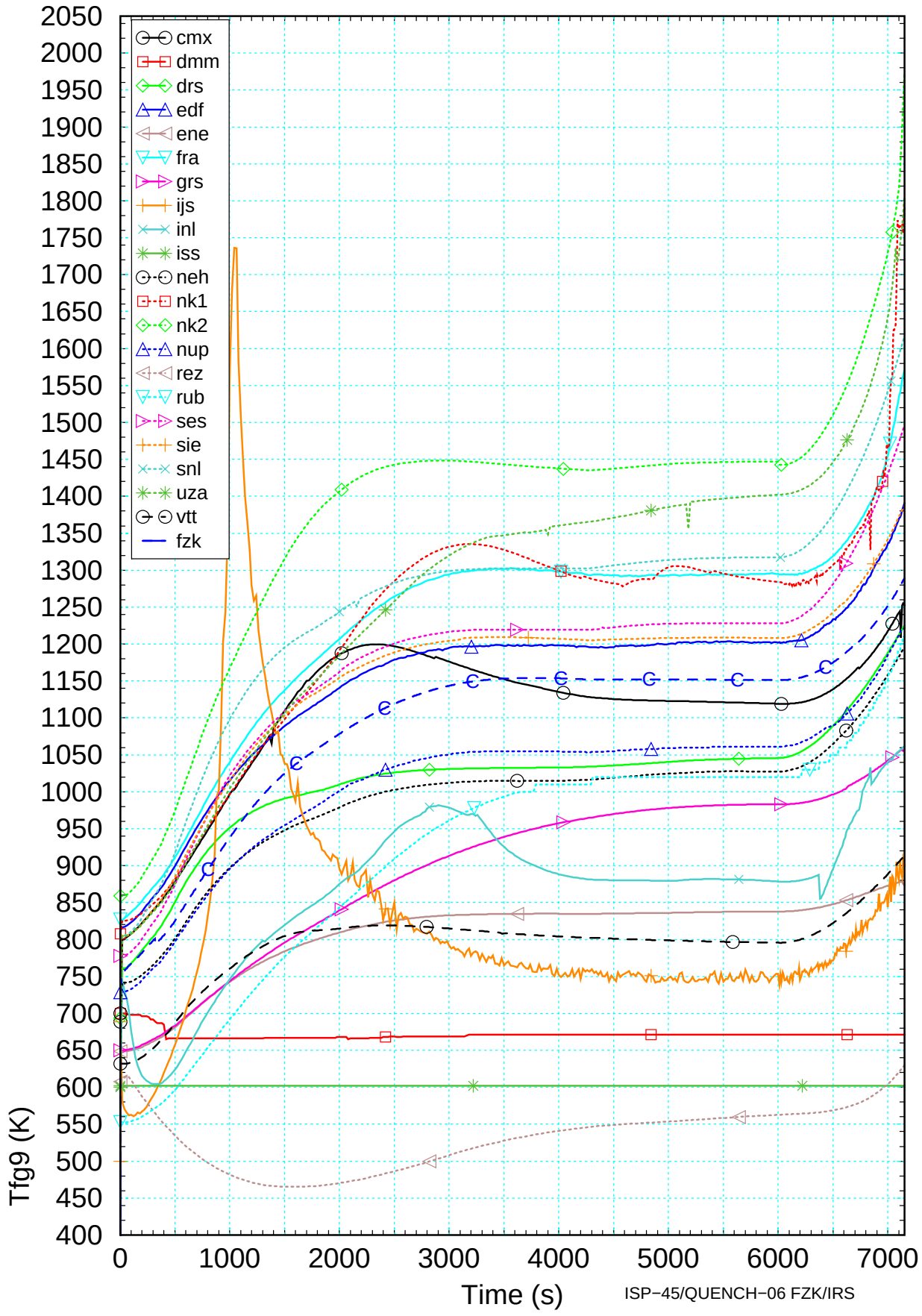

Figure 5.7 Fluid temperature at the bundle outlet (Tfg9) compared to FZK post-test analyses.

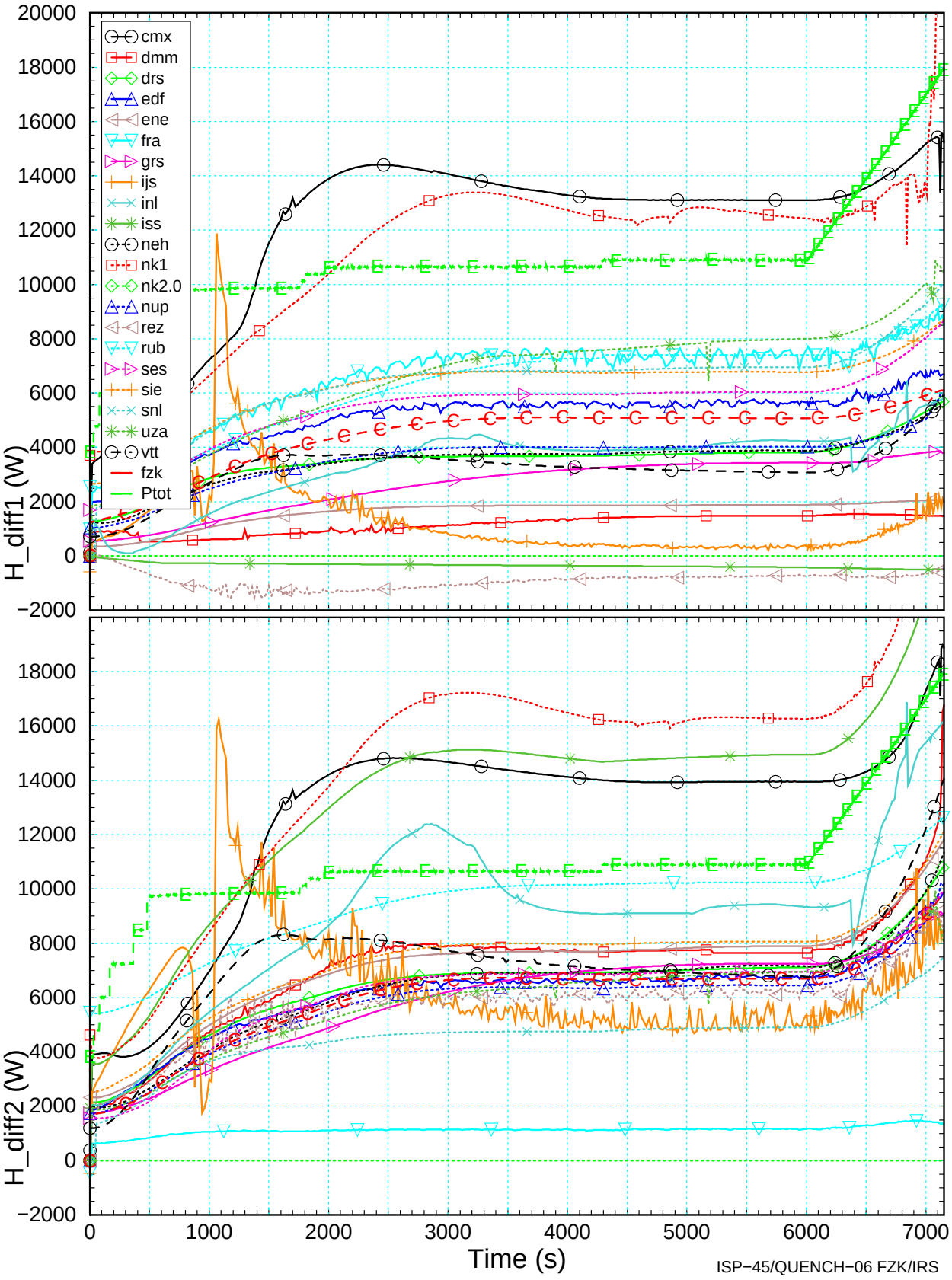

Figure 5.8 Fluid enthalpy balance for the whole bundle (top) and one for the heated part of the test section (bottom).

A comparison between both graphics of Figure 5.8 revealed that the spreading of the results is significantly reduced if the upper electrode zone is excluded. This indicates that a non-negligible part of the uncertainty is introduced by a facility effect, the radiative heat transfer in the annular

shroud gap (Table 5.1). Other uncertainties arise due to different axial positions where the outlet temperature was calculated, since some participants included parts of the off-gas-pipe.

Energy balances

The list of the global data allows to check the energy balance for the bundle between levels 1 and 16 and so to assess the achieved quality and the reliability of the simulations. For comparison purpose a coarse energy balance can be described by:

$$P_{elt} + P_{oxt} - P_{axt} - P_{shi} - H_{diff} - P_{store} = P_{res} \qquad (4.2)$$

with $P_{elt} = P_{el6} + P_{elb} + P_{el7}$

The energy source P_{elt} (Figure 5.9, sum of P_{el6} (lower electrode), P_{elb} (bundle), and P_{el7} (upper electrode, /22/) is the total electric energy released in the test section. The other energy source, the exothermal power P_{oxt}, amounts to only app. 700 W during pre-oxidation phase.

The energy sinks are given by P_{shi} (radial heat losses through shroud), P_{axt}, P_{fluid}, and P_{store}. P_{axt} is the axial heat loss due to heat conduction in the molybdenum and copper electrodes of the heater rods assessed by one-dimensional heat conduction calculation. Contribution of heat conduction in ZrO_2 pellets or in the Zry cladding can be neglected. P_{store} characterizes the increase of inner energy of fluid and structures in case of heat-up. P_{res} should be zero for a perfect calculation.

Based on these equations, a coarse power balance was performed for all participants and summarized in Figure 5.10. Since the axial nodalization varies between participants, influencing the axial heat flux to water-cooled ends, heat losses due to axial heat conduction in the electrodes were not considered. From our experience these heat losses sum up to app. 2000 W for both, the upper and the lower connections of the heater rod molybdenum wires to the water-cooled ends. Also, this sink term is rather stationary as demonstrated in /22/, because the axial boundary temperatures do not vary strongly during test. Even during final heat-up phase, this term increases by 20 % only. For a more detailed analysis the variation of the local temperatures in the bundle due to oxidation or convective cooling should be considered, too. But this is beyond schedule.

The main part of the difference in the power balance is attributed to the storage term, P_{store}. In the fast heat-up phase, this term deviates significantly, whereas during the pre-oxidation phase the value decreases to the error level of this coarse energy balance since the temperatures in the bundle are no strictly stationary. P_{store} amounts to app. 500 W (app. 6 % of the total energy source), which is in the range of the oxidation power P_{oxt} during pre-oxidation phase.

As shown in Table 5.1 the definition of the mainstream concerning Pbal is oriented at the experimental value at 6000 s (app. 2 kW), allowing a span of 100 %. Nevertheless, only a few participants are in the mainstream as can be seen in Figure 5.10. The most probably reasons may be difficulties to simulated QUENCH peculiarities such as heater rod or shroud, and/or overestimated Zircaloy oxidation. Also early melt relocation may have contributed in two cases to the observed spreading in the energy / power balance.

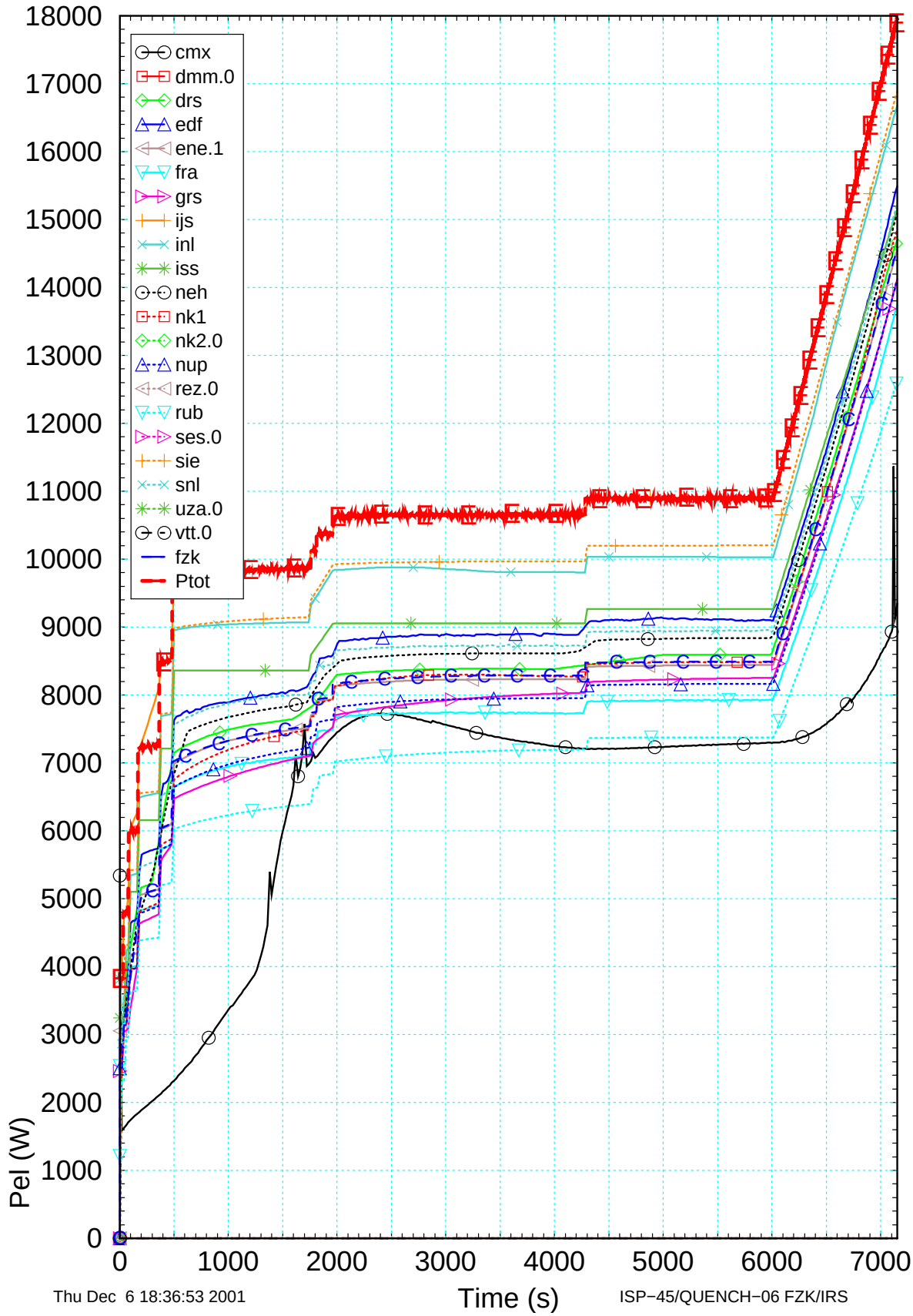

Figure 5.9 Total electrical power released in the whole test section compared to FZK posttest analyses (-C-) and the measured total electrical power (-E-).

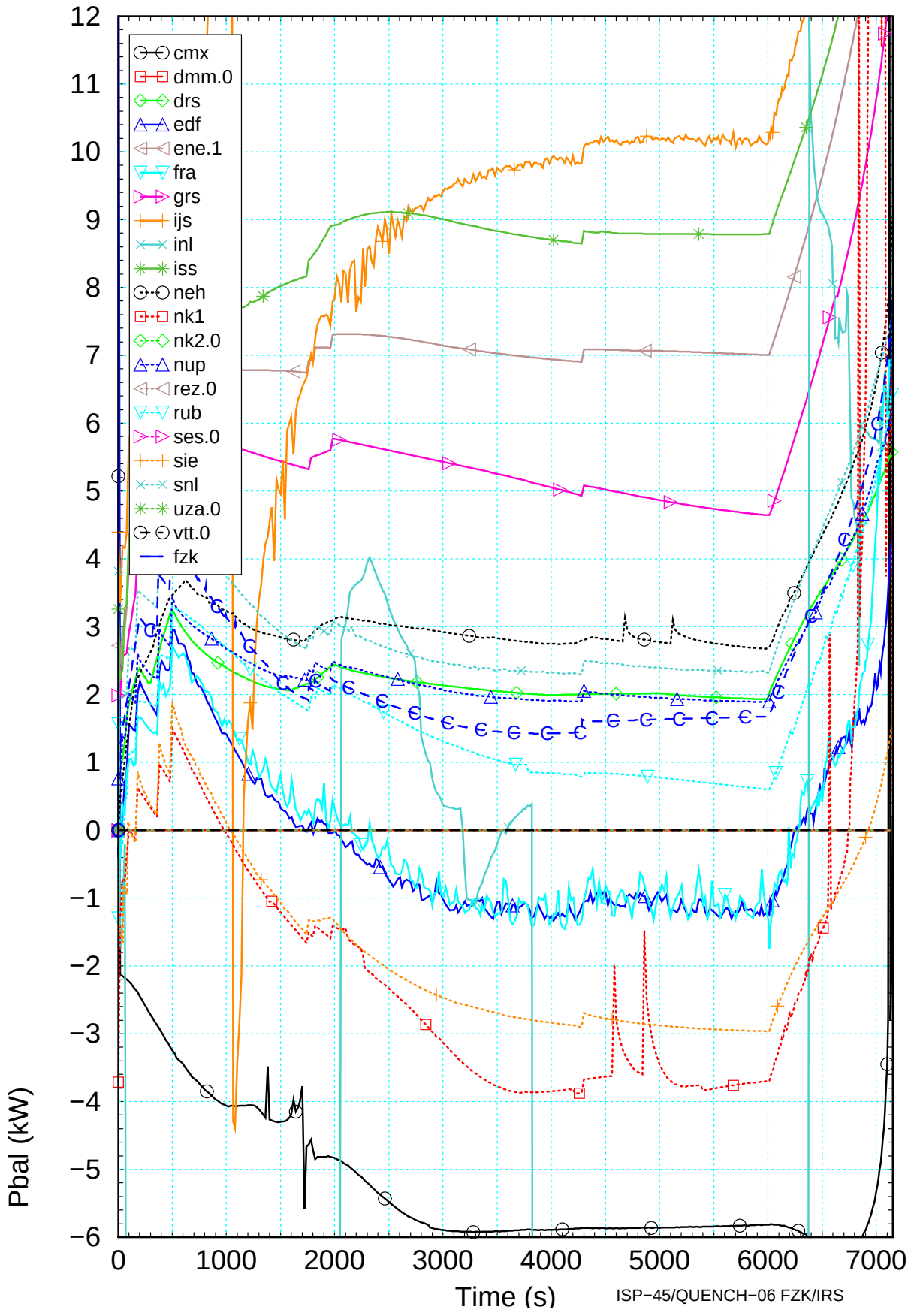

Figure 5.10 Power balance derived from data delivered by the participants without consideration of axial heat losses in the electrodes compared to FZK post-test results (-C-).

5.1.2 Bundle state prior to reflood

While the FZKA-6677 /22/ includes all relevant axial profiles at 6000 s, at 6620 s when the corner rod was withdrawn (Figure 5.11), and at 7170 s, this section is restricted to the specification of the bundle state at 7170 s. In the time interval of 550 s between the corner rod withdrawal and the reflood initiation, electrical power and exothermal heat of the cladding oxidation drive the temperature at 0.75 m up to 2000 K just before reflood with a heat-up rate of more than 2.0 K/s as can be depicted from Figure 5.2.

The average axial temperature gradient amounts to 950 K/m in the lower half of the heated zone and more than 2000 K/m in the upper third, due to the temperature escalation. These values can be compared to calculated axial profiles for reactor conditions, which are around 800 K/m. In the lower half the radial temperature spreading is nearly maintained as before, whereas above 0.7 m values up to 200 K are measured. In the upper electrode zone that variation is even more than 500 K. These experimental conditions increase the scatter of the calculations considerably.

At the time of reflood initiation, which will be discussed in section 5.2, the experimental temperatures up to mid of the bundle correspond to design basis accident (DBA) conditions. At reflood initiation the following situation is found: at 0.0 m the wall superheat is app. 300 K, in the center of the bundle app. 900 K, and in the hottest position app. 1600 K. Based on the temperature level, which is below the melting temperature of oxygen stabilized α-Zr(O), and the stability of slowly grown ZrO_2 scales the fuel rod claddings should still be intact, which is confirmed by inner fuel rod pressure measurements /7/.

Temperature

In Figure 5.12 the minimum and maximum measured temperatures at a given elevation are shown, indicating that in the experiment the lateral temperature profile is rather flat below 1.0 m, but radial temperature differences increase in the upper electrode zone, mainly due to the increased radiative heat flux in radial direction.

In the calculations deviations to the experiment increase after the experimentally detected temperature excursion (app. 7000 s), mainly due to the more or less abrupt change between the low and high temperature oxidation correlations used in the codes. The related sudden increase in the heat release of the exothermal Zircaloy/steam reaction at the switch temperature may cause energy balance problems, because the heat removal by radiation and convection require some time. Besides the shroud insulation heats up markedly. For the time scale relevant in this context conduction through the shroud and the insulation are not increased noticeably. Therefore two effects determine the bundle heat-up rate, the local heat generation and the behavior of shroud insulation both of which are difficult to model.

All participants delivered results within a band of -200 K and +100 K around the experimental data, except for CMX, who underestimates the axial temperature profile by app. 300 K and VTT due to the lacking heater rod model (see below) and an error in the modeling of the Urbanic-Heidrick oxidation correlation (Figure 5.14). With the onset of escalation above 0.8 m the deviation increases because the calculated temperature rise is delayed with respect to measured one. In the upper electrode zone the difficulties of the participants to simulate adequately the radiative heat transfer in the shroud spreads that band to app. 1000 K.

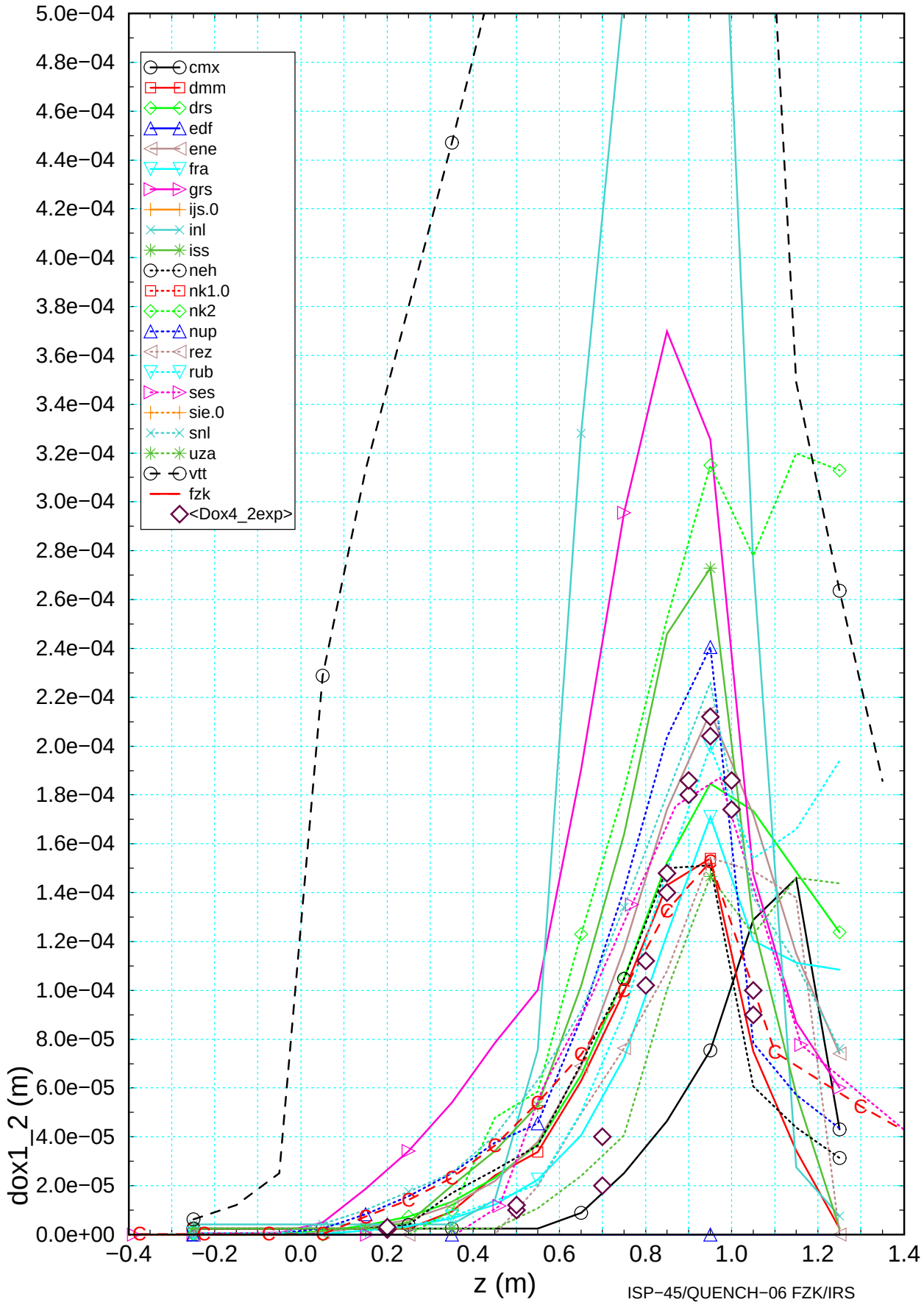

Figure 5.11 Axial oxide layer profile at t=6620 s compared to experimental minimum and maximum values (diamonds) and the results of FZK post-test calculations.

DMM calculated the largest axial temperature difference of 1700 K, from 550 K at –0.25 m to 2250 K at 0.95 m leading to an axial temperature gradient of app. 1400 K/m. This is somewhat higher than the experimental gradient, but in the range of axial gradients calculated for reactor conditions. The NK1 and NK2 calculations show very high temperatures in the upper electrode zone indicating either overestimated shroud insulation or lacking axial heat conduction in the heater rods to the water-cooled ends. The axial temperature profiles of NK1 and UZA show rather cold lower ends, whereas the very high peak temperature is produced. In essence the temperature at 1.35 m varies from 950 K (ISS) to 2120 K (NK2). The temperature history is discussed in detail in /22/.

Axial power distribution

Exothermal heat increases the local rod temperature and hence the electrical resistance of the tungsten wire, which in turn increases the local heating power (Figure 5.13). Below 0.5 m nearly all participants forming the mainstream are close together, the scatter is only 1800 W/m (10 % of maximum value). However, in the upper third the values spread, also enforced by power redistribution.

The strong deviations observed for VTT originate from the lack of an electrical heater rod model in the GENFLO code. After code improvement, the axial power distribution could be simulated adequately (see appendix).

Oxide layer thickness

Unfortunately no experimental data are available at 7170 s, so that a reliable description of the pre-reflood situation may rely on the data of the corner rod extracted 550 s earlier (Figure 5.11). However, when a temperature escalation is calculated, this time interval may lead to more a difference of than 1000 K. In Figure 5.11 the range of the experimental data is indicated as measured in each elevation. The variation indicates the minimum and maximum value obtained for a given elevation during post-test analysis /7/ reflecting an experimental uncertainties of app. 5 %.

Based on post-test calculations with Russian mechanistic SVECHA code /17/ which uses the measured temperature and oxide scales measured at the corner rod at 6620 s as input conditions a supporting axial oxide layer profile is estimated and used for comparison at 7170 s (Figure 5.14). A SVECHA calculation starts from the beginning to check the influence of the axial oxide profile of the corner rod.

Figure 5.11 (6620 s) and Figure 5.14 (7170 s) show that the participants significantly overestimated the low temperature oxidation, which occurred below 0.4 m, due to the conservative approach realized in the oxidation models. The curves in Figure 5.14 form a mainstream with a bandwidth of app. 200 µm that increases to app. 250 µm in the hot spot. CMX underestimated the oxide layer thickness, probably due to the lower temperatures (Figure 5.12), whereas INL and VTT delivered overestimated results. GRS also overestimated the oxidation and calculated a peak value of app. 480 µm 0.1 m below the peak value position of the main stream and the post-test analyses. NK1, NK2, and RUB calculated rather high oxide layers at 1.25 m bundle elevation, depending on the local temperature there.

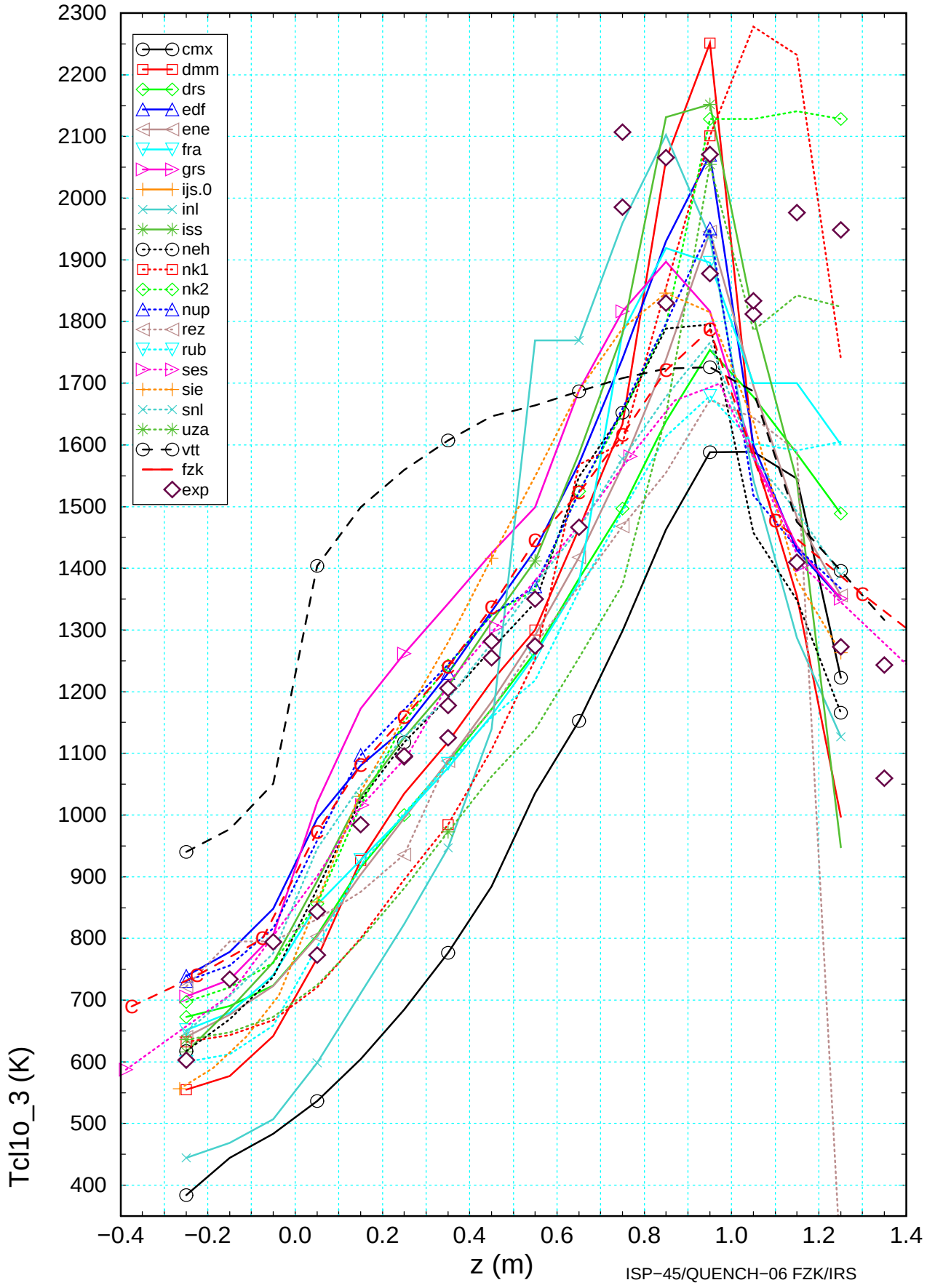

Figure 5.12 Axial surface temperature profile of the unheated fuel rod at t=7170 s compared to measurements and results of FZK post-test calculations (-C-).

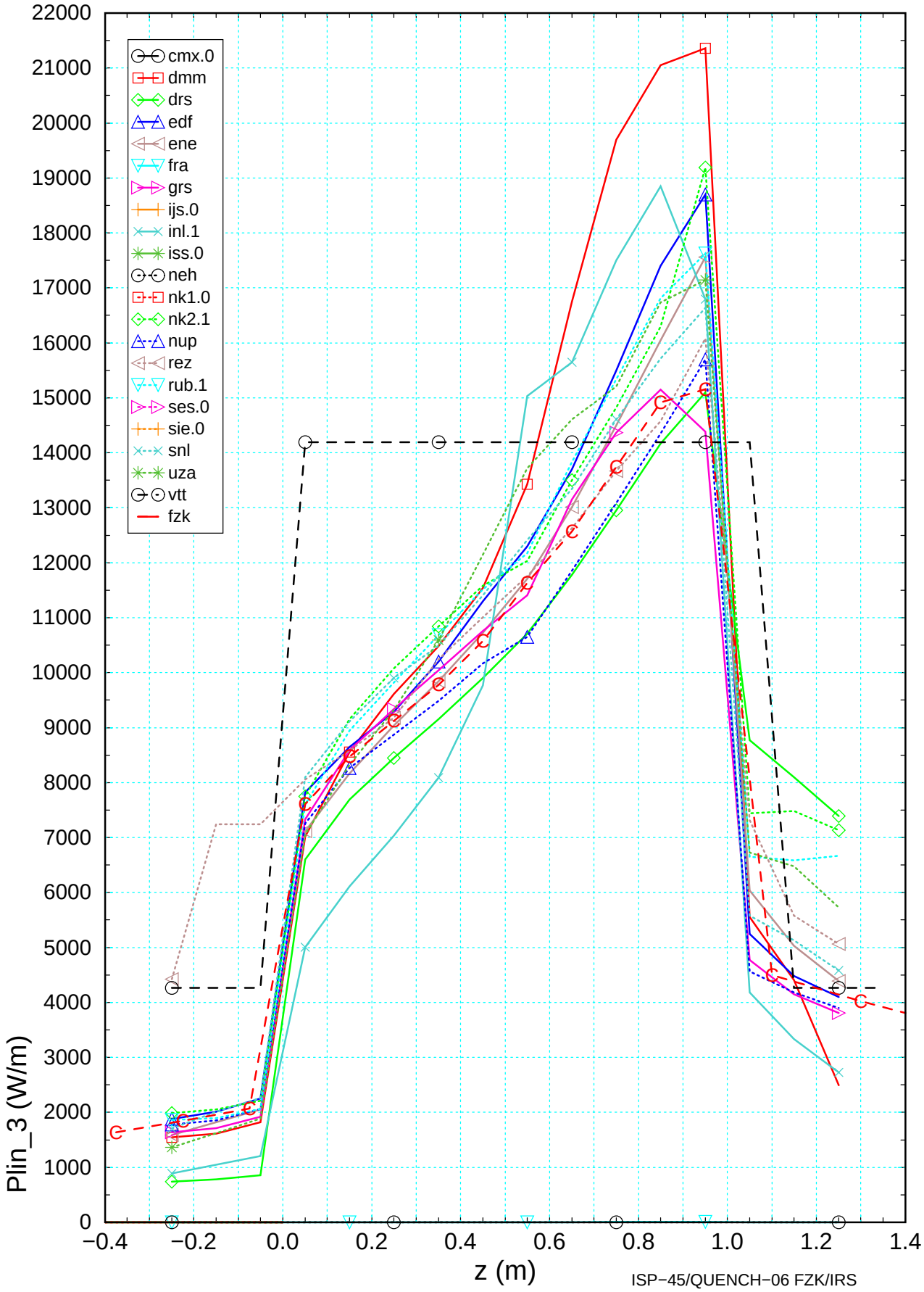

Figure 5.13 Axial power profile at t=7170 s compared to experimental results (-E-) and the results of FZK post-test calculations (-C-).

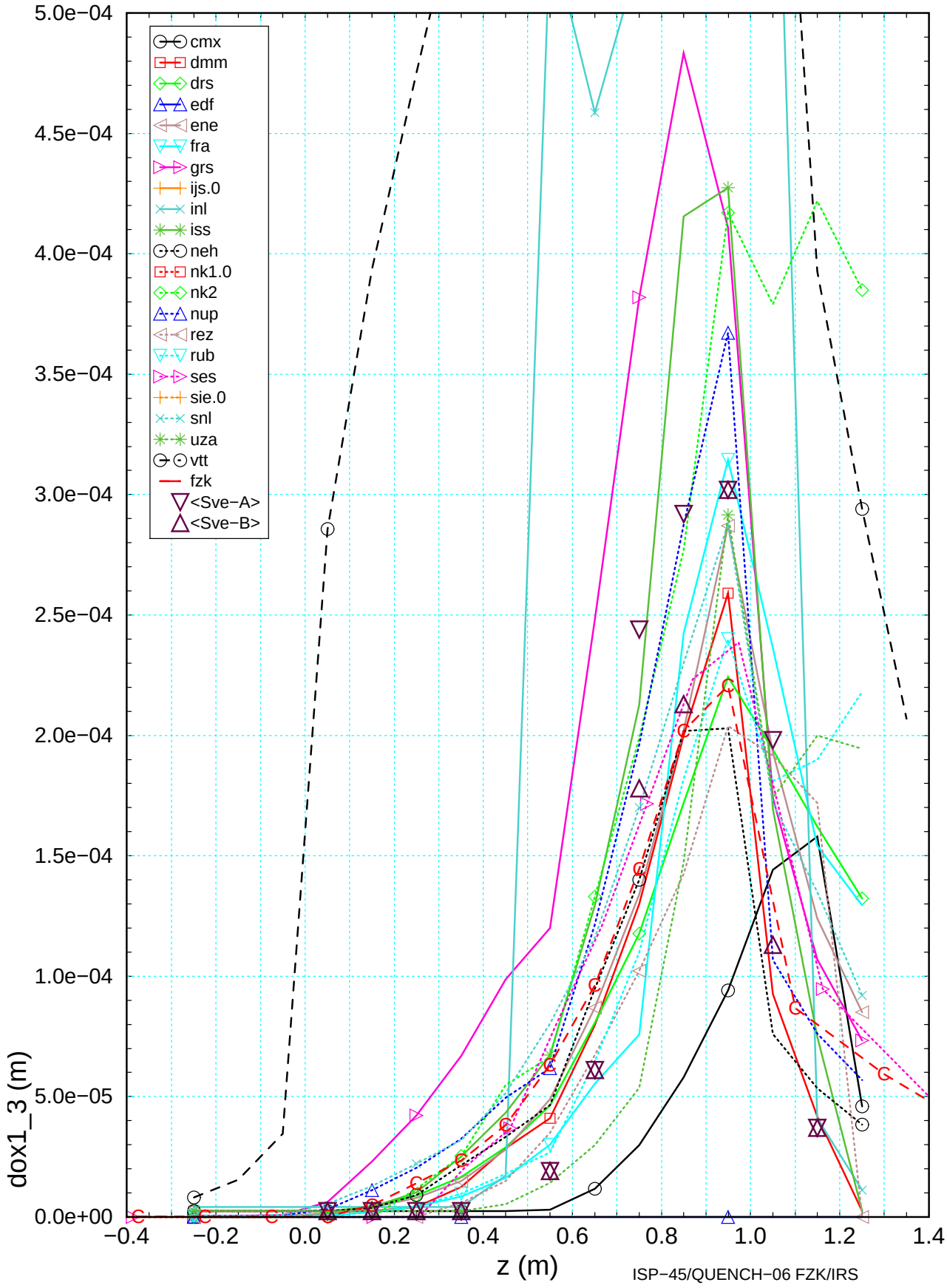

Figure 5.14 Axial oxide layer profile at t=7170 s compared to experimental based calculations using SVECHA (diamonds) and the results of FZK post-test calculations.

Net flow area

In the QUENCH Program two tests (QUENCH-02 and QUENCH-03, /3/) showed significant bundle degradation due to high temperature, however, main bundle damage was initiated prior to reflood initiation. From the post-test examination of QUENCH-06 /7/ no significant bundle damage is found as described in section 3.3 and in detail in /7/. SES calculated the flow area to be constant throughout the transient.

The fluid flow area data of DRS, REZ, and FRA deviate from specified geometry of the intact bundle. EDF, ENE, ISS, NK1, NK2, RUB, SIE, SNL, and VTT delivered no sufficient information.

From the various data (af, mzry, mzro, etc.) versus time, an overview was extracted as shown in Table 5.3. In the first column the axial node indicates at which elevation the participants calculated fuel rod or shroud damage. Next the assumed or identified phenomena are given together with the token of the participant who calculated the damage. In the last column a brief attempt was made to explain and to quantify the calculated results. From A_f slope an identification of the basic mechanism is feasible (ballooning, melt relocation). Generally all participants calculated the QUENCH facility to remain intact. All participants calculated the lower zones to remain more or less intact. The results of IJS are excluded from the discussion, because melt relocation and release down to 0.15 m at 1000 s were calculated.

Clad failure

In the experiment fuel rod cladding failure was detected at the onset of reflood at 7179 s (section 3), mainly caused by thermal shock. One second later the shroud failed, too. This quantity was not asked by the participants due to difficulties in modeling the small plena and the rather large volumes of the fuel rod pressure system, which remains at room temperature level. However, the participants were asked to explain the position and type of clad failure calculated by their code (section 4.6 in /8/). Some participants mentioned that they had to reduce the inner rod pressure to avoid early clad failure as observed in early S/R5irs calculations. SES calculated the bundle and the shroud to be intact throughout the transient.

In all codes participating in ISP-45 the clad failure was calculated from user defined parameters such as local cladding temperature and oxide layer thickness, bounding physical phenomena. The temperature value range is reasonable between 2200 K and 2500 K, compared to earlier ISPs (ISP-31).

Melt formation and release

Nevertheless some participants calculated temperatures high enough to produce clad failure with subsequent melt release and relocation. In some cases blockages at the upper most elevation was observed, probably due to code error. The melt accumulates in the 15^{th} and 16^{th} axial zone (CMX, IJS, NEH, UZA).

No direct experimental information is available for the bundle state prior to reflood. As mentioned in section 3.3 no significant blockage formation was found in QUENCH-06 after the test, so that this holds true for the bundle state prior to reflood. For those participants who calculated blockages the results are summarized in Table 5.3 indicating time and axial location of calculated debris formation and other identified phenomena.

Table 5.3 Overview of local effects derived from participant's time dependant data

#	Effect	Participant	Remark
16	melting ballooning ?	IJS NEH, UZA FRA	assumed ZrO_2 pellets nearly all melted at 1000 s NEH: 1500s-2500s and UZA: 3000 s - 3500 s small unexpected increase of Af
15	melting ballooning ?	IJS CMX,NEH,UZA FRA	assumed ZrO_2 pellets nearly all melted at 1000 s ballooning between 1000 s and 3500 s small unexpected increase of Af
14	melting ballooning	IJS CMX, UZA, DMM, FZK FRA	assumed ZrO_2 pellets completely melted at 1000 s 10 - 20 % ballooning < 5% ballooning small unexpected increase of Af
13	ballooning	DMM, FZK, CMX,NEH,UZA	up to 20 % up to 10 %
12	blockage ballooning	IJS CMX, NEH, UZA DMM	intermediate blockage at 1000 s + subseq. relocation 5 % reduction between 1000 s and 1500 s (and 3500 s) 20 % reduction between 1000 s and 1500 s
11	ballooning blockage ?	DMM, CMX, NEH, FZK, UZA FRA IJS	nearly all participants up to 15 % (1000 s to 3000 s) 20 % at 7200 s blockage formation plus subsequent re-melting
10	blockage ballooning	IJS CMX, UZA	50 % blockage at 1000s 5 % reduction between 1000s and 1500s (3000s)
9	blockage ballooning ?	IJS DMM,NEH,FZK CMX, UZA	40 % blockage at 1000s ballooning between 1000s and 3500s ballooning with subsequent clad relocation ? unclear
8	blockage ballooning	IJS CMX, UZA,NEH, FZK, DMM	50 % blockage at 1000s 5 % reduction between 1000s and 1500s (3000s)
7	blockage ballooning	IJS CMX, UZA	20 % blockage at 1000s 5 % reduction between 1000s and 1500s (3000s)
6	blockage	IJS	12 % blockage at 1000s
5	blockage	IJS	8 % blockage at 1000s
4	blockage spacer ?	IJS IJS, NEH, DMM, REZ, FRA	first blockage at 1000s initial value 0.0024 m² initial value 0.0026 m²
3	Blockage	FRA	slight blockage at 7200s
2	-		intact bundle: no variation of Af
1	-		intact bundle: no variation of Af

Please note: No data available from EDF, ENE, ISS, NK1, NK2, RUB, SIE, SNL, and VTT. In the experiment Zircaloy spacers are located in axial zone 9,14, and 16, the Inconel spacer is located in level 4.

5.2 Reflood phase

The main objective of the test ISP45 (QUENCH 06) was to investigate the behavior on reflood and hydrogen release. Therefore, as an extension to the FZKA-6677 report /22/, which analyses in detail the code predictions at several elevations, the reflood process will be analyzed in detail focused on code capabilities.

First, the cool-down behavior is explained based on temperatures history at a representative elevation in the next section, a discussion of water level behavior and quench front movement follows (section 5.2.2). The hydrogen source term and total mass is given in section 5.3 which is necessary for comparison with the results of the open calculations.

5.2.1 Reflood progression

Conditions at reflood initiation are described in section 5.1.2, water injection conditions were explained in specification report /8/, as well as in /22/. The measured data for water levels and quench front movement in the reflood phase are given in section 3.2.

Generally, all participants calculated the reflood phase. It was assumed that all participants used the same quench water mass flow rate as specified in /8/. The data were assessed and qualified considering the participants' statements and removing erroneous data from further discussion /22/. Inspection of the various data showed that a clear mainstream formed by 10 participants can be seen in the vicinity of the experimental results. For the overall flooding rate, however, this mainstream appears to slightly overestimate experimental data.

As a first result the collapsed water level is compared to the experimental results (Figure 5.15). They include the wetting of thermocouples (TFS at fuel rod cladding outer surface and TSH at shroud inner surface) and the differential pressure sensor (Lm 501 averaged; diamond). Though they indicate different physical quantities, they are used to generate an experimental range of uncertainty for the accuracy of the calculated water levels. The indications from the TFS are used as an uppermost limit for droplet flow and those of the TSH as a lower limit for nearly pure liquid flow.

The scatter band including the remaining participants starts in the lower section of the heated region with rather a small uncertainty of app. 0.3 m, but it spreads to app. 0.7 m in the hot spot (above 0.5 m Figure 5.15). This may partly be explained by different evaporation rates due to different rod temperatures prior to reflood initiation.

It should be mentioned that some curves show strong oscillations that originate from two-phase flow near the pure liquid region. Possible reasons may be too large axial nodes or oscillations in the heat flux and hence boiling rates due to changes between different heat transfer regimes.

Since the temperature history during reflood was discussed extensively in /22/, this report illustrates the different behavior of the codes at one selected elevation (0.75 m) only as shown in Figure 5.16. This figure is representative for results calculated between 0.35 m and 1.25 m in the bundle. The maximum cladding temperature (Tbp) is not appropriate for this purpose because its position may vary due to different cool-down behaviors.

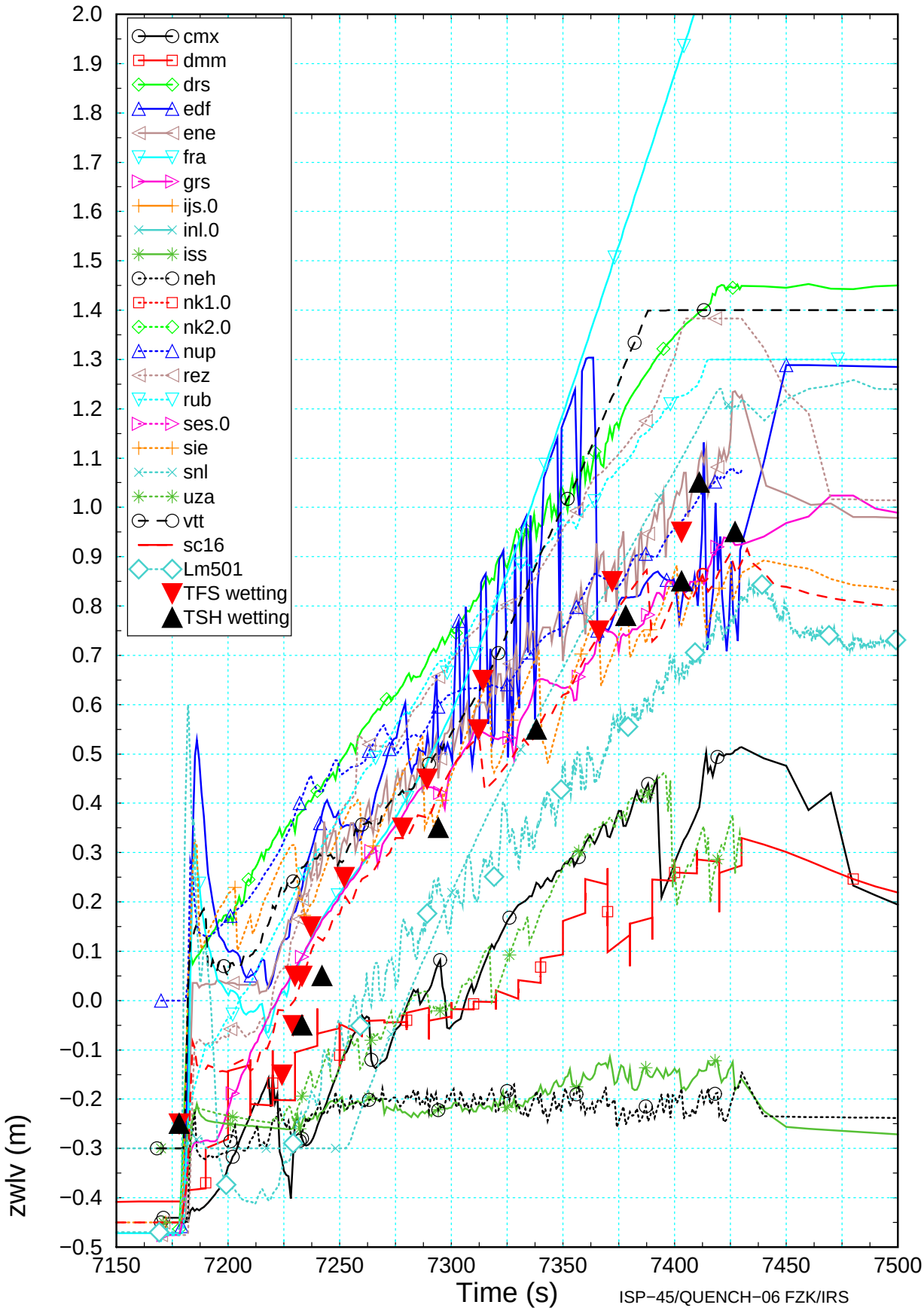

Figure 5.15 Collapsed water level compared with experimental measurements, thermocouple readings, and results of post-test calculations (-C-).

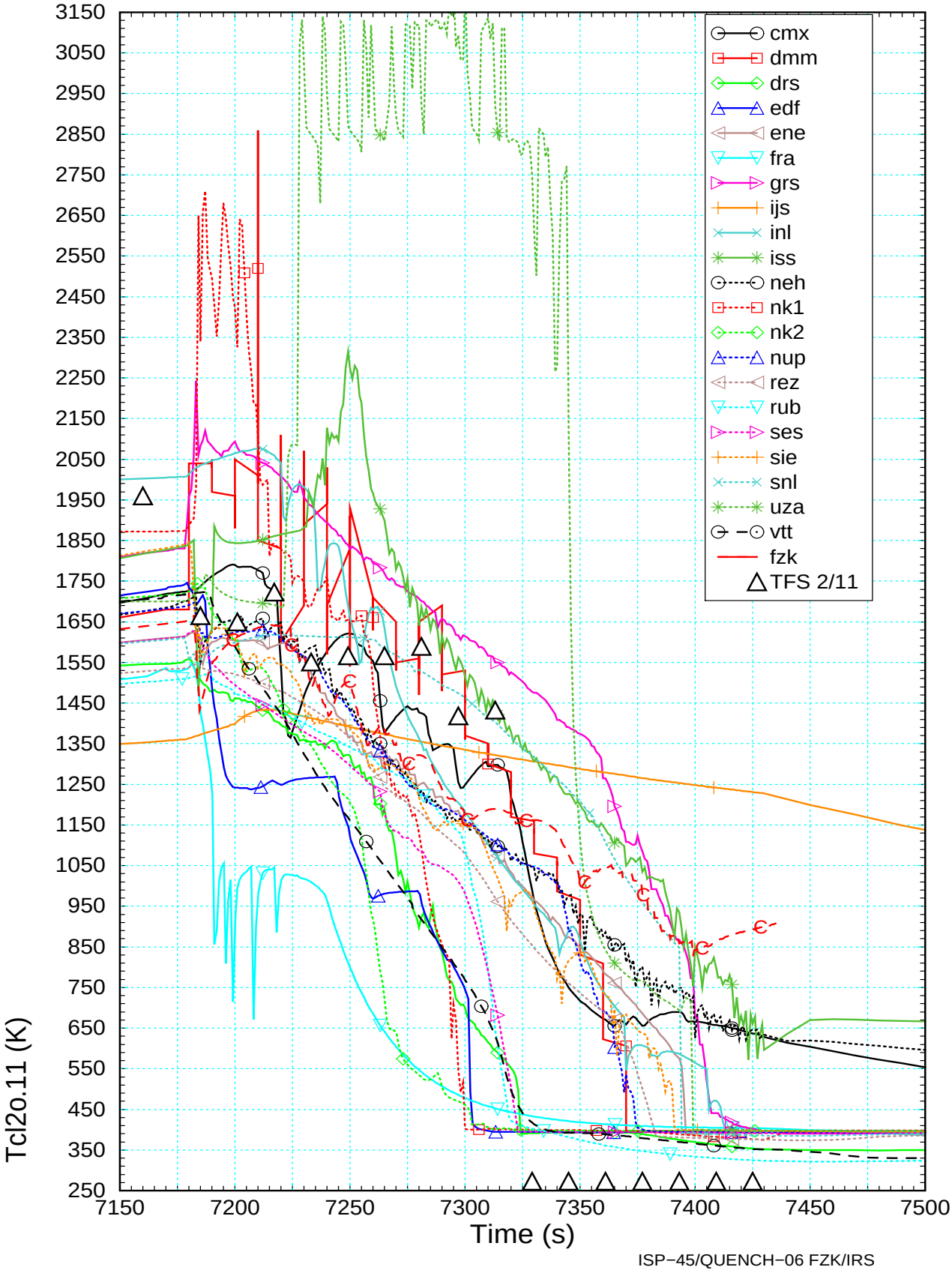

Figure 5.16 Cladding temperature (First Ring) at elevation 0.75 m compared to experimental result TFS2/11 and that of FZK post-test calculation (-C-).

In Figure 5.16 three different forms of cool-down curves can be identified:

1. A smooth cool-down to app. 550 – 750 K indicating the convective heat transfer to the steam, followed by a rapid cool-down (quenching). The calculated quench temperature i.e. the sharp change of the temperature slope depends on the thermal-hydraulic model and varied slightly with elevation.
2. Rapid drop of clad temperature at reflood initiation so that no distinct quench temperature can be identified
3. Rapid temperature increase above 2500 K at or just after reflood initiation due to activated shattering model. In some cases multiple temperature spikes or oscillations were found. For these participants the reflood process is also influenced by relocated melt and local blockages.

In the upper third of the bundle, the scatter band of the mainstream amounts to app. 300 K at 7170 s, but increases to 600 K app. 200 s later, neglecting the high temperatures triggered by shattering and subsequent strong oxidation. Even with this restriction, it can be stated that

1. The reflood behavior in the hot region of the bundle is not yet adequately simulated. Furthermore geometry changes due to clad failure or melt relocations may have influenced the calculated cool-down.
2. The slopes of experimental and calculated curves differ generally. There is a constant decrease in the calculations whereas the thermocouple readings show a more complicated behavior in the beginning of the quench phase, perhaps due to the fast water injection.
3. Some participants, including the FZK post-test calculations with 16 axial nodes (mesh length 0.1 m in the heated section) did not reach the saturation level. Possible explanations are mass error or overestimated evaporation.

5.2.2 Capability of thermal-hydraulic models

Quench front progression

To further identify the capabilities of the thermal-hydraulic code packages the development of the quench front (zTq), delivered by DRS, EDF, FRA, GRS, IJS, NEH, NUP, REZ, RUB, SNL, and VTT, are shown in Figure 5.17. The result of IJS, calculated by a MELCOR version without a dedicated reflood model, was very noisy; so it had to be removed. The axial offset in the VTT results was corrected subtracting 0.5 m. The experimental data are derived from TSF thermocouples indicated by -e- and shroud thermocouples TSH -E-, respectively. Their slopes are approximated by thick straight lines. The results of TCRI/C thermocouples, which are used for support, are indicated by "s".

As mentioned in section 2.3 the TSH signals are representative for the onset of nucleate boiling, whereas the surface mounted TFS thermocouples give hints of the elevation of the droplet zone in the two phase region. In this sense, the TSH line is considered to be the lowest elevation for "wetting". As can be seen clearly at quench initiation the distance between both lines is affected by the mass flow rate. During the short period of fast water injection, that distance increases to app. 0.5 m but after 7250 s it decreases to 0.1 m - 0.2 m.

Despite the axially increasing surface temperatures (Figure 5.12) this difference remains nearly stationary up to the upper end of the heated section, which is reached after 7400 s. This indicates that the dominant parameter is the flooding rate.

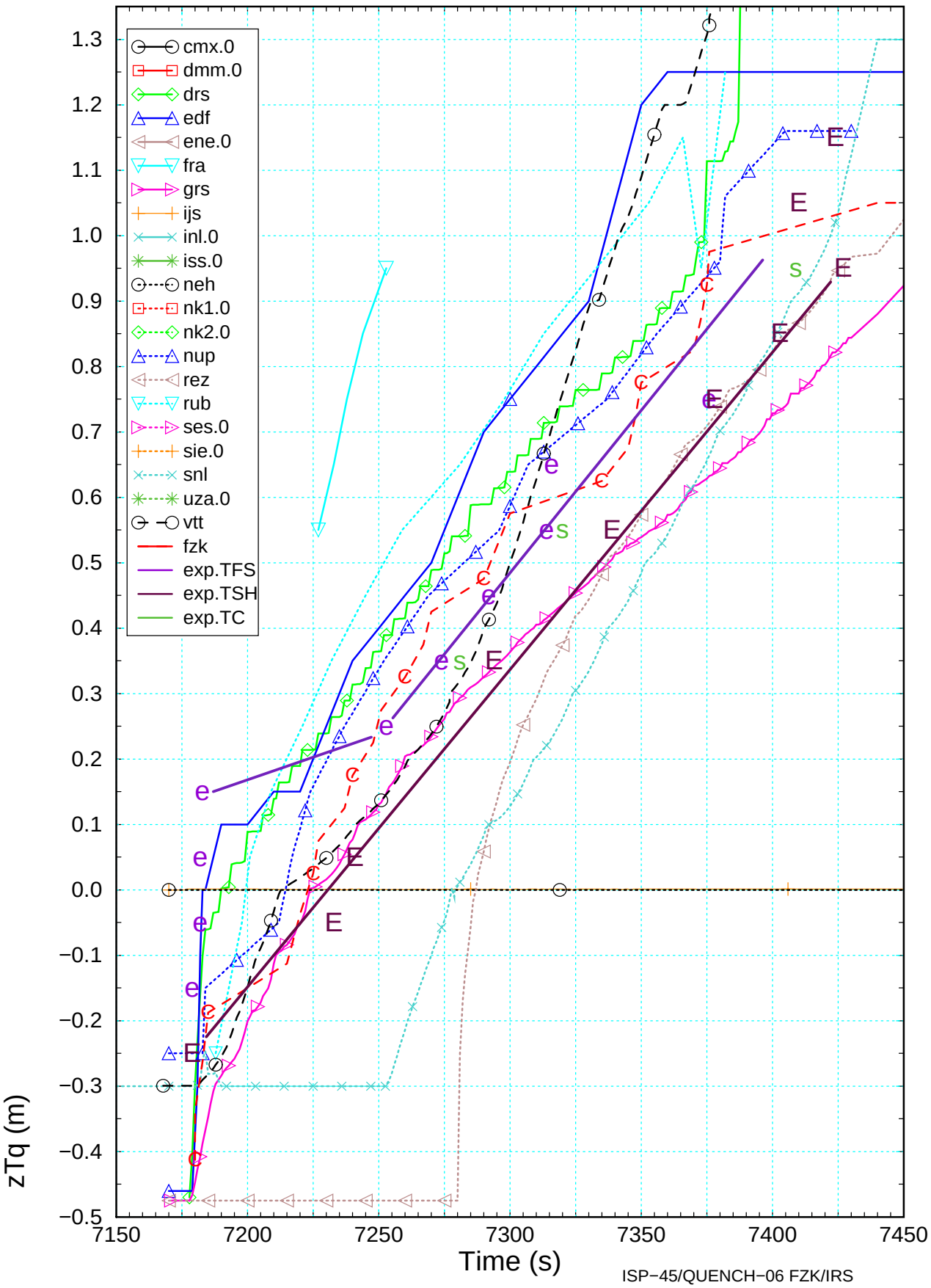

Figure 5.17 Development of the quench front calculated by various participants and compared to experimental results derived from TFS (-e-), TSH (-E-), and TCR (s) thermocouples and the results of FZK post-test calculation (-C-).

In the calculations there is a tendency to slightly over-predict the quench progression during fast water injection leading to an offset of app. 0.2 m. A fraction of fast-injected water evaporates in contact with the hot structures of the inlet pipe and enters the bundle as vapor at app. 400 K (section 1). That vapor mass flow rate may be the origin of the observed deviations in the local void fraction calculation of some participants (DRS, EDF).

Two MELCOR results (SNL and REZ) show an unexpected delay of app. 80 s until the quench front starts to propagate upwards. At that time the quench front (zTq) is calculated to be app. 1.0 m below the collapsed water level (zwlv) as can be seen in Figure 5.15. This is rather unrealistic, especially since below 0.5 m the temperatures are rather low. For SNL this can be explained be a delay in the quench water injection. For the lower half of the bundle these plots are out of the mainstream, mainly linked to the over-estimated fixed temperature (600 K) in the simplified model.

Also the MAAP (FRA) results are located above the mainstream, probably due to lacking or erroneous reflood models. The results of ATHLET-CD code calculations of GRS and RUB are somewhat contradicting, insofar as GRS quench front meets the TSH line, while RUB overestimates the experimental results. This could be explained by the artificial oxide scale cracking modeled by GRS. The results of EDF, DRS, and VTT also overestimate the quench front velocity in the bundle.

Above 0.25 m, the result of the FZK calculation, which was used to define the water mass flow rate at the bundle entrance follows roughly the TFS line. The spreading of most slopes in Figure 5.17 is rather small considering the differences in the surface temperatures and oxide layer thickness at reflood initiation (Figure 5.12). The oxide scales change local heat removal due to the different material property data and surface roughness.

On the other side, the calculation of the quench temperature reflects the capability of the models to simulate the interaction of the fuel rod behavior and the very turbulent two-phase flow in the cooling channel. Here codes with thermal-hydraulic code packages developed for DBA are advantageous, especially if the strongly varying radial heat fluxes can be calculated in a fine axial mesh as mentioned in /10/. Since mesh refinement techniques are not available so far, the axial mesh length should be restricted to 0.075 m (3").

Model capabilities

To identify the interplay between fuel rod or shroud models and the thermal-hydraulic models the difference between the calculated quench positions (zTq, Figure 5.17) and the collapsed water level (zwlv, Figure 5.15) was investigated, as shown in Figure 5.18 (dzQ). The experimental data, corresponding to the collapsed water level, is the pressure difference Lm 501 (Figure 5.18 top) signal. However, it can be used only during the second part of the reflood phase (t > 7240 s). After that time a clear tendency can be seen (Figure 3.2, Figure 5.18 top): the experimental quench positions are always app. 0.2 m above the Lm 501 signal.

The level difference between the collapsed water level and the quench level primarily depends on the local mass flow rate and the wall superheat. During fast water injection nearly all codes calculate a large negative value, due to the extended inversed annular flow caused by the high mass flow rate. Between 7240 s and 7360 s, in the lower half of the bundle, nearly all values

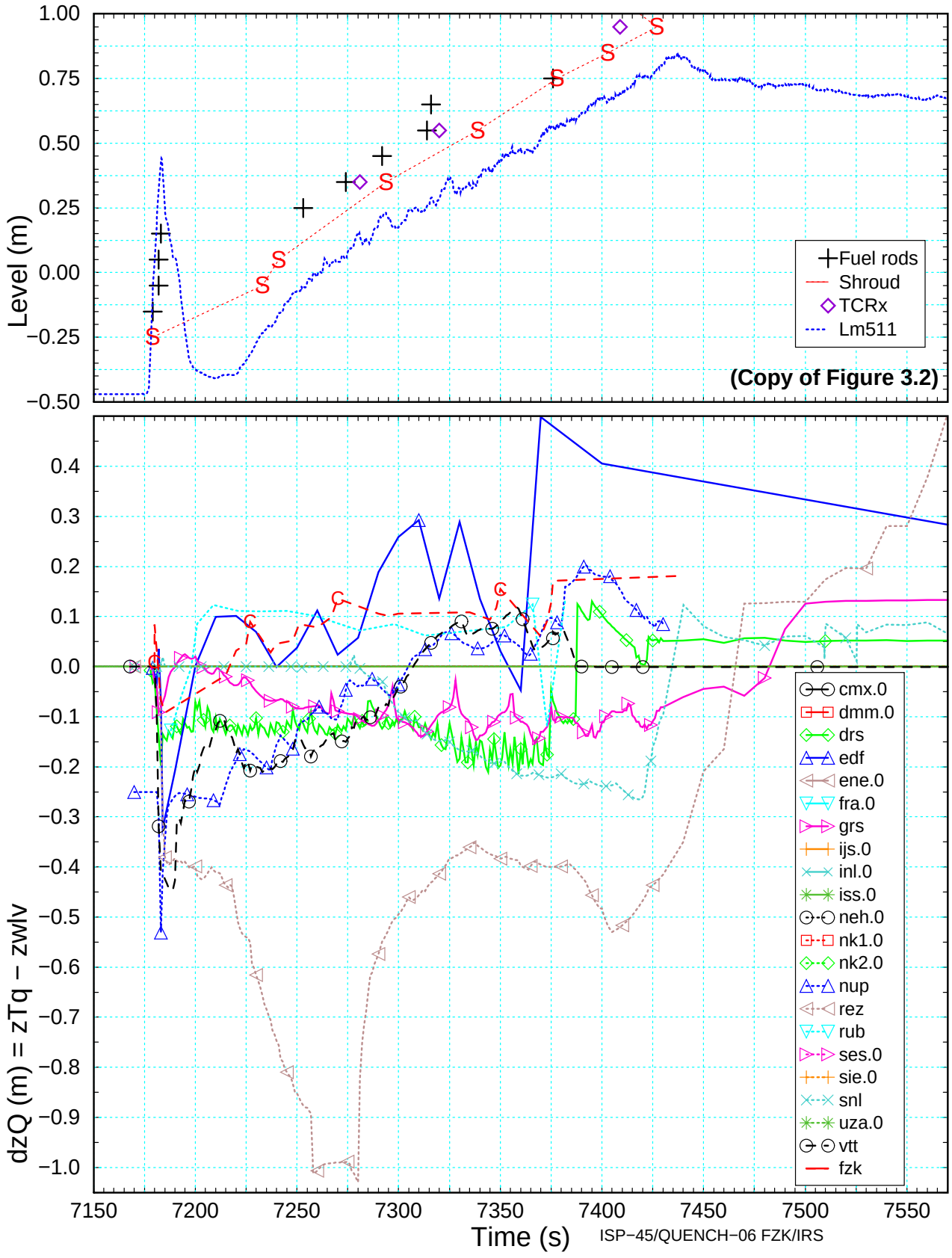

Figure 5.18 Water and quench levels, deduced from experiment (top) and difference between the calculated quench temperature positions and the calculated collapsed water level (bottom).

are within - 0.2 and 0.1 m. A negative value states that the flooding rate is still high enough to establish an inversed annular flow regime significantly above quench position. Two curves show a similar increasing trend (NUP, VTT) starting from app. –0.2 m (7200 s) to 0.1 m (7360 s). The two MELCOR results (SNL, REZ) show strong discrepancies which can be taken as strong influence of the surface temperature, which controls nearly directly the reflood advancement of the MECLOR reflood model. The EDF curve may be influenced by the oscillations found in the zwlv data (Figure 5.15).

General speaking, codes with detailed thermal-hydraulic models delivered more reliable results, however, the opposite sign reflects that the physics of the coupled energy and mass transport problem is not yet simulated adequately.

More detailed analyses should be performed, but the contribution of the participants is needed, since details about the computation of the quench temperature are required.

5.2.3 Hydrogen source term

In particular, the QUENCH-06 experiment was performed to assess SFD computer codes under reflood conditions, especially fuel rod behavior under transient cool-down conditions and hydrogen release. So a special emphasis on the accumulated hydrogen generation for the bundle plus shroud during reflood is given in this section. All available results are compared to FZK post-test calculation (-C-) and data from experiment (-E-) in Figure 5.19.

As shown in Table 5.4 only a few grams of hydrogen have been released during reflood. The calculated hydrogen production spreads of around 20 g observed for the mainstream of 14 participants at 7179 s and around 180 g for 8000 s (Figure 5.19). The scatter band, which started with a range of uncertainty of app. 67 % at 7179 s, has grown up to more then 480 % 420 s later. No specific code tendency could be identified. Thus, thermal-hydraulic modeling, activation of shattering options by the user, or severe bundle damage prior to reflood initiation has to be considered.

- First, most of the participants, the so-called mainstream, did not calculate significant oxide layer thickness increase during reflood (Figure 5.19, bottom). The results of 7 participants (EDF, FRA, REZ, RUB, SES, SNL, and VTT), who did not apply shattering options, form a narrow group around the experimental value.
- Second, a large increase is found only above 0.35 m as mentioned before. This indicated that a minimum oxide layer thickness is implemented in the shattering options of the different codes, or that the option must obey to a temperature criterion.

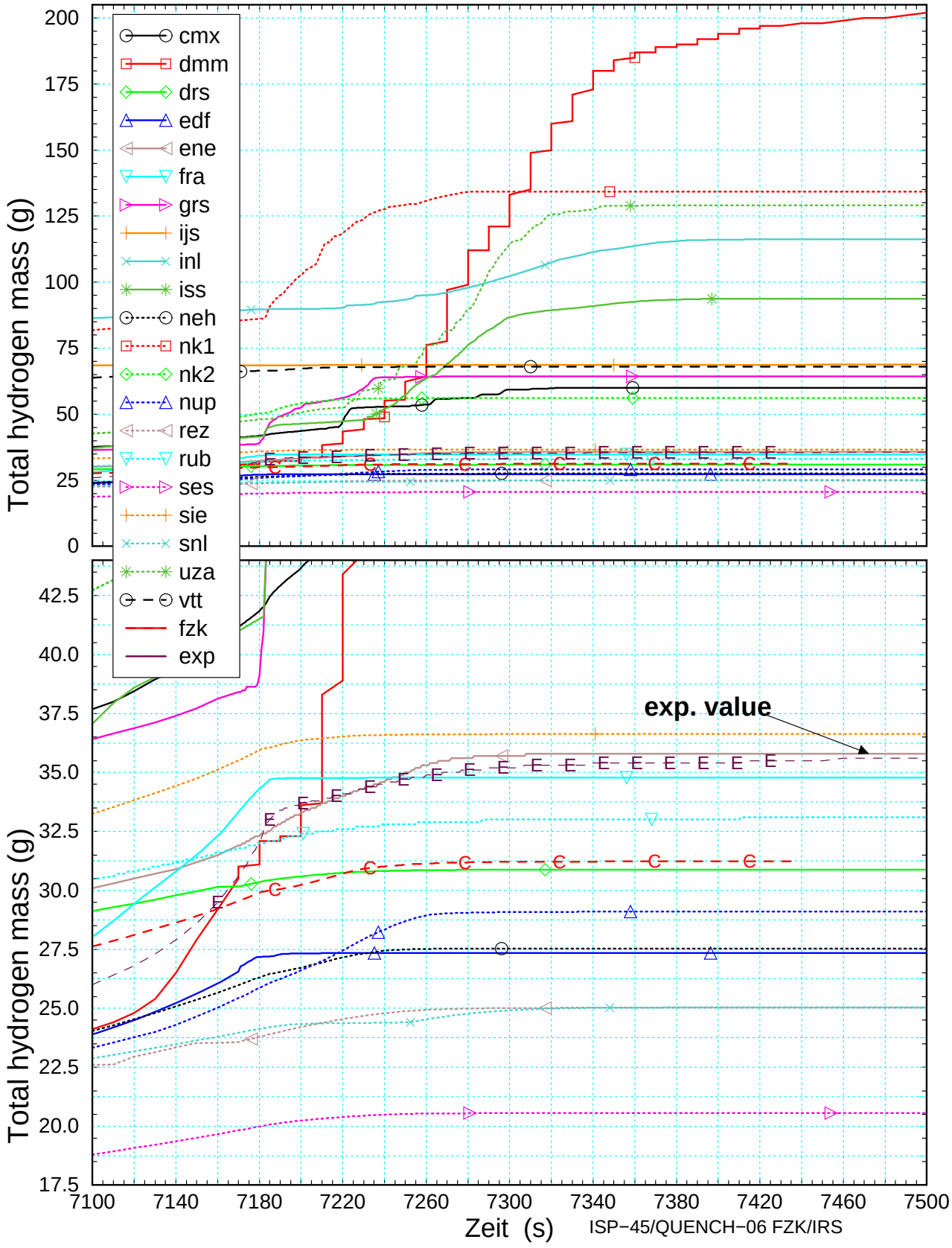

Figure 5.19 Hydrogen mass calculated during reflood phase compared to experimental data (-E-) and post-test analyses with S/R5irs (-C-): top: total field of results, bottom: magnified for mainstream.

Table 5.4 Hydrogen source term during flooding

		bundle state prior to reflood (t=7179s)			final bundle state (t=8000s)	
code	**participant**	**Tbp K**	**δox μm**	**mht_1 g**	**mht_2 g**	**shattering option**
QUENCH-06		***2050***	***≅ 300 (#)***	***31***	***4,6***	
quenching at Tbp < 2050K : total 14 calculations						
ATHLET-CD	**RUB**	1675	250	32	1	(-)
GENFLO	**VTT**	1725	330	66	1,8	(0) (*)
MELCOR	**REZ**	1750	260	23,5	1,3	(0)
ICARE/ CATHARE	**DRS**	1775	250	30,5	0,5	(-)
MELCOR	**SES**	1775	250	20	0,5	(0)
MELCOR	**SNL**	1800	310	24	1,1	(0)
SCDAPSIM	**NEH**	1825	220	26	1,2	(+)
S/R5.irs	***FZK***	***1825***	***220***	***30***	***1,2***	***(+)***
SCDAPSIM	**SIE**	1875	300	41	0,8	(+)
MAAP 4.04	**FRA**	1900	310	34,5	0,5	(0)
ATHLET/CD	**GRS**	1900	510	39	27	(++)
ICARE/ CATHARE	**ENE**	1950	310	32	3,5	(+)
IMPACT/ SAMPSON	**NUP**	1950	400	25,5	3	(+)
MAAP 4.04	**EDF**	2050	370	27,5	0,2	(0)
quenching at 2050 < Tbp : total 7 calculations						
SCDAPSIM	**UZA**	2100	360	47,5	80	(+)
SCDAP-3D	**INL**	2150	680	90	26	(+) (**)
SCDAPSIM	**ISS**	2175	450	42	53	(+)
MELCOR	**NK2**	2175	630	50	5	(0)
SCDAPSIM	**CMX**	2225	320	42	18	(+) (*)
SCDAPSIM	**DMM**	2275	280	32	175	(+)
SCDAPSIM	**NK1**	2300	1100	86	50	(+)

(#) preliminary value from SVECHA
(+) shattering option activated
(++) shattering amplified by user
(-) shattering option deactivated
(0) shattering not available
(*) erroneous axial dynamic power redistribution
(**) erroneous heater rod model

IJS excluded due to early blockage formation
δox : oxide layer thickness
mht_1 : Accumulated H_2 mass up to reflood
mht_2 : Accumulated H_2 mass starting at reflood

5.3 Final state

As discussed in section 3.3.3 no significant change in the bundle cross section was found, except for some debris of spacer grids. The final oxide layer profiles are given in Figure 3.7 and have to be compared with the calculational results shown in Figure 5.20.

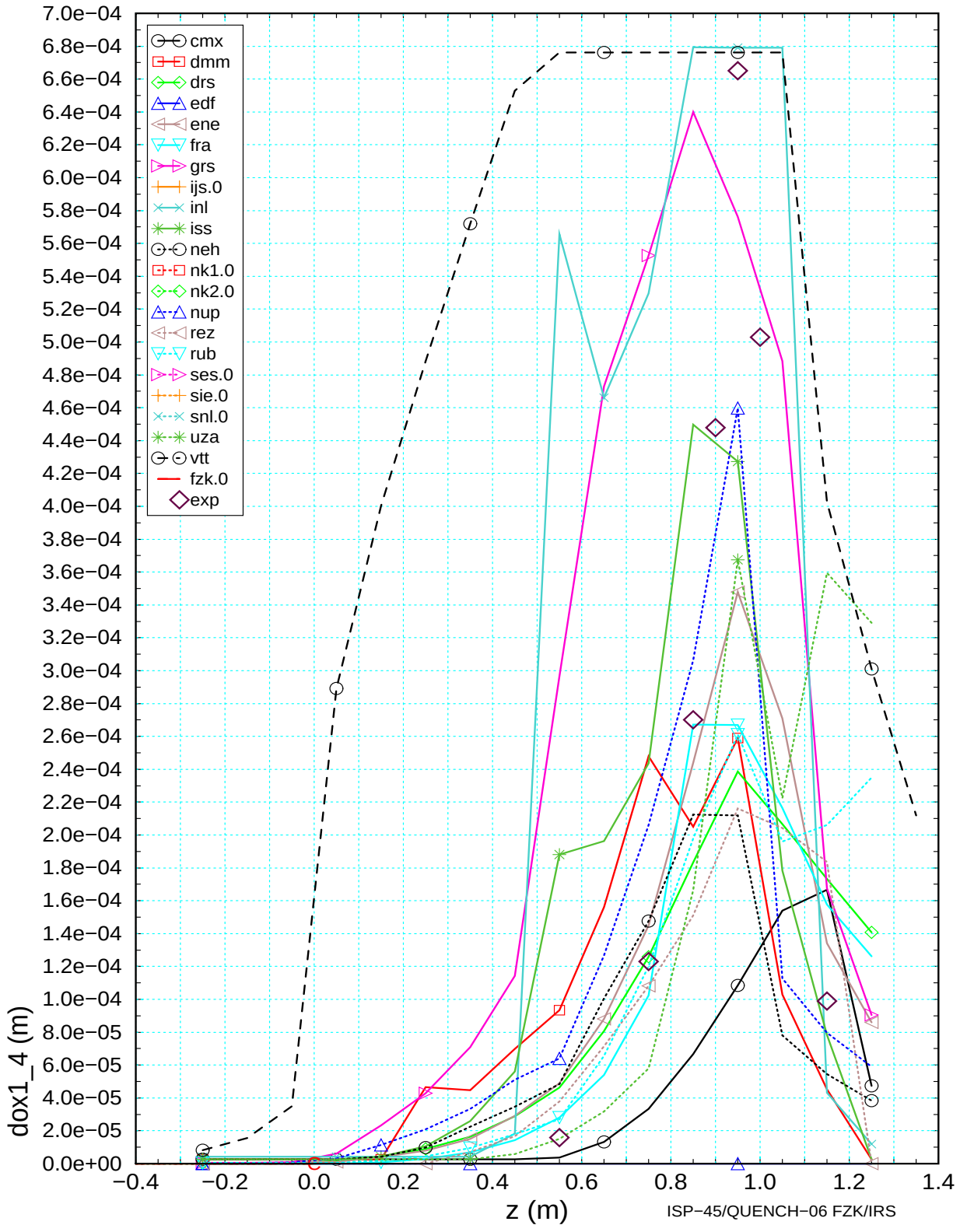

Figure 5.20 Axial oxide scale profile of the central unheated rod calculated by the participants for t=8000 s compared to experimental results.

Ballooning was calculated by some participants, leading to light reduction of the net flow area. This was rather difficult task since the external volumes of pressure lines and gauges reduced the pressure increase in the fuel rods so that they failed in the experiment due to thermal shock at reflood initiation.

The main contribution to the deviations in the final state is caused by use of an outdated heater rod model and by application of a shattering model. As a consequence, oxidation is over-predicted, and melt formation was calculated due to very high temperature in the upper third of the bundle.

5.4 Summary of blind phase

The International Standard Problem No. 45 of the OECD/NEA/CSNI on the out-of-pile reflood test QUENCH-06, performed at FZK, fills the gap between various ISPs dedicated to reflood situations of design basis accidents and ISPs in the severe core damage area ISP-31 (CORA-13) and the LOFT LP-FP2.

Apart from obvious user errors, the calculated conditions prior to reflood do not deviate significantly from one another, so that a definition of a mainstream is justified. During quenching the lack of adequate hydraulic modeling becomes obvious: some participants could not match the observed cool-down rates, others had to use a very fine mesh to compensate code deficiencies. Even without any bundle damage, the calculated axial oxide layer thickness varied significantly.

5.4.1 Code capability

The simulation capability of the codes with respect to the electrically heated out-of-pile test facility has been significantly improved in comparison to previous ISPs (ISP-31, ISP-36) hosted at FZK. Nevertheless, for some codes the simulation of non-reactor specific environments causes difficulties. In the contest of the various codes the detailed mechanistic codes such as ICARE/CATHARE, SCDAP-3D, SCDAP/RELPA5, or SCDAPSIM have some in-built advantages due to their dedicated usage for experiment analyses (SCDAP designed for PBD, LOFT analyses and extended and optimized at FZK for CORA/QUENCH and Phebus experiments, ICARE2 for the Phebus SFD and Phebus FP programs).

The thermal-hydraulic packages of the codes span between detailed mechanistic versions, widely validated in the field of DBA experiments, and single phase approaches, which can only handle either liquid or vapor in one cell. To overcome such deficiencies for both integral codes MAAP and MELCOR, new models for reflood were used.

The results with respect to energy balance, thermal-hydraulics, and bundle degradation are considered to be reasonable if they are in the confidence range as indicated in Table 5.5, forming the so called “mainstream”. That mainstream comprises app. 80 % of the participants.

The energy balance of the different code systems showed unexpected large deviations compared to experimental values and post-test analyses at the end of the pre-oxidation phase, when a quasi steady state situation in the bundle is given. This may not be attributed to user effects alone.

Table 5.5 Code and user specific effects found during ISP-45 exercise.

Code	Type	Input source	Code variants	User experience	Fluid mass balance	Energy balance	Thermal-hydraulics heat-up	Thermal-hydraulics reflood	Bundle degradation heat-up	Bundle degradation reflood	Possible errors Code	Possible errors User
ATHLET-CD	d	RUB	RUB	E	± OK	± OK	± OK	± OK	n/a	n/a		IT
		"	GRS	D / E	± OK	++	± OK	++	± OK	± OK		SO
GENFLO	d	VTT	VTT	G	++	n/a	++	++	n/a	n/a	OC	HR, IT
ICARE/ CATHARE	d	DRS	DRS	D / E	± OK	± OK	± OK	± OK	± OK	± OK		PI
		ENE	ENE	E	± OK	++	± OK	± OK	n/a	n/a		
IMPACT/ SAMPSON	d	NUP	NUP	D / E	± OK	± OK	± OK	± OK	±OK	±OK		
MAAP 4.04	I	EDF	EDF	E / D	± OK	--	± OK	± OK	n/a	n/a		
		FRA	FRA	E	± OK	--	± OK	± OK	±OK	MR	RM	IT
MELCOR (R)	I	SNL	SNL	D / E	± OK	± OK	± OK	± OK	n/a	n/a		
		REZ	REZ	E	± OK	n/a	± OK	± OK	±OK	± OK		
		SES	SES	G	± OK	n/a	± OK	± OK	n/a	n/a		
MELCOR (-)	I	NK2	NK2	G	± OK	n/a	++	++	n/a	n/a	RM	
		IJS	IJS	G	---	++	++	++	MR		RM	HR IT
SCDAPSIM	d	ISS	CMX	G	++	--	++	++	B	± OK		RF, IT ,SO
		"	ISS	D / G	++	++	± OK	++	± OK	± OK		SO
		"	NEH	G	± OK	± OK	± OK	± OK	B	± OK		SO
		"	NK1	G	++	--	++	++	n/a	n/a		SO
		"	UZA	G	± OK	n/a	++	++	B	± OK		RF, SO
		DMM	DMM	E	± OK	n/a	± OK	++	B	± OK		IT, SO
		SIE	SIE	E	n/a	--	± OK	± OK	n/a	n/a		PI, IT
SCDAP-3D	d	ISS	INL	D / E	/\/	/\/	++	++	±OK	± OK	HR	PI, IT
SCDAP/ RELAP5.irs	d	FZK	FZK	E / D	± OK	± OK	± OK	± OK	B	± OK		

Confidence range for : ± OK | ± 40% | ± 40% | ± 15% | ± 40%

underpredicted -- < nn%
overpredicted ++ > nn%

no sufficient information given: n/a
oscillating behaviour : /\/

Code classification

Integral fast running tool : I
detailed mechanistic tool : d

User experience

Code developer : D
More experienced : E
Less experienced : G

Bundle degradation

Baloonning : B
Clad failure : CF
Melt relocation : MR

Possible deficiencies

Power input : PI
Oxidation correlation : OC
Inlet gas temperature : IT
No specific reflood model : RM
Radiation deactivated : RF
Elec. heating model deficiency : HR
Shattering option : SO

During reflood various data such as water level and temperatures, reflect the different thermal-hydraulic capabilities of the codes. The results vary between no reflood effects, the temperatures simply drop to saturation value, and temperature increases up to 3100 K.

In Table 5.5 possible deficiencies are indicated. It was found that a code developer suggested inappropriate code options to the code users such deactivating rod-to-rod radiative heat transfer, so that unrealistic high cladding temperatures were found.

ISP-45 was continued with user comments on the report on the blind phase /22/ and open calculations to extend code validation and to deepen learning. No perfect simulation of the QUENCH-06 using all adjustments of the codes was intended, but a reasonable simulation of the relevant phenomena and their interaction. So all participants were invited to participate in open calculations and to use other QUENCH experiments without modifying the main code parameters.

5.4.2 Participants experience

The user's experience ranged from beginners to code developers, who know the code in much detail. Therefore, the participants were grouped according to their experience - of course, with some reservation.

The first group comprises the more experienced users, indicated by "E" in Table 5.5. They have already analyzed CORA experiments or QUENCH experiments before ISP-45. Experience with analyses of experiments in the French Phebus facility was also taken into account. Participants in this group are: ENE, FRA, REZ, DMM, and SIE. The group of the more experienced users also contains the code developers, such as DRS (ICARE/ CATHARE), GRS (ATHELT-CD), INL (SCDAP-3D), ISS (SCDAPSIM), NUP (IMPACT/ SAMPSON), and SNL (MELCOR). They are indicated by "D" in Table 5.5. EDF (MAAP4) was also ranked as "D" because they developed models or improved their code. Since the code developers also validate their codes, "E" is also indicated for them in Table 5.5.

The group indicated by "G" for "general", combines all users who are not so experienced in analyzing integral severe accident experiments or nuclear power plants. In this category the participants CMX, IJS, ISS (Honaiser), NEH, NK1, NK2, SES, UZA, and VTT were placed.

Analysis of the results showed that with some reservation the participants who knew the capabilities of their code as well as the experimental peculiarities rather well had most success.

6 RESULTS OF OPEN PHASE

As usual the blind phase of an ISP exercise is followed by open calculations to identify sources of deviations observed during comparison of blind calculation results.

6.1 Participants and codes

Except for MAAP, GENFLO[1] /23/, and SCDAP-3D, all codes participating in the blind phase are represented in the open phase. In sum 8 participants who had engaged in the blind phase and Volchek, A., token NK3 and same address as NK1 and NK2, delivered results for the open phase (Table 6.1). Besides, VTT delivered results after the end of the open phase, given in the Appendix. The others did not participate; e.g. because the results of their blind phase calculations could actually not be improved due to various reasons. In the following sections the results of the open phase calculations i.e. of DRS, ENE, NK3 (ICARE/CATHARE), GRS (ATHLET-CD), IJS (MELCOR), NEH, UZA (both using SCDAPSIM), and NUP (IMPACT/SAMPSON) are compared to post-test results and experimental data similarly to the blind phase data in section **5**.

Table 6.1 List of participants for ISP-45 open calculations

Token	Code	Open calculation	Delivered data
CMX	SCDAPSIM	No opt. 30, global data available	
DMM	SCDAPSIM	No shattering, fluid inlet temp corrected	
DRS	ICARE/CATHARE	Some global data available	Tbp, mht
EDF	MAAP 4.04	No	
ENE	ICARE/CATHARE	Global data available	All
FRA	MAAP 4.04	No	
GRS	ATHLET-CD	Global data available	All
IJS	MELCOR	Global data available	All
INL	SCDAP-3D	No	
ISS	SCDAPSIM	No	
NEH	SCDAPSIM	Global data available	All but Tfg.01
NK1	SCDAPSIM	No	
NK2	MELCOR	No	
NK3	ICARE/CATHARE	Some global data available	Tbp, mht
NUP	IMPACT/SAMPSON	Global data available	All
REZ	MELCOR	No	
RUB	ATHLET-CD	No	
SES	MELCOR	No	
SIE	SCDAPSIM	No	
SNL	MELCOR	Blind phase data used	All
UZA	SCDAPSIM	Some global data available	Tbp, mht
VTT	GENFLO	Delayed (see Appendix)	Tbp, mht

[1] After end of open phase VTT presented results with an improved GENFLO code as mentioned in the appendix

6.1.1 Input modifications

In Table 6.2 the most important modifications are given. As requested during the comparison workshop, the participants should deliver those parameters which differ from the default values and which are responsible for their calculations. The most relevant parameters summarized in Table 6.2, the detailed lists are given in the appendix (section 11.1).

Table 6.2 List of input modifications

	Type	Blind calculation	Open calculation
DRS	Delay in reflood initiation: Outer circuit resistance (bundle): "Bug" in input file (details see **Table 11.1**)	Not taken into account 0.2 mΩ (4 mΩ/rod) Bad power distribution in heated rods	Taken into account 0.25 mΩ (5 mΩ/rod) "Bug" corrected
ENE	Zircaloy grid spacer perimeter per rod (input data error correction)	0.1128 m	0.0564 m
	Correlation used for Zircaloy oxidation at temperature below 1853 K	URBANIC	CATHCART
	Stop of fast water injection (according to experimental measurement)	7184.5 s	7184 s
	Temperature of fast water injection at bundle inlet (-0.45 m)	340 K	390 K
	Fraction of fast injected water that evaporates in contact with the hot structures of inlet pipe and enter the bundle at -0.45 m elevation as vapor at 400 K	0%	15% (0.6 kg)
GRS	Limitation of protective oxide layer thickness (details see **Table 11.2**) Inlet temperature	0.02 Tfg.01	Rods: no, shroud: 0.2 Tfg.01 + 20 K
IJS	Water injection before quench fluid inlet temperature	Input error: Steam: 437K / Ar: 294K	No water injection TFS2/1 used
	Modeling of bundle heating	DECAY heat	MELCOR ELHEAT
	Min temperature for oxidation (1100 K)	900 K	900 k
	Radiative heat transfer in the shroud	No	No
	Mass flow of quench water (details see **Table 11.3**)	No quench water	Ar, steam, and water correctly modeled
NEH	Code option to improve coupling Double side oxidation > strain (%)	Opt. 30 used 7 %	No Option 30. 18 %
NUP	Contact Resistance (mΩ/rod): ZrO_2 Thermal Conductivity multiplier	5.0 x 1	4.3 x 2.5
UZA	Electric power input: Contact Resistance (mΩ/rod): Shroud gap in upper electrode zone: Quench water temperature: (details see **Table 11.4**)	Ptot (t) 4.2 Argon 297.6 K	0.945 * P tot (t) 4.0 Artificial material 370.0 K

6.1.2 Code features

From the information delivered by the participants no hints about code modifications necessary to simulate QUENCH-06, were found. In the appendix (section 11.2) some of the participants' statements are comprised, focused on the code family. In one case (ENE) the oxidation correlation was modified.

6.2 Pre-reflood

In the blind phase the pre-reflood phase was discussed in detail (section 5.1) in order to identify code deficiencies, which may influence the reflood phase. For the open phase, only a brief check will be given based on the available global data. Especially the fluid mass and enthalpy balance as well as the energy balance are discussed and compared with the findings of the blind phase exercise outlined in section 5.1.1.

6.2.1 Global data

Similarly to section 5.1.1 a brief overview will be given, but restricted to the maximum bundle temperature and the total hydrogen mass.

Maximum bundle temperature

The maximum bundle temperatures shown in Figure 6.1 reflect the improvement to simulate the QUENCH-06 experiment, attained in the open phase. The data are in the vicinity of either the experimental value of TIT A/13 or the FZK post-test calculations. The deviation up to 6000 s is reduced from about 150 to 200 K to app. 100 to 120 K. It should be pointed out that such an agreement could only be reached, when the experimental conditions, above all the thermal boundary conditions for the radial direction, are sufficiently well defined. However, it should also be noted that the measured temperature refers to the centerline of an unheated corner rod, whereas the calculated values are surface temperatures of heated rods so that there is some underestimation of experimental data common for all codes.

The variation in the peak temperature prior to reflood amounts to app. 500 K. During reflood phase the temperature drops more or less rapidly to saturation temperature, depending on the axial position of the maximum value. From participants' statements, the input modifications were not tremendous, except for correcting obvious errors found in the blind phase.

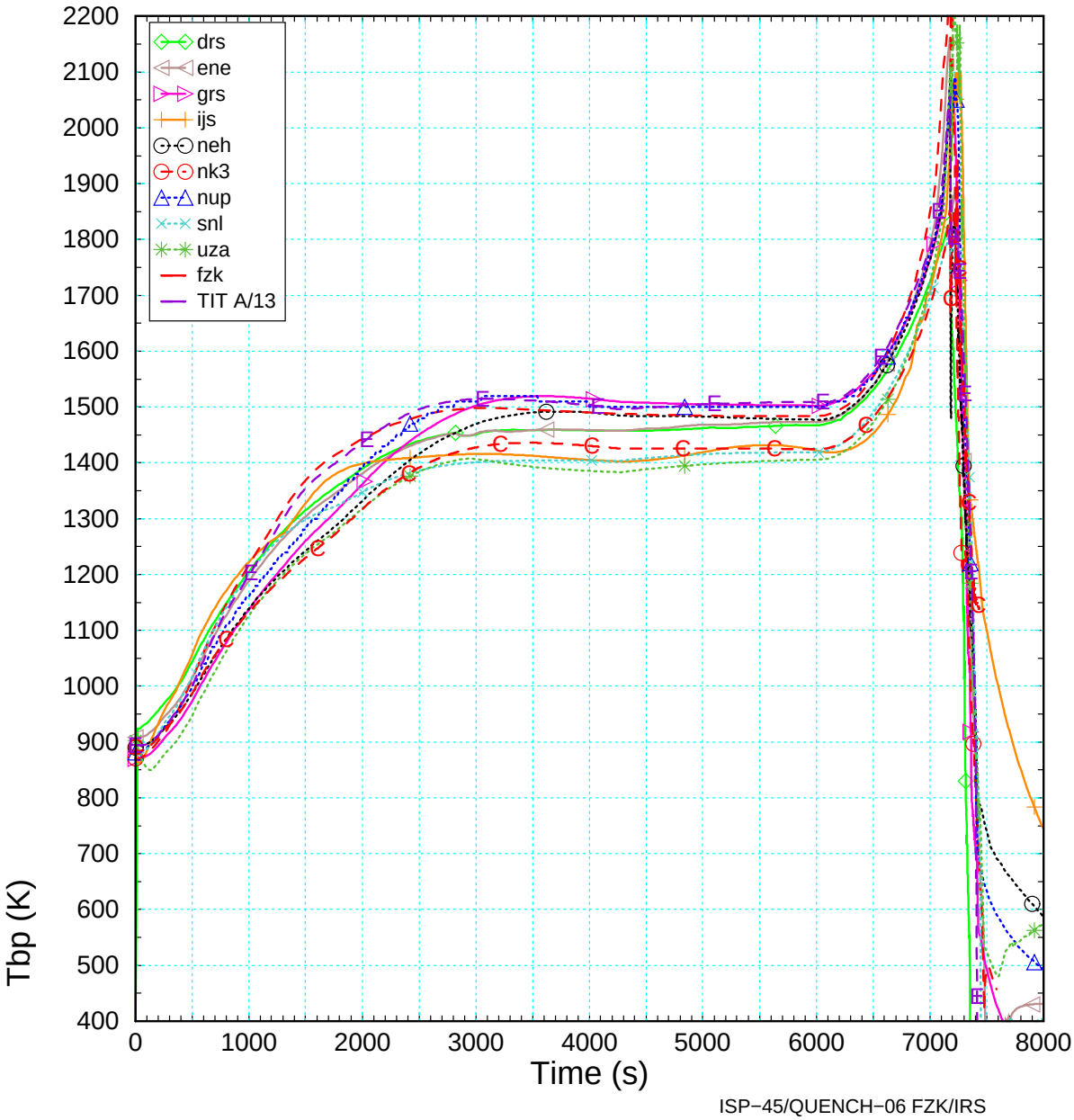

Figure 6.1 Maximum bundle temperature calculated during open phase.

Hydrogen production

Table 6.3 Relative deviation from experimental value

Time	7178	8000
DRS	3%	-7%
ENE	1%	-1%
GRS	1%	1%
IJS	116%	105%
NEH	3%	1%
NK3	3%	1%
NUP	-5%	-8%
SNL	-24%	-30%
UZA	-15%	-3%
FZK	-9%	-11%

In Figure 6.2 the total hydrogen mass is given together with the FZK post-test results of S/R (-C-) and the experimental data (-E-). Furthermore, a bandwidth of 15 % around the experimental data is shown. At a first glance nearly all participants are within that bounds, except for DRS, who slightly overestimated the hydrogen mass in the pre-reflood phase. In the IJS model the radiation heat losses in the upper electrode zone from the shroud to the coolant jacket were not taken into account. Therefore the temperature in the upper electrode zone and hence hydrogen release were over-predicted.

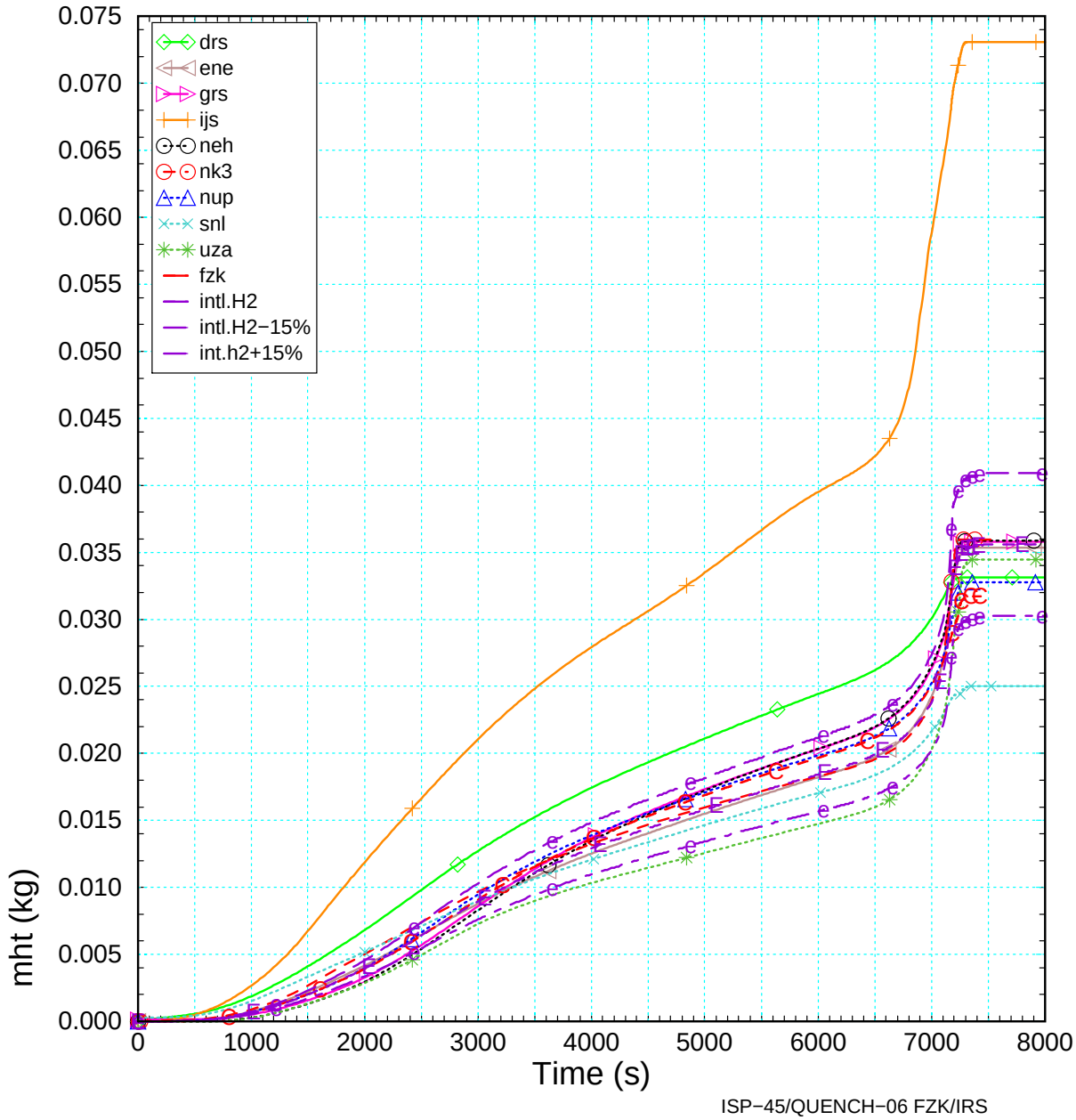

Figure 6.2 Total hydrogen mass calculated during open phase.

6.2.2 Data checks and global balances

Fluid mass balance

Compared to the blind phase (Figure 5.1) the fluid temperature at level 1, Tfg.01, measured by the thermocouple reading TFS 2/1, does not vary significantly. The participants mentioned only slight modifications necessary to adopt shortcomings in simulation of the inlet region. At the end of reflood phase, however, the fluid temperature varies between 300 K and saturation temperature. This may be attributed to the different thermal-hydraulic code packages.

In a next step the mass balance (Figure 6.4) was set up, and compared to the blind phase (Figure 5.6). As expected, the results only reflect numerical oscillations, which may be explained by numerical difficulties of the code. Since oxidation is taken into account by the hydrogen mass flow rate, another explanation may be a code error, in not exactly transferring the hydrogen source term into the fluid.

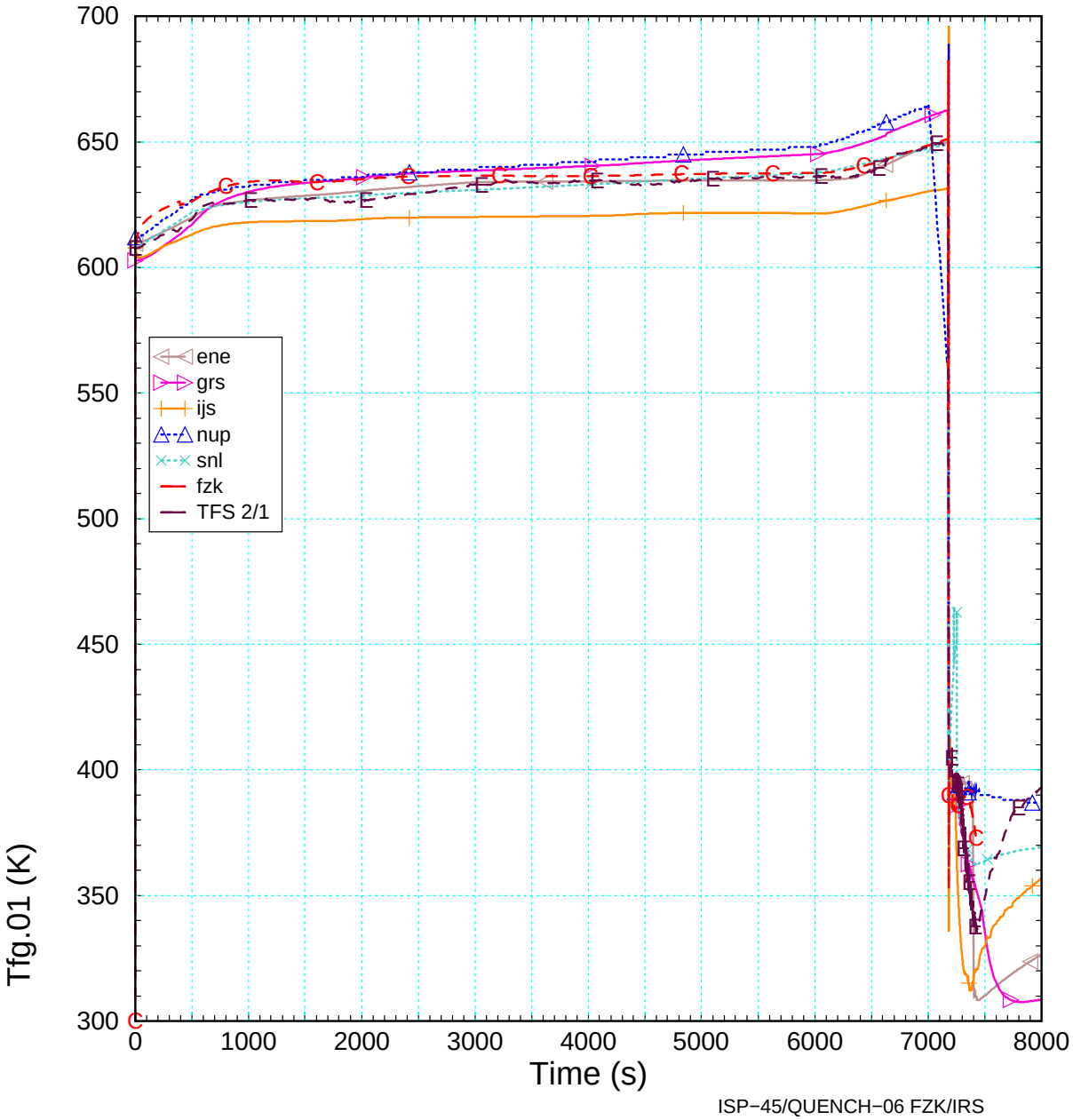

Figure 6.3 Open phase fluid temperature (Tfg.01) at lowest bundle elevation calculated by the participants compared with post-test calculation with S/R5irs (-C-) and delivered fluid temperature derived from TFS 2/1.

For RELAP5 based codes, another possible explanation of the unexpected deviation found for IJS may be the use of the nearly implicit scheme. In that case large time steps are formally allowed but due to code errors an intolerable increase in the mass error may result. (Remark: The authors made similar experiences with SCDAP/RELAP5 mod3.2 with respect to the PHEBUS FP and QUENCH tests.)

Fluid enthalpy balance

As described in section 5.1.1 as well in /22/ in detail, the fluid enthalpy balance is the basis to assess the convective heat losses in the test section. Inspection of H_diff1 revealed that a better simulation of the test section is obtained; the scatter band is reduced. Nevertheless, it shows that an adequate modeling of the QUENCH test section peculiarities is still challenging.

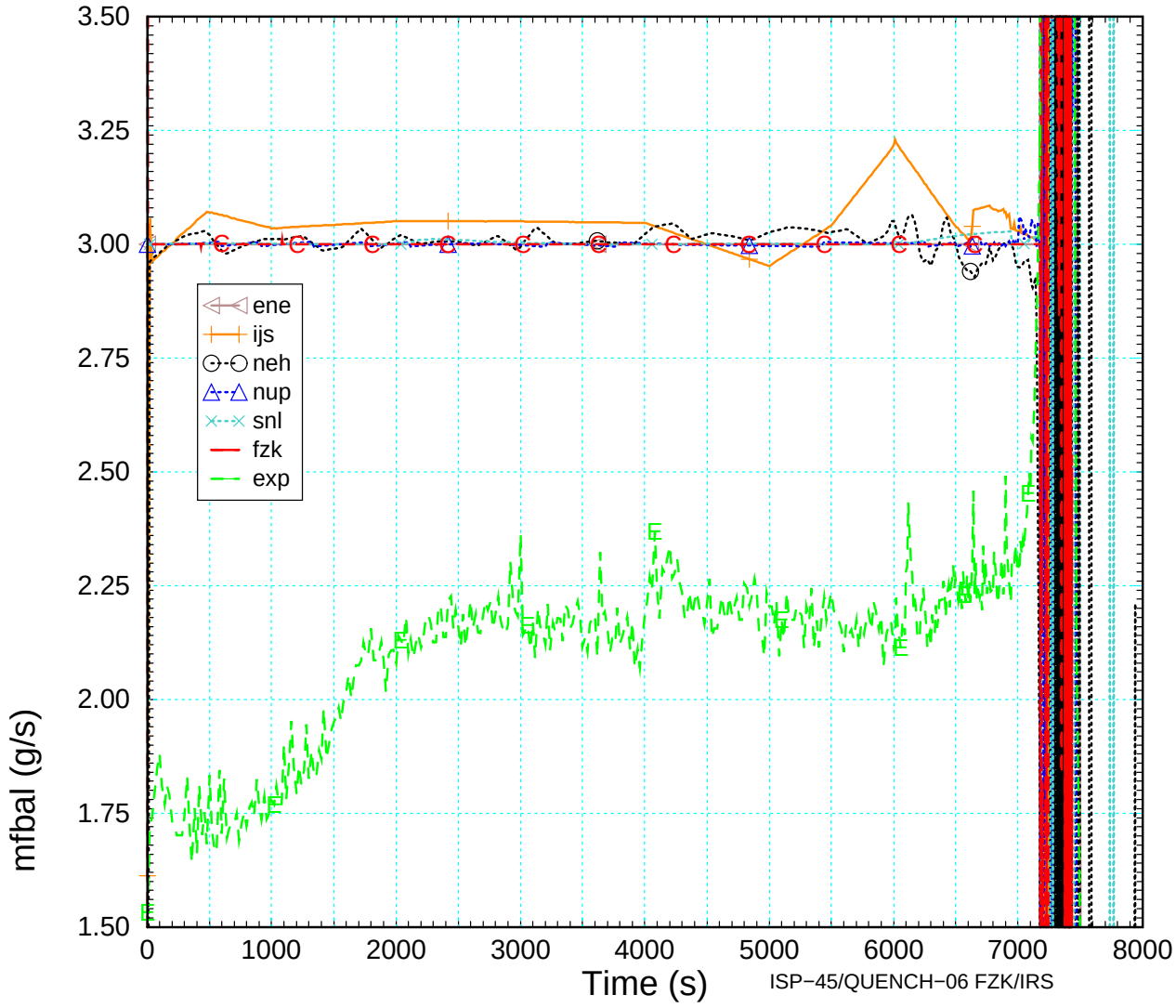

Figure 6.4 Fluid temperature Tfg.01 at lowest bundle elevation calculated in the open phase by participants compared with FZK post-test analyses (-C-) and delivered fluid temperature TFS 2/1.

To circumvent the difficulties in modeling the upper electrode zone, a second check of the fluid enthalpy balance is done, neglecting the upper electrode zone. However, in the open phase the fluid temperatures at the upper end of the heated zone (at 1.0 m) were not available. As an alternative the maximum bundle temperature was used. Therefore, the results of H_diff2 in Figure 5.8 may differ somewhat to those shown in Figure 6.5 (H_diff2*). Nevertheless, the results of this “artificial” enthalpy balance shows only slight scattering among the participants and the posttest calculations.

It is stressed and appreciated that the participants did not tune their codes for a perfect agreement with the experimental results, because this would devaluate the results. The uncertainties are due to the limitations of the codes, which are primarily dedicated to reactor applications. However, radiative heat transfer from the core to the liner and to the core barrel is not negligible in low-pressure severe accident scenarios.

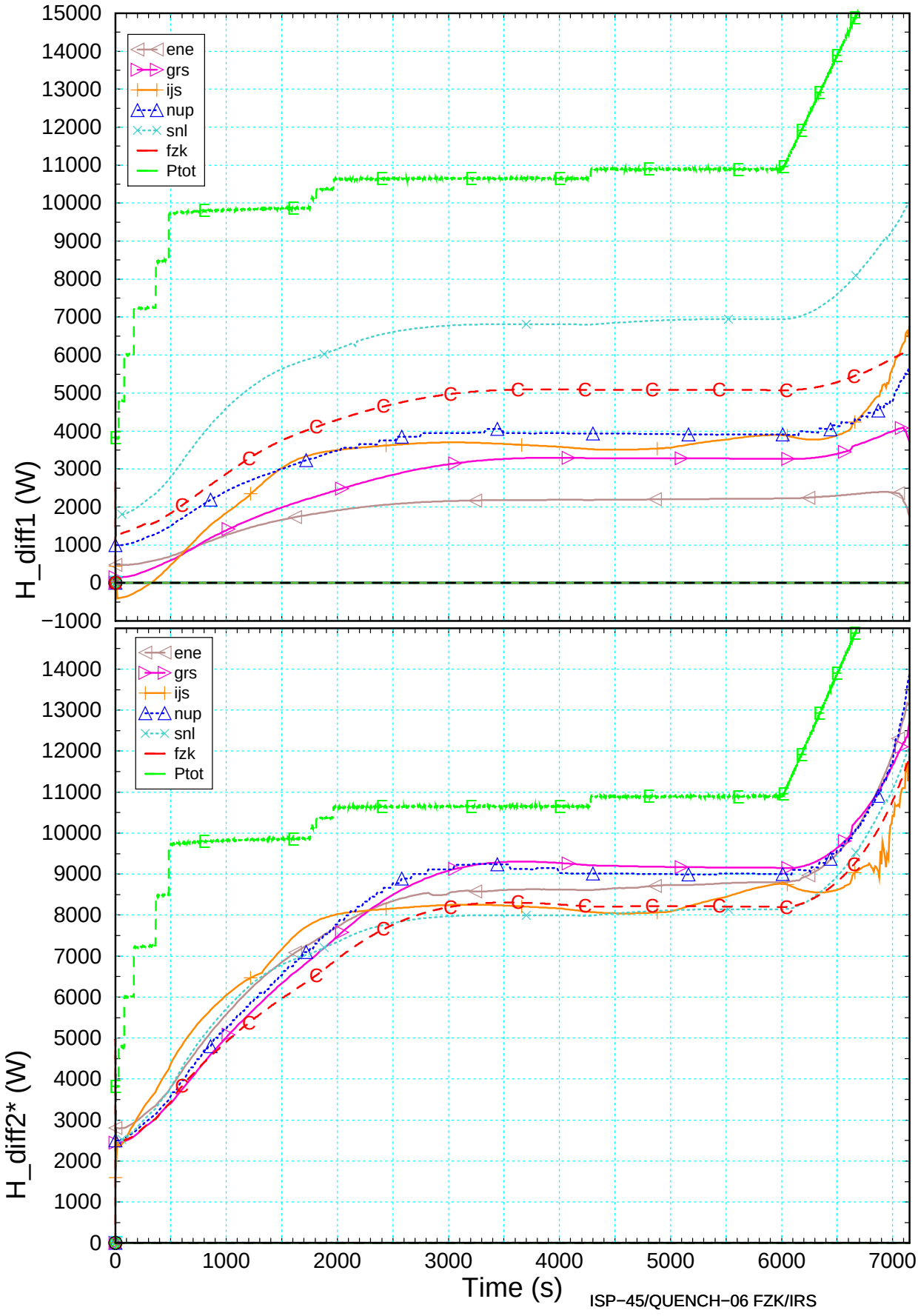

Figure 6.5 Open phase fluid enthalpy balance for the whole bundle (top) and for the heated section (bottom).

Power balance

As mentioned in section 5.1.1, the total electric power released in the test section P_{el} has to be lower than the total measured power due to losses in the flexible wires and the sliding contacts, given by a resistance R_v per rod. This value decreases with increasing temperatures and thus the resistance by (~ R_v / R_{total}).

As can be seen in Figure 6.6, the scatter band is comparable considering participants of the open phase only. It is rather small (app. 6 %) compared to that of the mainstream in the blind phase (app. 10%) shown in Figure 5.9. Unfortunately, not all participants who had problems with the power release participated in the open phase.

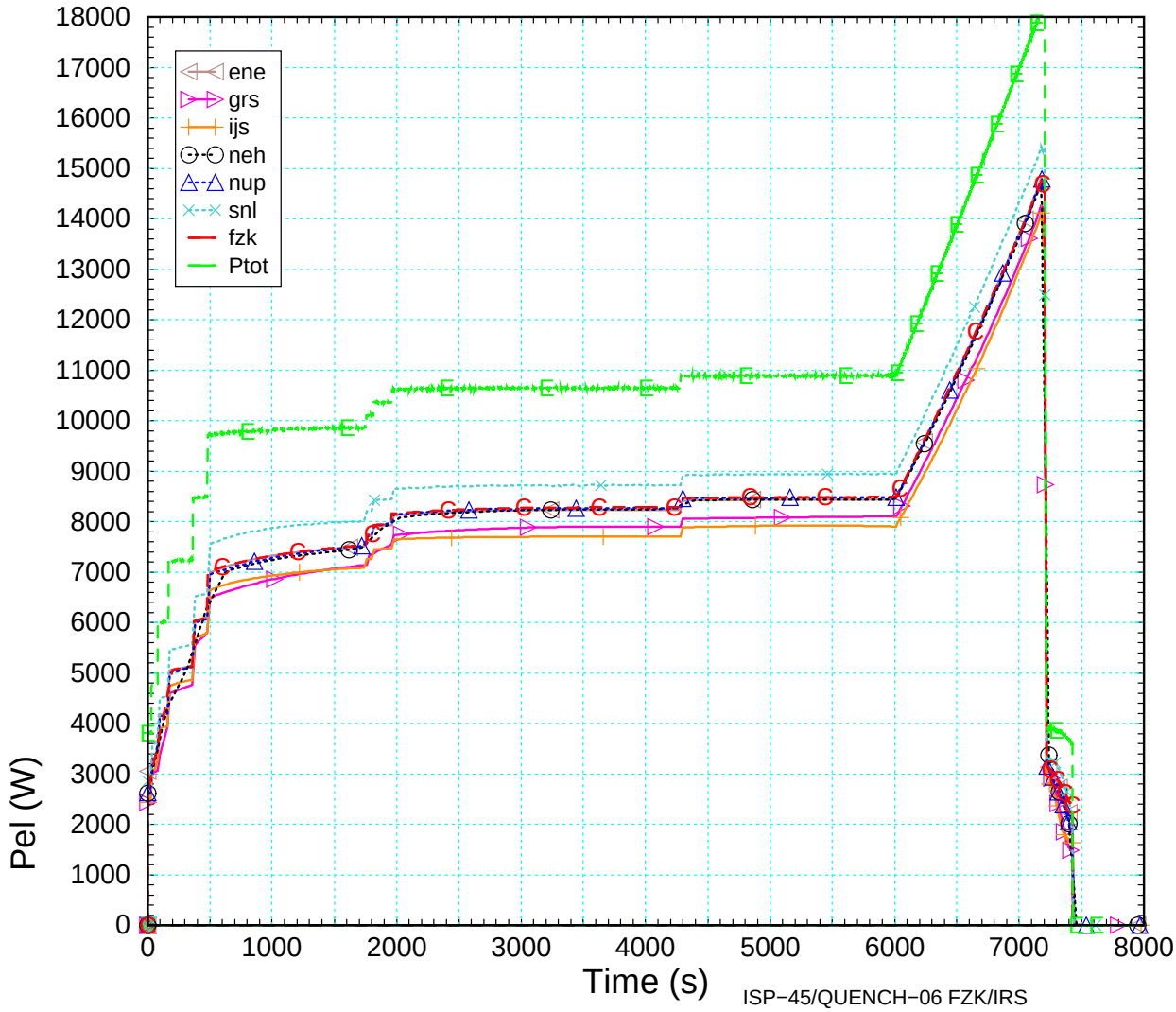

Figure 6.6 Open phase total electrical power released in the whole test section compared to FZK posttest analyses (-C-) and the measured total electrical power (-E-).

As can be seen in Figure 6.7 the global power balance reveals rather reasonable values, if the uncertainties in the convective heat losses are considered as mentioned above. As discussed in section 5.1.1 higher value indicate that the convective losses are underestimated, assuming that the electric energy is calculated reasonably and the exothermal energy is small (which is fulfilled at the end of the pre-oxidation phase).

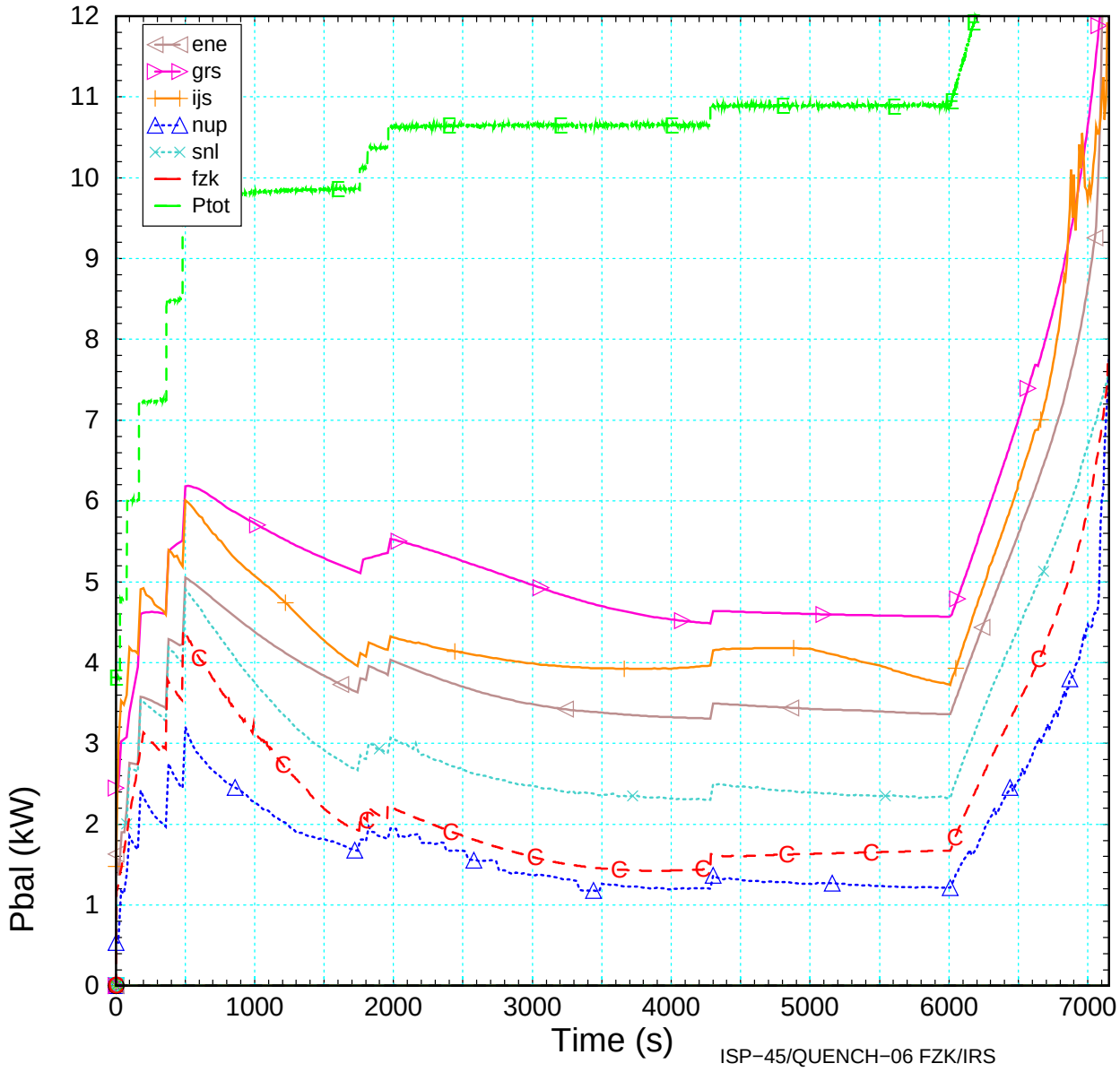

Figure 6.7 Open phase power balance derived from data delivered by the participants without consideration of axial heat losses in the electrodes compared to FZK post-test results (-C-).

In detail, GRS maintained the rather high residual energy of app. 4.8 kW at 6000 s, IJS significantly reduced its value from 10.2 to less than 4 kW and NUP slightly reduced their value from app. 2 kW by 10 %. The value of ENE dropped from 7 kW to app. 3.4 kW, which is still above the FZK value. The difference may be explained by the missing heat losses through the shroud above the heated section as mentioned by the participant. Compared to the total electrical power input, the residual power is still too high, but for a final explanation, the contributions to the values used for this energy balance have to be checked in detail by the participants.

6.2.3 Reflood phase

As can be seen in Figure 6.8 the local heat release due to clad oxidation is in the range of the total electrical power input (Figure 6.6). As can be seen clearly, the oxidation is reduced due to the fast water injection for a short period of time in the experiment, and this effect is reproduced in most calculations.

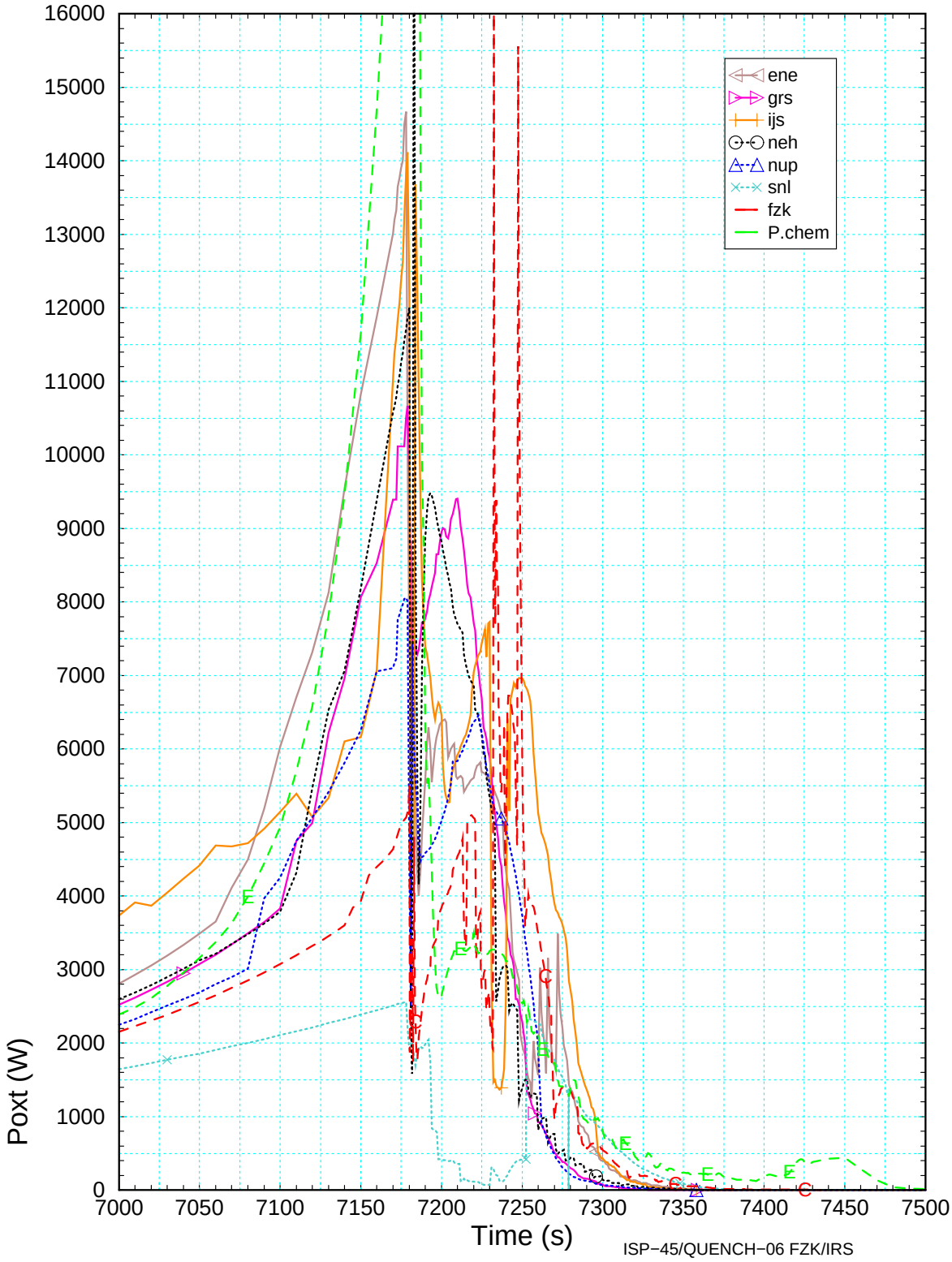

Figure 6.8 Open phase exothermal energy released during reflood phase compared to experimental data (-E-) and post-test analyses with S/R5irs (-C-).

In FZK calculation, two spikes indicate shattering in two meshes, however, as it is modeled in S/R5irs, with reduced surface area to account for crack oxidation. They increase the temperatures locally, but do not significantly delay the cool-down process, as can be seen in Figure 6.9. For comparison the steep curve (-q-) shows a rapid quenching without additional energy release due to oxidation, when it is assumed that no delay for the quench water injection into the lower plenum has occurred.

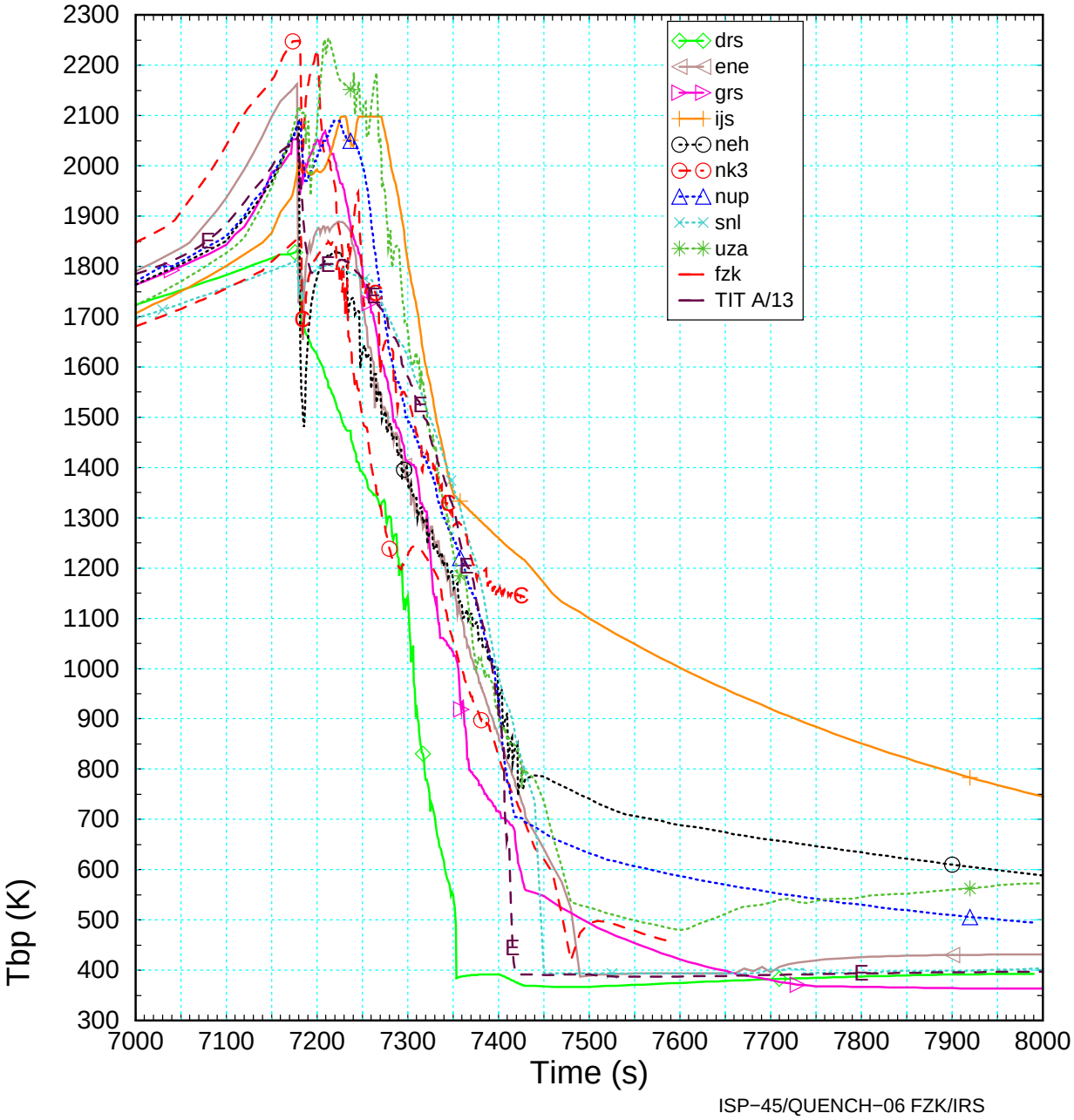

Figure 6.9 Open phase cool-down behavior compared to experimental results (TIT A/13) and FZK post-test analyses (16 axial meshes: -C-, 32 axial meshes: -c-).

In nearly all cases, the temperature drop very fast to 400–800 K, but then a slow cool-down is calculated due to the un-wetted sections in the upper electrode zone. This cool-down curve is caused by heat transfer from the clad surfaces to the evaporated steam. The reason for the deviation of the IJS curve is that during the temperature excursion some of the modeled thermocouples were partly converted into debris, which caused an excessive surface blockage in one cell of the second radial ring at axial level 0.75 m. So only in this cell the clad did not cool as fast as it should, and at some time it becomes the hottest cell. Everywhere else the cool-down rate was correctly predicted. This example shows that modeling of unessential details can in some cases significantly influence the simulation results.

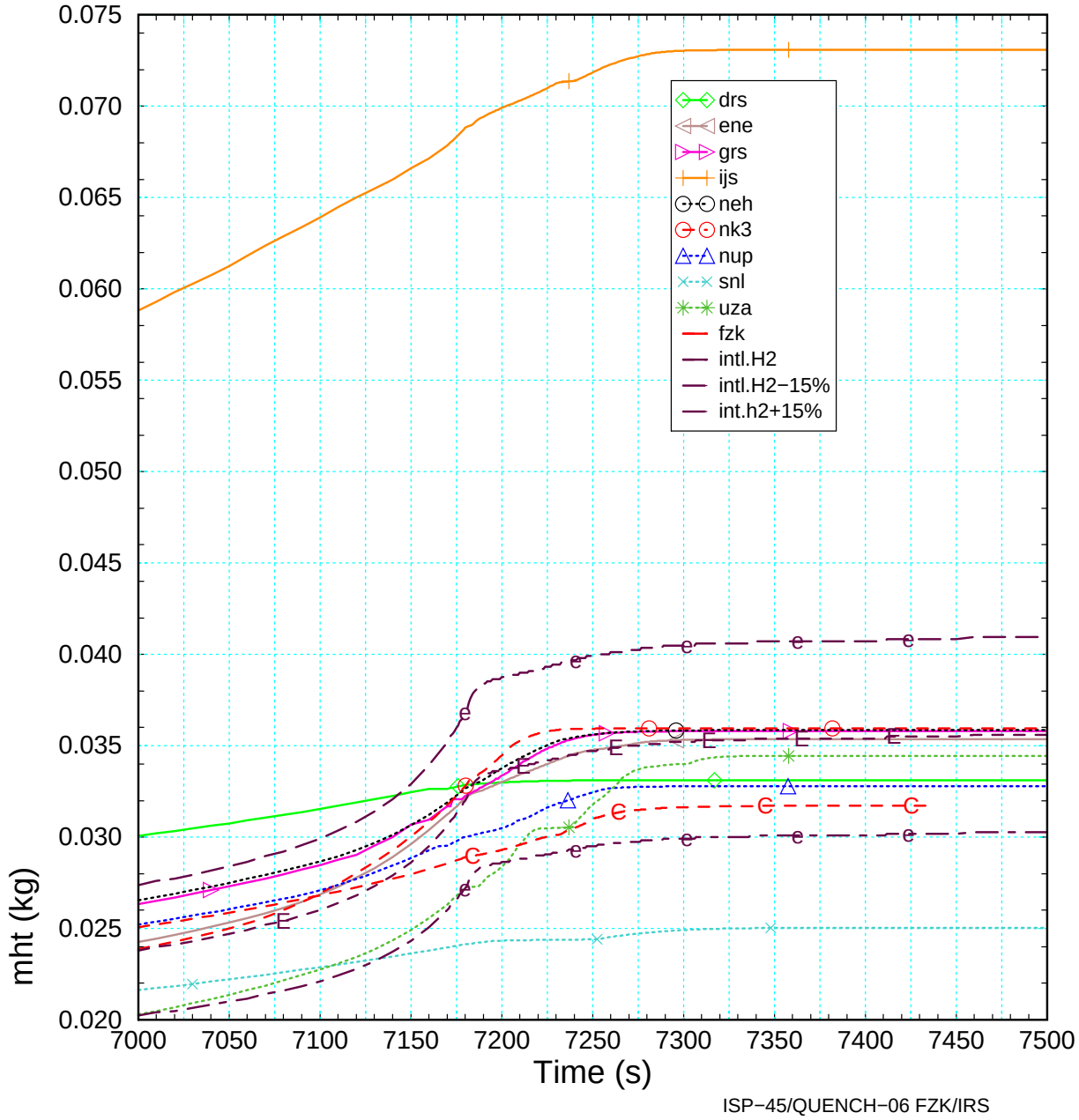

Figure 6.10 Open phase hydrogen mass-produced during reflood phase.

6.3 Summary of open phase

The participants in the open phase improve their modeling of QUENCH-06 solely by input deck optimization. However, the results still show difficulties of the code users to simulate adequately non-reactor specific environments, especially the shroud component. Similar problems arose in the PHEBUS facility, where the annular gaps in the shroud are closed due to thermal expansion of the insulating material during test.

The non-use of so-called shattering options or models or even modification of the activation criteria significantly reduced the deviation to experimental data and the spreading within the participants.

Other participants, who could not deliver the results in time, showed that their codes are able to simulate QUENCH-06 adequately. Their comments are given in the appendix.

7 RECOMMENDATIONS FOR OECD AND FUTURE ISPS ORGANISATORS

Based on our experience we would like to give the following recommendations for the OECD/NEA/CSNI as well as for the organizers of future ISPs to enhance efficiency of the organization and to improve the worth of ISPs.

1. Share experience between organizers of different ISPs of different types (e. g. problems of containment ISPs may be similar to in-vessel ones) to reduce organizers' work and improve efficiency. For instance, CSNI groups ISPs devoted to a given topic and tries to bring together organizers and participants.
2. Data and information transfer by E-mail is very efficient. Establishing a web server for information, e.g. for frequently asked questions or for the transfer of large amounts of data may be rather time consuming without giving an adequate benefit. An ftp server may be sufficient for this purpose, but consumes less maintenance work.
3. Request clear statements about all the code modifications and clear descriptions why they were performed (e. g. for ISP-45: thermal-hydraulics of MAAP and MELCOR improved, deficiencies in SCDAPSIM, MAAP, MELCOR found, model shortcomings identified)
4. Encourage exchange of information and experience among participants prior to the ISP, e.g. by encouraging the code developers to present their code and their ability to transfer knowledge to all interested participants.
5. Prefer blind exercises, which give more insight into code capabilities, but encourage participants to participate in open phase to deepen knowledge and to learn from errors. Since more and more scientific personal has to work on more and more different projects, the users and their organizations should be aware that the benefit for the users experience is substantially increased when more than only a short portion of their working time is dedicated to an ISP.
6. For blind ISPs use experiments, where similar tests have already been run in the same facility and make all details available for the participants, to allow them to become familiar with the facility.
7. Encourage participants to use the experience gained from other experiments of the same or a similar program. After an ISP all participants should have gained enough experience to adequately simulate experiments in that specific facility.
8. Taking in mind e.g. the ongoing alternation of generations or organizations with less experience in the field of the given ISP, be aware that there may be two groups of participants:
   (1) more experienced users, who mainly aim at code validation and assessment
   (2) less experienced users, who also aim at user training and know-how transfer.
9. Request from the participants a statement of their code assessment work. Code developers and code users have to be considered differently, because code developers are supposed to have a broader basis for and to spend more time on code verification than most users.
10. Be aware that the participation in an ISP needs much courage, because delivering results outside the main stream may be considered as a failure, not only of the participant himself – which is discouraging enough - but also of his organization.

8 SUMMARY

The OECD/NEA/CSNI International Standard Problem No. 45 refers to the FZK out-of-pile experiment QUENCH-06, where an overheated bundle of electrically heated fuel rod simulators in a geometry representative for Western Light Water Reactors has been quenched with water. In a first, the blind phase of the exercise, where only those data were released which were absolutely necessary for the calculations, 21 participants from 13 countries contributed with 8 different codes. In a second, the open, phase all experimental data were made available to the participants, and in sum 10 participants delivered results. The summary of this effort has to address several rather different facets, as will be discussed hereafter.

Experiment

The QUENCH-06 bundle has withstood the experimental transient with essentially intact geometry, whereas considerable cracking and some fragmentation of clad and ZrO_2 pellets occurred during the phase of water quenching. This behavior was dominated by the strong steam oxidation of the fuel rod simulator cladding (external side), the corresponding ZrO_2 scale growth, and the embrittlement of the residual metallic material. Interaction between the cladding and the ZrO_2 simulator pellets, rod-internal melt formation, and internal oxidation by steam ingress along through-wall cracks were of secondary importance. These post-test examination results correspond reasonably well to those of the temperature and hydrogen evolution measurements.

Hydrogen release

Close similarities are seen between QUENCH-06 and QUENCH-04 and QUENCH-05 - the two latter ones being rapidly steam-cooled - concerning the moderate response of bundle temperature and H_2 production during quench or cool-down. On the other hand in QUENCH-01 important crack surface oxidation was found, and in QUENCH-02 and QUENCH-03 considerable melt relocation and oxidation had taken place, connected with a temperature excursion during the quench phase.

Some participants would have preferred to investigate a test with a massive hydrogen release as found in QUENCH-02, QUENCH-03, and CORA-13 (ISP-31). However, so far most of the participants as well as the organizers cannot adequately simulate these experiments. Hence a test like QUENCH-03 would not have been more appropriate for this ISP, but should be considered in a future ISP, when the respective modeling work is more advanced.

Code performance and nodalization

As asserted by the participants and also believed by the organizers, the codes, used in this exercise, were assumed to be qualified for such scenarios, to include all features to simulate the FZK out-of-pile experiments CORA and QUENCH, and hence to participate successfully in ISP-45. Nevertheless FZK delivered code improvements to code developers especially for this ISP to reduce the uncertainty of modeling the peculiarities of the QUENCH facility, namely the electric heater and shroud models.

Whilst during heat-up and oxidation, no significant model weaknesses were found, the codes still suffer from inadequate simulation of the reflood phase. The ICARE/CATHARE code only used the simplified built-in thermal-hydraulics model of ICARE2V3; therefore the involved par-

ticipants should repeat the exercise with the extended capabilities of the combined code. During the ISP-45 exercise code improvements were performed by EDF for MAAP and by SNL for MELCOR. The models are still in a fabric state, but they may reduce the respective insufficiencies. Thermal-hydraulic packages developed for design basis accidents seem to be more appropriate (ATHLET-CD, SCDAPSIM), but still have difficulties at high surface temperatures.

Further improvements may be desirable with respect to the oxidation correlations and the clad failure criteria, which is still a user parameter and cannot appropriately describe thermal shock triggered clad failure as observed in QUENCH-06.

Participants found - and this is strongly supported by the organizers' experience - that for a reasonable modeling, the maximum axial mesh length should not exceed app. 0.07 m. Such a mesh length may give problems for reactor applications. Therefore, as a minimum requirement for realistic calculations, some code developers suggest an automated mesh refinement strategy at least for calculations of reflood situations.

Participants' experience

Depending on their experience with severe accident codes the participants could be divided into two groups: more and less experienced users. The first group includes code developers as well. Their members were able to correctly analyze the case and deliver mostly results within the mainstream. Nevertheless their results also tended to over-predict the hydrogen production during reflood.

The second group includes users starting with analyses of severe accidents or of out-of-pile experiments, e.g. younger scientists and engineers and partly members of Eastern European countries. They firstly had to get experience during the performance of these analyses. For this reason their results were evaluated separately. However, they profited significantly from the knowledge of the first group of participants in identifying errors and adopting techniques for efficient modeling, as could be deduced from the comparison of blind and open phase results. For this group ISP-45 could be considered as a successful training associated with transfer of know-how, as it should be for the sake of continuity of work and knowledge.

Participation in the exercise has maintained or even improved the expertise of participants, not only for those in the second group. The participants also understood the difficulties in modeling the combined problem of thermal-hydraulics and fuel rod behavior under fast transient conditions.

Organizers' experience

The organizers, who work on experimental analyses since the CORA program, realized that during the years a lot of experience had been collected and transferred into the in-house code versions of SCDAP/RELAP5. Most of the improvements were published and made available to code developers, but even the newest code versions SCDAP/RELAP5 mod 3.3 and SCDAPSIM did not take credit of the available improvements.

General findings

Despite some large discrepancies between some measured and calculated results, especially during the quench phase, a blind exercise like ISP-45 has turned out to be valuable, because

the participants are forced to assess the code capabilities in a more profound way than simply to modify input parameters to fit the code predictions to known experimental results. However, it should be followed by an open phase for a more sophisticated evaluation and a more extended verification of code or facility models.

Comparing results of the blind phase indicates not only differences in the mechanistic treatment of phenomena but also some inadequate balancing between them. It is most important for the simulation of severe situations not only to consider all pertinent phenomena, but also their inter-dependencies. A reasonably revised ranking of the relevant phenomena will help to limit the necessary analytical effort also for more severely damaged bundles. It is emphasized that this ranking must be done carefully to avoid inappropriate model development. As an example the large over-prediction of hydrogen release in ISP-45 was mainly caused by application of the shattering models, originally developed to explain the measured hydrogen source term of ISP-31.

ISP-45 may be considered to be a first step for further code validation concerning the aims of the QUENCH program. So the organizers invite the participants of ISP-45 to actively participate in the ongoing QUENCH experiments. Future tests are intended to enlarge, to verify or to precise the findings drawn from the past tests, including the influence of absorber components. This will contribute to an improvement of the mechanistic basis for future code development and verification efforts.

9 ACKNOWLEDGMENT

The broad support needed for preparation and execution of the OECD/NEA/CSNI ISP-45 is gratefully acknowledged. In particular, the authors would like to thank the QUENCH staff at IMF for all the work that is related to such a project. They also appreciate the contribution of all participants to clarify unexpected data. Especially we appreciate the careful reading of the manuscript and the valuable comments by J. Royen as well as R. Krieg and U. Imke.

Last but not least the authors thank all participants for the time and effort they spent on this work and for their courage to join an adventure the outcome of which nobody knows in advance.

10 LITERATURE

/1/ Hofmann P., Homann C., Leiling W., Miassoedov A., Piel D., Schmidt L., Sepold L., Steinbrück M.; Results of the Commissioning Tests, Wissenschaftliche Berichte, FZKA-6099 (August 1998).

/2/ Hofmann P., Hering W., Homann C., Leiling W., Miassoedov A., Piel D., Schmidt L., Sepold L., Steinbrück M.; QUENCH-01 Experimental and Calculational Results, Wissenschaftliche Berichte, FZKA-6100 (November 98).

/3/ Hofmann P., Homann C., Leiling W., Miassoedov A., Piel D., Schanz G., Schmidt L., Sepold L., Steinbrück M.; Experimental and Calculational Results of the Experiments QUENCH-02 and QUENCH-03, Wissenschaftliche Berichte, FZKA-6295 (July 2000).

/4/ Hering W., Homann C.; Improvement of the Severe Accident Code SCDAP/RELAP5 mod 3.2 with respect to the FZK QUENCH Facility, FZKA 6566 (December 2001).

/5/ PSF-Information: http://psf-nt-server.fzk.de/psfhome.htm.

/6/ ZIRCONIA Insulation Boards and Discs Types ZYFB-6 and ZYFB-3 (http://www.zircarzirconia.com/ZYFB-3ZYFB-6.htm).

/7/ Sepold L., Homann C., Miassoedov A., Piel D., Schanz G., Schmidt L., Stegmaier U., Steinbrück M.; Experimental and Calculational Results of the QUENCH-06 Test (OECD ISP-45), Wissenschaftliche Berichte, FZKA-6664 (in preparation).

/8/ Hering W., Homann Ch., Miassoedov A., Steinbrück M.; Specification of the International Standard Problem ISP-45 (QUENCH-06), OECD/NEA/CSNI/R(2001)1, Internal Report Nuklear-3355, (http://www.fzk.de/isp45).

/9/ Hering W., Homann Ch., Lamy J.-S.; First survey of global data of ISP-45 blind phase, Internal Report Nuklear-3359 (August 2001).

/10/ Frepoli C., Hochreiter L.E., Mahaffy J., Cheung F.B.; A noding sensitivity analysis using COBRA-TF and the effect of spacer grids during core reflood, ICONE-8711, Proceedings of ICONE-8, April 2-6, 2000, Baltimore, MD, USA.

/11/ Olander D. R.; Materials chemistry and transport modeling for severe accident analyses in light water reactors, I: External cladding oxidation, NED 148 (1994), pages 253-271.

/12/ Firnhaber M., Trambauer K., Hagen S., Hofmann P.; CORA-13 experiment on severe fuel damage : OECD/NEA-CSNI international standard problem no. 31 ; ISP-31 ; comparison report, OECD/NEA/CSNI/R(93)17, Wissenschaftliche Berichte KFK-5287, GRS-106, July 1993.

/13/ Firnhaber M., Trambauer K., Hagen S., Hofmann P.; CORA-W2 experiment on severe fuel damage for a Russian type PWR; comparison report; OECD/NEA-CSNI international standard problem ISP 36, Wissenschaftliche Berichte, FZKA-5711 (1996).

/14/ Analytis G. Th.; Developmental assessment of RELAP5/MOD3.1 with the separate-effect and integral experiments: Model changes and options. PSI-Ber.96-09 (April 1996).

/15/ Elias E., Sanchez V., Hering W.; Development and validation of a transition boiling model for RELAP5/MOD3 reflood simulations, NEDEA 183 177-332 (1998).

/16/ Cole R.; ELCOR Core Reflood Modeling and Applications to QUENCH Experiments, CSARP Meeting, May 7-9, 2001, Bethesda, Maryland, USA.

/17/ Berdyshev A.V., Boldyrev A.V., Palagin A.V., Shestak V.E., Veshchunov M.S.; SVECHA/ QUENCH Code for The Modeling of Reflooding Phenomena in Severe Accidents Conditions. Proceedings of the Ninth International Topical Meeting on Nuclear Reactor Thermal Hydraulics (NURETH-9), paper Log_19 (CD-ROM edition), San Francisco, California, 1999. (http://www.ibrae.ac.ru/english/kiselevae.html).

/18/ Allison C. ; private communication, October 2001.

/19/ Mühl B.; Programm Nukleare Sicherheitsforschung, Jahresbericht 2000, Wissenschaftliche Berichte, FZKA-6653, p. 239-250 (September 2001).

/20/ Stuckert J.; private communication, November 2001.

/21/ Leskovar M.; private communication, November 2001.

/22/ Hering W., Homann Ch., Lamy J.-S.; Comparison Report on the Blind Phase of the OECD International Standard Problem No. 45 Exercise (QUENCH-06), FZKA-6677, March 2002.

/23/ Miettinen J., Hämäläinen A.; private communication, March 2002.

11 APPENDIX

11.1 Open phase database received

Modifications

Table 11.1 List of modifications for DRS ICARE/CATHARE open phase calculations

Model	Parameter (default value)	Blind	Open	Comments
Reflooding	MESH (LARGE)	LARGE	LARGE	Means that an additional convective flux is used to minimize the error on the axial conduction in the cladding
	ALFA (0.995)	0.995	0.995	Limit void fraction for which the model considers that enough water is present for reflooding.
Zircaloy oxidation	PHYS (URBANIC)	URBANIC	URBANIC	Correlation selected.
	AREA (REDUCED)	REDU-CED	REDU-CED	In this case the surface is automatically reduced if a contact is detected.
	FGAI (0.0)	0.0	0.0	Distribution factor used to calculate the oxygen gain in the zirconia phase when all the β-Zr has been consumed.
	MULT (1.0)	1.0	1.0	Multiplying factor of the exchange surface where oxidation occurs.
	PHYSM (PROTECTI)	PRO-TECTI	PRO-TECTI	Oxidation mode for a material located in a mix-ture relocated on a component face.
	STOP (10^{10})	10^{10} 6900.s	10^{10} 6900.s	Time at which the oxidation stops (6900 s for the withdrawn corner rod).
	STAR (0.)	0.	0.	Time at which the oxidation starts (s).
	TBEG (600.)	600.	600.	Temperature at which the oxidation starts (K).
	OSTA (NO)	NO	NO	Option to account for ZrO2 dissolution in fully starvation conditions.
	GEFI (NO)	NO	NO	Option to allow the oxidation process after the disappearance of the β-Zr layer according to the Pawel approximation.
	TDER (NO)	NO	NO	Option to take into account the derivative of the temperature in the evaluation of the oxidation reaction.
Heat conduc-tion	CONT (0.0)	0.0	0.0	Contact resistance.
	FVOL (1.0)	1.0	1.0	Volume fraction of the component participating in the conduction (1.0 means full participation).
Concentric cylinders	CONT (10^{10})	0.0	0.0	Instant of contact by means of which the contact between cylinders can be enforced as soon as the calculated value exceeds this value.

Model	Parameter (default value)	Blind	Open	Comments
Electrical supply	STAR (0.0)	0.2	0.25	Outer circuit resistance (mΩ).
Radiation exchange	GAS (TRANSPARENT)	GREY	GREY	Spectral integration model.
	MULT (1.0)	1.0	1.0	Multiplying factor for geometric mean bean length. In this case the values are automatically calculated by the code (PHEBUS type bundle).
	PGAS (10^{10})	1.0	1.0	Time step separating two updates of the gas absorption properties.
	PHYS (LEBOURGEOIS)	LEBOURGEOIS	LEBOURGEOIS	Correlation for the calculation of the steam absorption band characteristics.
Decanting (radial movement of materials)	STAT (DISLOCATE)	DISLOCATE	DISLOCATE	Condition to allow the decanting through layers present on a cylinder. In this case, the layers have to be DISLOCATE.
	BLOC (NO)	NO	NO	Option to allow or not the decanting process in blocked meshes.
	LIQF (0.0)	1.0	1.0	Liquid mass fraction in a layer above which the partially molten materials can move radially.
	RULE (CONTINUE)	CONTINUE	CONTINUE	The decanting process is not sudden.
	TYPE (STANDARD)	STANDARD	STANDARD	Option for decanting mode. In this case it obtains to the standard ICARE2 rules for the mixing of molten materials.

Table 11.2 List of modifications for GRS ATHLET-CD open phase calculations

Type		**blind calculation**	**open calculation**
material properties of plug / electrodes	ρ, c_p, λ		revised
electrical resistance of electrodes		Wo	Wo and Cu
material properties of rod / heated zone	ρ, c_p, λ		revised
gap heat transfer coefficient of rod	α_{gap} [kW/m^2/K]	15.0	0.5
axial heat transfer coefficient at rod end	α_{axial} [kW/m^2/K]	1000.0	1.0
hydraulic diameter of rod (BUNDLE)	d_{hyd} [mm]	d_{hyd} / 0.36 d_{hyd}	0.5 d_{hyd} / d_{hyd}
inlet fluid temperature (INPIPE)	T_{fluid} [K]	TFS 2/1	TFS 2/1 + 20.0
thickness of porous ZrO_2, elev. –0.3 to –0.2m	d_{porous} [mm]	$d_{(ZrO2)}$	0.27 $d_{(ZrO2)}$
heat capacity of porous ZrO_2	c_p [J/kg/K]	630.0	315.0
artificial heat conductivity of Ar-gap (SHRTOP)	$\lambda(T)$ [W/m/K]	$\lambda_{(Ar)}$	0.5 $\lambda_{(Ar)}$
thickness of Ar-gap, elev. 1.20 to 1.30 m	d_{Ar} [mm]	d_0	0.32 d_0
number of steel layers at elev. 1.30 to 1.50 m	n_{TOPSHR} [-]	1	2
heat transfer coefficient between steel layers	α_{TOPSHR} [W/m^2/K]	--	200.0
oxlim of rod after quench (t > 7179 s)	$d_{oxlim,rod}$ [mm]	0.020	no limitation
oxlim of shroud after quench (t > 7179 s)	$d_{oxlim,shroud}$ [mm]	0.020	0.200
oxlim of shroud before quench (t < 7179 s)	$d_{oxlim,shroud}$ [mm]	no limitation	0.200

Note: plug calculation, material properties
limitation of protective oxide layer (structure), oxlim
wall condensation with non-condensible gases

Table 11.3 List of modifications for IJS MELCOR open phase calculations

IJS Type	blind calculation	open calculation
Electrical heating system modeling	- electric heating modeled with DCH package as decay heat - time independent axial power density profile CORZjj03 determined from resistivities of W, Mo and Cu electrode zones at average temperatures - time independent radial power density profile CORRii03 determined from approximate ratio of electric power of inner and outer ring (40%/60%)	- electrical heating modeled with user subroutine ELHEAT - W, Mo, Cu temperature dependent resistivities considered - inner and outer ring electric power considered - above (>1.5 m) and bellow the simulated region (<-0.475 m) electrode resistivities calculated at approximate average temperatures (0.5* [T_boundary + 300 K(water cooled)]) - 4.2 mO additional resistivity due to wires
COR000NS – global support rule for nonsupporting structure (mostly ZrO2 pellets)	- support rule for NS: ROD - temperature above which NS will collapse: 1700 K (steel melting temperature) - for some cells different support rules were specified	- support rule for NS: FIXED (since the pellets are hold by the W electrodes) - temperature above which NS will collapse: 2990 K (ZrO2 melting temperature); for the inner unheated rod (COR01NS): 2400 K (default cladding failure temperature)
COR000SS – global support rule for supporting structure	failure temperature: 2500 K ((Zr shroud and grid spacer)	failure temperature: 2400 K (default maximum ZrO2 temperature to hold up molten Zr)
CORijj06 – surface area record	surface of fuel, cladding and shroud determined as the whole surface (inner, outer, upper, lower) – about 2x too large	surface of fuel, cladding and shroud determined correctly
Sensitivity coefficient 1132 (1) – core component failure parameters	temperature to which fuel rods can stand in the absence of unoxidized Zr in the cladding: 2990 K (ZrO2 melting temperature) – not correct since ZrO2 pellets were modeled as NS	temperature to which fuel rods can stand in the absence of unoxidized Zr in the cladding: 3695 K (W melting temperature), since the fuel is composed of W
Mass flow rate of quench water	as in q06_boundcond.dat (see also last row in the table)	0 kg/s till the quench phase due to quench water pipe draining, otherwise as in q06_boundcond.dat
Steam and argon inlet temperature	- steam: 437.5 K - argon: 294 K	- steam: 607.7 K (as TFS 2/1) - argon: 607.7 K (as TFS 2/1)
Heat structure package	- shroud not modeled as heat structure, so the heat flux from control volumes on the inner side of the shroud to control volumes on the outer side of the shroud is not correct - heat structure on the top of the simulated region (1.5 m) isolated	- shroud modeled as heat structure - heat structure on the top of the simulated region (1.5 m) cooled with water to increase axial losses
Mass flow: argon, steam, water	Mass flow defined with tabular functions: mass flow as a function of time. But when the mass flow was calculated instead of the argument "time" the argument "mass flow" was taken (input bug). So the mass flow was the initial mass flow during the whole simulation (Ar: 3 g/s, steam: 3 g/s, water: 0.6 g/s – that means no quench water at all)	The mass flow of argon, steam and water was calculated correctly as a function of time.

For blind and open calculations minimum oxidation temperature is assumed to be 900 K instead of the code standard value of 1100 K. For open calculations mainly user errors have been corrected.

Table 11.4 List of modifications for UZA SCDAPSIM open phase calculations

Type	Blind calculation	Open calculation
Option 30	Option 30 is used.	Option 30 is switched off. This option causes a large increase in the heating of the system, especially in the quench phase.
Control option	On the time step control cards control option 39 is used (it allows automatic selection of the semi-implicit or the nearly-implicit advancement scheme based on the current time step and Courant limit).	Control option 3 is used (it specifies the semi-implicit advancement scheme), because it increases stability of the calculation.
Argon injection	Argon is injected into the lower plenum at all time during the experiment.	At the beginning of the water quench phase argon is no longer injected into the lower, but into the upper plenum (it is represented with time dependent volume 050 and with time dependent junction 051 in figure 2).
Quench water temperature	Temperature of quench water is 297.6 K	Temperature of quench water is 370.0 K.
Fast quench water injection	Fast quench water mass flow rate was determined in order to fill the lower plenum within 5 seconds.	Fast quench water fills the lower plenum up to –300 mm in the time interval from 7179 s to 7182 s.
Argon cooling of jacket	Argon cooling of jacket is modelled directly with one pipe, two time dependent volumes, one time dependent junction and one single junction component (figure 1).	Argon cooling of jacket is modelled with series of 13 time dependent volumes and junctions connected to a dummy pipe component. This means that temperature boundary conditions are applied to the outer surface of the shroud and to the inner surface of the cooling jacket (heat structure 13) – figure 2.
Electric power input	The electric power input is as specified.	Electric power input equals 0.945*Ptot(t). When power factor is 1.0 then there's a high bundle peak clad surface temperature increase during the quench phase.
Upper part of the shroud insulation	There are used argon properties that include low thermal conductivity and low heat capacity for the last 3 nodes of the shroud insulation.	Argon in the upper part of the shroud insulation is replaced with an artificial null material that has very high thermal conductivity and low heat capacity.
Lower part of the shroud insulation	Built-in ZrO_2 properties are used for bottom 13 nodes of the shroud insulation.	Specified shroud fibre insulation properties are used (reference 2). Use of the new thermal conductivity values, as they were given in the final draft of the ISP-45 specification, results in high temperature gradient between shroud inner and outer surface. This causes an increased heating in the bundle test section so the lower values of the electricity power input have to be used.

Type	Blind calculation	Open calculation
Shroud outer surface boundary conditions	RELAP5 control volumes that provide boundary conditions are pipe 034 and pipe 040 components. The fluid used in pipe 034 is argon, and in pipe 040 that fluid is water.	Time dependent volumes 060–084 provide boundary conditions as described in argon cooling of jacket section. The boundary conditions (inner cooling jacket temperatures at various elevations) are obtained from the data file q06_boundcond.txt. The interpolation was used to calculate temperatures at all 13 elevations. Same as in the blind calculation component pipe 040 is used for upper 3 nodes to provide boundary conditions.
Cooling jacket inner surface boundary conditions	The boundary conditions are the same as for the shroud outer surface in the blind calculation.	The boundary conditions for the upper 3 nodes are the same as for the shroud outer surface in the open calculation. Temperatures needed to describe boundary conditions for the bottom 13 nodes of the cooling jacket inner surface are entered in the general tables.
Cooling jacket outer surface boundary conditions	They are defined as temperature boundary conditions. These temperatures are entered in the general tables.	Same as for blind calculation, but for bottom 10 nodes temperature values are 20 K less (than they were in the blind calculation), and for 3 nodes above them temperatures are 10 K less. This is based on the reference input [1].
Fluid distribution tube in lower plenum	modeled, as heat structure 022.	not modeled.
Plenum length of the unheated rod	0.06 m	0.066 m
Plenum void volume of the unheated rod	$1.0 \cdot 10^{-6}$ m^3	$2.435 \cdot 10^{-5}$ m^3
Material specifications for the unheated rod	not used.	used.
Helium inventory in the unheated rod	$2.7368 \cdot 10^{-5}$ kg	$1.391 \cdot 10^{-5}$ kg
Plenum length of heated rods	0.06 m	0.01 m
Plenum volume of heated rods	$1.0 \cdot 10^{-6}$ m^3	$7.45 \cdot 10^{-5}$ m^3
Resistance of flexible wires, heated rods	0.0042 Ω/rod	0.004 Ω/rod
Inner heated rods power multiplier	0.41614	0.41
Outer heated rods power multiplier	0.58386	0.59
Helium inventory in heated rods	$2.7368 \cdot 10^{-5}$ kg	$1.24 \cdot 10^{-5}$ kg

11.2 List of participants' findings on their codes

ATHLET-CD

The oxidation limiting parameter (oxlim) that simulates shattering has been deactivated for rods in GRS. Uncertainties in material properties of the thermal insulation (shroud) have also a big impact (Argon gap) because no radiative heat transfer calculated

Improvements for open calculation

Heat transfers in the upper region because of an excursion of temperature at the outlet (RUB). Heat transfers between the rods and to the fluid, the axial heat conduction to the bottom and top ends, the heat transfers in the gap. Material properties also revised for rods, shroud insulation and Argon gas. Fluid inlet temperature revised (GRS)

GENFLO

The blind calculation with GENFLO showed three shortcomings /23/: 1. The absence of an electrical heater rod model to calculate the axial- and time-dependent heat release, 2. Radial heat losses through the shroud insulation were modeled using factory data for the insulation material, and 3. The time-discretization of the oxidation model.

Improvements for open calculation

The shortcomings mentioned above were corrected and open calculations were performed, unfortunately due to time restrictions not in time. The participant delivered some results (see section 11.3) that demonstrated the successful code improvement.

ICARE/CATHARE V1 Mod1.1

ICARE2 thermal-hydraulics package used, not CATHARE.
Small discrepancies before the quench phase at the bottom of the bundle.
Small discrepancies on clad temperature during the reflood phase.

Improvements for open calculation

Cathcart correlation gives better results than the Urbanic-Heidrick one regarding mdh9 and Tbp before reflooding.
Fluid inlet temperature modified to improve reflood prediction capability.
Fast water injection taking into account vaporization in the inlet circuit (ENE).

Fast water injection, power distribution and R_v (DRS). Problem still existing due to heat exchanges in the bottom of the bundle (Fixed temperature boundary condition in the lower electrode zone) and leading to over-estimation of quench front velocity

IMPACT/SAMPSON

Further improvements should be focused on temperature distribution in the bundle and the hydrogen generation correlation.

Improvements for open calculation

Insulation conductivity increased and static resistance R_v
Recalculation of QUENCH-01 initiated using same parameters

MAAP

In the ISP-45 two MAAP versions participate, the original version, used by FRA and an extended version used by EDF.

Original version (FRA)

Smoothing of cooling rates due to single phase thermal-hydraulics

Estimation of surface available for oxidation not clearly known and therefore mechanics during reflood missing
Coping with too conservative oxidation correlations

EDF version

For reflood scenarios code improvements with a dedicated two-phase flow model.
Urbanic correlation is somewhat better than BJ one regarding mdh9 and Tbp before reflooding.

Improvements for open calculation

Coupling with a detailed thermal-mechanical code that calculates mechanical stresses and visco-plastic deformations due to an imposed 2-D or 3-D temperature field. This allows to couple oxidation and mechanics calculation and finally permits to implement in MAAP a global fissuring model.

MELCOR 1.8QZ

Clad failure temperature is still an outstanding question.

Impact of user effects (IJS)

A need to improve and to transmit the knowledge to less experienced users.

Improvements for open calculation

Problems:
- No axial rod conduction at top end and no radiation from shroud and bundle to Ar gap (thus upper electrode zone too hot).

Problems solved:
- Geometry corrected
- Gas inlet temperature
- Shroud modeled as a heat structure and wrong mass flow rates including water during the whole calculation corrected

MELCOR 1.8RB

Electrical heating system well modeled.
Quench front tracking model that does not give so good results.

Contribution of the shroud and the upper electrode zone to hydrogen production are not negligible and underline the problem of modeling ability of user more the code efficiency.
Errors mainly depend on boundary conditions and heat losses to the shroud.
The shroud is not representative of a commercial reactor and is therefore difficult to be modeled (REZ).

Hydrogen rates with respect to their origin are uncertain up to now and cracking and oxidation during quenching are not well reproduced due to a lack of sophisticated models (artificial shattering or only increased steam availability).

SCDAP-3D

The participant mentioned that the code included an outdated heater rod model, which is not applicable to QUENCH heater rods. Therefore the temperatures were overestimated.

SCDAPSIM mod 3.2

New: Implementation of FZK heater rod model based on /4/.
Local material properties for the shroud instead of FZK-shroud model developed for PHEBUS FT facility (Gap handling)
Option 30 (radiative HT stabilization erroneous), deactivating radiative heat transfer

The crucial point for a good simulation is the proper adaptation of the boundary conditions to the potentialities of the codes.

SCDAPSIM mod 3.2(bd)
The radiative term has a very significant impact on the calculation of Tbp (overestimated) and other parameters (like radial temperature difference between heated and unheated rods overestimation) because this option deactivates radiative heat transfers from heated rods. Impact can be checked comparing blind/open results of CMX, UZA.

SCDAPSIM mod 3.2(bg4)
The code calculated wrong heat transfer coefficients for Argon containing volumes
Adjustment of thermal properties of the shroud
Radiation and convection considered in Argon gap
Input model developed by SIE
Tbp, mdh9 reduced due to modifications in the upper region (Argon gap). Besides, the shroud insulation properties result in temperatures in the lower part of the test section higher than expected.

Original reference input model have proved to be inadequate underlining that the specific conditions of the facility had a strong impact on the simulation. Coding errors in the original code version (bd) had a negative impact on 2 submittals.

11.3 Individual remarks by some participants

IJS: MELCOR

The reason for the obvious deviations of the blind phase calculation is a combination of the not modeled specific features of the electric heater system and some user errors; both caused due to the inexperience of the analyst (M. Stanojevic). In the open calculation, which was indeed performed as a blind calculation by another analyst (M. Leskovar), the electric heater system has been adequately modeled with the user subroutine ELHEAT and identified user errors were corrected. Since in the model the radiation heat losses from the shroud to the coolant jacket were not taken into account the temperature in the upper electrode zone was overestimated, with all known consequences (hydrogen mass over-prediction...). Since, however, electrical power release is rather small in that region, consequences for the heated zone should be limited.

NK3: ICARE/CATHARE

Simulated length is from –0.475 m to 1.5 m with 29 axial and 5 radial nodes. The corner rods are not taken into account. Inner cooling jacket temperature is imposed as a boundary condition. R_v = 0.22 mΩ is used.

The ISP-45 provided a good opportunity to assess the capabilities of the code to simulate the fuel rod bundle behavior in reflood/quench conditions without severe damage prior to reflood initiation. Our post-test simulation results of QUENCH-06 test were obtained with latest ICARE2 V3Mod1.1 code version.

The results of simulation are in good agreement with the experimental data. The simulated temperatures are close to the measured ones as during oxidation plateau as during escalation phase. Temperatures drop during quenching and further heat up are reproduced in ICARE2

calculations, while partial discrepancy in temperatures during middle and end of quench phase can be explained by a certain uncertainty in reflood conditions.

The sensitivity study for the QUENCH-06 test revealed that closest agreement with the experiment on hydrogen production could be received with Zr oxidation kinetics, obtained by Leistikow-Schanz, supplemented by Urbanic-Heidrick data at very high temperatures. The calculated hydrogen production for such combined correlation set corresponds to measured values both in timing and totals amount in the range of 1 g.

REZ: MELCOR

My opinion is the point discussing the benefit to plant application should be extended by the topic:

- Main difference of bundle behavior in Quench test in comparison with plant application is done by strong influence by shroud
- My personal contribution to plant application is also done by the tuning of some parameters where the default values were used up to now.

But the difference of new and default values is not significant (for example the minimum oxidation temperature was modified from 1100 K /default/ to 1040 K based on the Quench-01 open calculation).

RUB: ATHLET-CD

From our point of view we would like to stress the importance of the blind phase of the ISP. In general this is the real case, and hence what we are aiming at. Open calculations can serve as an extra opportunity for checking new models or adjusting parameters due to new findings from the experimental data, but the main attention should be turned to the blind phase.

Our intention was to stick as much as possible to the recommendations of the ATHLET-CD user-manual, thus reducing user-influence to a minimum. It is of course necessary to have a workable input-file (therefore calculations based on already performed tests are suggestive) and it is one of the crucial points in CFD that boundary conditions are implemented correctly. Keeping in mind, that the codes are developed for simulating NPPs, facilities like the QUENCH-facility need to be modeled with high additional expense.

It would be desirable to have more opportunities to perform blind calculations. Therefore it would be helpful to have a central contact-point where one can get information of planned experiments, in particular for users new in this field.

Last but not least, the ISP-45 led to an improved understanding of the handling of the ATHLET-CD code with view to user-influences.

VTT: GENFLO

Results have been delivered after the end of the open phase and could therefore not been included in section 6. Therefore the participants' results and comments are given hereafter.

The ISP-45 blind calculation with GENFLO showed three shortcomings:

1. The absence of an electrical heater rod model to calculate the axial- and time-dependent heat release (the heating power was described by the time dependent total power and fixed power profile),
2. Radial heat loss through the shroud insulation were modeled using factory data for the insulation material (the heat loss transported by the argon flow in the outer annulus was modeled by applying the total heat conduction through the insulation material taken from the factory data and using 293 K as the temperature boundary),
3. The time-discretization of the oxidation model.

The open calculation proved that our GENFLO improvement managed a fairly well agreement. We could say as well: "There are no mysterious phenomena, when the reflooding transients from temperatures below 2200 K are calculated."

Code improvements

For the open calculation the heater model was improved by programming a case specific heater module with following specific features: 1) user gives the voltage over the test section as a function of time, 2) Joule heating is modeled for the –450 mm – 1700 mm level of the test section including the molybdenum and tungsten heated sections, 3) around 20 % of the electric power are consumed by the sliding contacts and electrical cables not in contact with the fluid volumes.

Besides 1) the 6 g/s argon flow in the outer annulus was modeled, 2) the heat conduction in the insulation material was increased by 40 % based on the experiences from experiments at VTT, where factory data were found to be valid only for idealized packing conditions and 3) the geometry effect due to the cylindrical geometry was taken into the consideration.

Originally the formulation of the Urbanic-Heidrick oxidation model in the discretized form was implemented improperly, causing around 2.5 times too high oxidation. The discretized formula was needed in the application, where the GENFLO code is used for BWR recriticality calculation in the prompt power excursion conditions with the time step of 0.001 to 1.0 ms. In the post test calculation the Urbanic-Heidrick model was used in its original parabolic form. In QUENCH calculations the time step was 50 ms. Due to the modification the oxidation rate it dropped clearly. One-sided oxidation model was assumed. During the rewetting phase no scrubbing for the oxide material was assumed. The new values correspond rather well to the experimental data, as can be seen in Figure 11.1.

The maximum temperature is given in bottom left of Figure 11.1. The maximum temperature in the GENFLO -result it was 1880 K. In the experiment the maximum measured temperature was 2242 K on the 950 mm level for the peripheral rod, but a number of TCs had failed before. Thus the real experimental maximum temperatures may be even larger. Thus GENFLO underestimates the maximum temperature by 360 K or more even in the posttest calculation. In the blind calculation the measured maximum temperature of 2242 K was overestimated by 100 K.

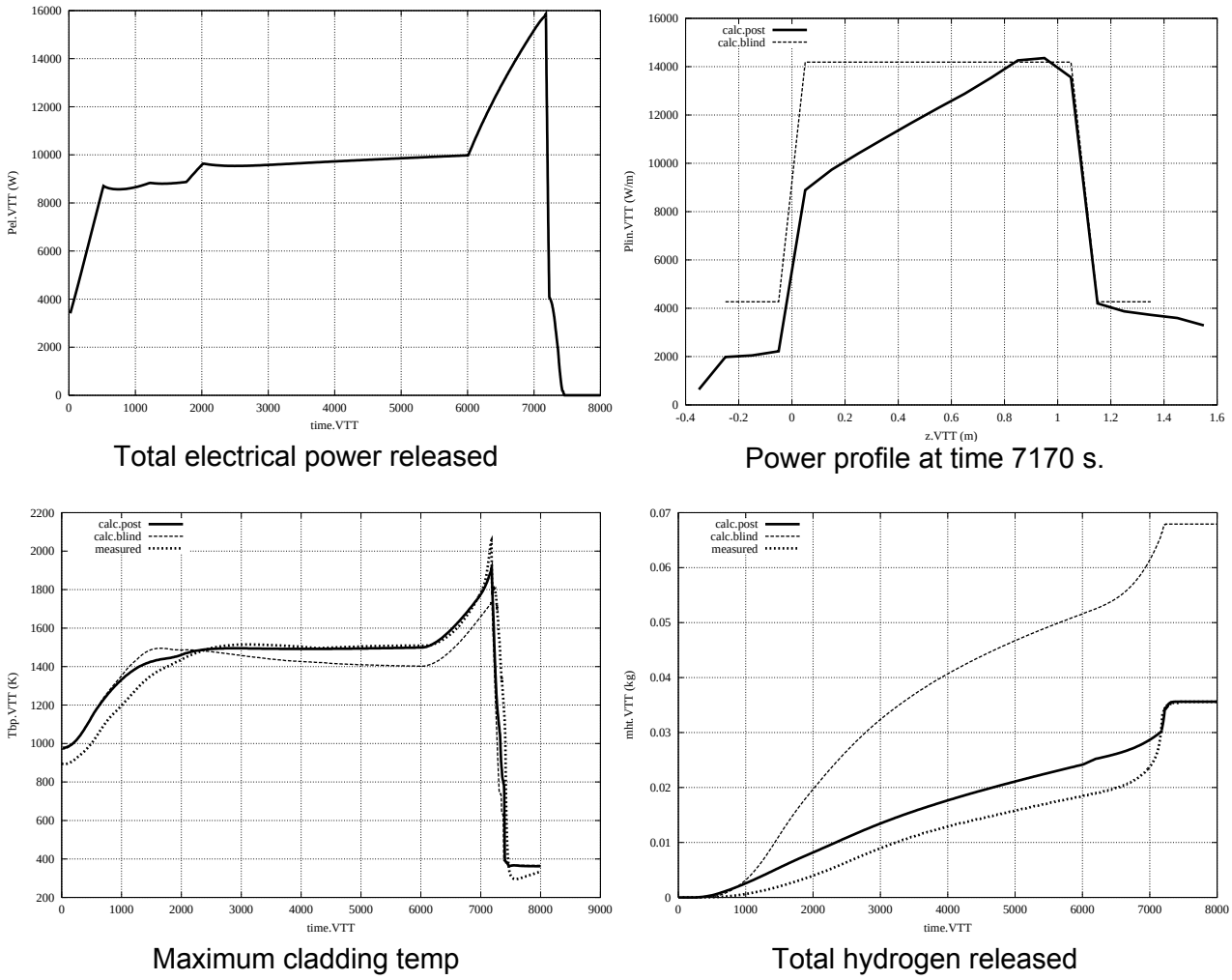

Figure 11.1 Summary of important result of blind and open calculations documenting the GENFLO code improvements achieved during ISP-45

11.4 Characteristics and normal usage of codes

In the ISP-45 specification report /8/ all participants were asked to give some information about normal application of their code, impact of ISP-45 results on their work on reactor safety, and experience to reactor safety, AMM, licensing, etc. The following sections comprise all available statements of the participants.

ATHLET-CD: GRS

The code system ATHLET-CD is developed by GRS especially for the investigation of beyond design basis accidents and accident management measures. For this the knowledge of the impact of quench processes on fuel elements is very important. The results of the well-defined and instrumented ISP experiment are a good basis to be compared with the analytical investigation with ATHLET-CD and for further improvements of the model. The ISP will be added to the validation matrix for the code and thus has a significant influence on the further development of ATHLET-CD.

ATHLET-CD: RUB

The range of application of the code ATHLET-CD comprises the whole spectrum of leaks and large breaks, as well as operational and abnormal transients for PWRs, BWRs, and VVERs. At present the analyses cover the in-vessel thermal-hydraulics, the core degradation processes in the core region, as well as fission products and aerosol release from the core and their transport in the reactor coolant system. The aim of the code development is to extend the simulation of core degradation up to failure of the reactor pressure vessel and to cover all physically reasonable accident sequences for western and eastern LWRs including RBMKs

GENFLO: VTT

The GENFLO (GENeral FLOw) code was developed at first for the BWR reactor recriticality analysis for severe accident reflood scenarios, which may be described through the following scenario:

1. BWR blackout
2. Core heat-up up to 1800 K.
3. Reflood injection will start after the depressurization.

The thermal hydraulics solution methods of the GENFLO code originate from the SMABRE code, a design basis accident code, mainly focused on the small break LOCA and used for twenty years for the safety analyses in Finland.

At present, the GENFLO code is being used in three different applications. In a code called RECRIT, the model is coupled with the 2-D transient neutronics model TWODIN for calculating thermal hydraulics during re-criticality accidents in a BWR plant. For this purpose the whole BWR vessel is modeled for GENFLO. In APROS-SA application, the model is used to calculate the PWR pressure vessel thermal hydraulics during a severe accident until the core melting and relocation and pool generation at the bottom of the reactor vessel is simulated. In the current FRAPTRAN application the model is coupled with a transient fuel behavior code to study complex fuel transients whereby special attention is given to realistic description of the thermal hydraulics in the sub-channel. Additional new applications are the severe accident thermal-hydraulics for PWR and BWR plants and subchannel models for detailed fuel analyses, mostly for DNB-conditions, but the hot pin may experience higher temperatures as 1200 c as well.

Before the ISP-45 (QUENCH-06) the GENFLO-module has only been validated against reflooding experiments, starting at surface temperatures of 870 to 1000 K. Under these conditions radiation heat transfer and Zircaloy oxidation are not important. Within the ISP-45 the physical models of the GENFLO -code were validated firstly against severe accident conditions, including cladding oxidation, radiation heat transfer, and reflooding of superheated surfaces.

ICARE/CATHARE: DRS

The ICARE2 module of the ICARE/CATHARE code was developed at IPSN and is primarily devoted to calculate the behavior of a Light Water Reactor (LWR) vessel during a severe accident, but it is also intensively used to simulate core-degradation experiments.

In the actual V3mod1 version, ICARE2 is able to represent the structures and the fluid of the vessel, as well as the degradation phenomena during the early phase of an accident (heat-up, oxidation and early material interactions) and during the late phase (melting and creation of a

debris bed, progression and flowing of the corium until the formation of a magma pool). Reflooding issues are accounted for, but partial validation is confirmed only in intact geometry.

ICARE2 already benefits from a large validation matrix on separate effect tests and on integral experiments concerning the different aspects of degradation phenomena. In particular, calculations of the CORA tests exhibited a large under-estimation of the hydrogen production during the quench phase. In order to investigate further this phenomenon and to evaluate the capability of the code to predict the thermal-hydraulics of reflooding, a part of the QUENCH program is included in the validation matrix of ICARE2: the QUENCH-01 test was calculated to assess the modeling of the test section and to validate the different code parameters; the present exercise belongs to the validation matrix too and is the occasion to check the prediction capability of the code.

ICARE/CATHARE: ENE

Information about normal application of the code, impact of ISP-45 results on our work on reactor safety, AMM, licensing, etc.

There are no nuclear power plants in operation in Italy. At present, the main objectives of our nuclear safety research is to maintain the knowledge and the expertise in this field, through the participation in international projects and collaborations with other institutions, looking forward to advanced reactors with new safety concepts including passive systems.

With this aim, we participate in various research projects on severe accidents promoted by the European Commission (Framework Program on Nuclear Fission) and the OECD/CSNI. We also have a bilateral agreement with IPSN-France. In this framework, we are largely involved in the development and validation of computer codes used in the analysis of severe accident, such as ICARE/CATHARE. Therefore, our main interest is not in nuclear plant applications, but in code model development, validation and testing.

Code models for the reflood phase computation are still under development. The ISP-45 is providing a good opportunity to assess the capability of the code (including a simple quench model), in evaluating hydrogen generation under reflood conditions starting from hot core temperatures, by comparing the results with experimental data and other code calculations.

Because of the particular situation in Italy, without nuclear power plants in operation, there are no information regarding the application of ISP5-45 results to AMM, licensing, etc.

ICARE/CATHARE: NK3

The ICARE/CATHARE code is used in NSI RRC KI for the analyses of accident transients on VVER-type NPPs. Since ISP 36 the last versions of the ICARE2 code are continuously and intensively validated in NSI RRC KI to provide better understanding of the main processes during severe accidents on VVER and other ones bundle types. The main strategy in examinations is intended to reduce the uncertainty of weakly known or undefined code parameters and to define a creditable basis for code application.

The ICARE2 V3Mod1 code (developed in IPSN, France) includes new and updated models for severe accident in-vessel phenomena covering early and late phases of the accident. This version is coupled with the thermal-hydraulic CATHARE code and both developments seem to be

particularly useful for the interpretation and planning of experiments and for scaling to the reactor conditions. In the frames of collaboration between NSI RRC KI and IPSN additional efforts were provided by NSI RRC KI to validate the new version of the ICARE/CATHARE code against a number of integral tests for PWR and VVER bundles, which belong to IPSN validation matrix. These activities apart from general examinations concerned different degradation phenomena.

- Impact of B_4C absorber rod on VVER bundles behavior in accident conditions (on the basis of CORA-W1 and CORA-W2 tests),
- Impact of SIC absorber on PWR bundle (on the basis of CORA-2 and CORA-5 tests),
- Damaged bundle behavior in quenching conditions (on the basis of CORA-12 and CORA-13 experiments),
- Molten pool and debris formation (on the basis of RASPLAV AW-200-4 test).

IMPACT/SAMPSON: NUP

The IMPACT/SAMPSON code has been developed since 1993 by the sponsorship of the Ministry of Economy, Trade and Industry, Government of Japan. Its 10-year program will end in the fiscal year of 2002. The code will be applied to detailed analyses of postulated severe accidents in PWR and BWR. The code consists of eleven modules. The QUENCH analysis validated two modules, Fuel Rod Heat-up Analysis and Molten Core Relocation Analysis modules. Other modules are being validated by the analysis of Phebus-ISP. Steam explosion analysis module, VESUVIUS has already been applied to the severe accident analysis of commercial PWR. Other modules will be applied to the analyses of actual commercial nuclear power plants in turn. The code is also expected to analyze accidents due to such as hydrogen detonation.

MAAP: EDF

For the last decade, Electricité de France has been using the MAAP code for severe accident analyses. MAAP stands for Modular Accident Analysis Program. It is developed under the leadership of EPRI (USA) by the contractor Fauske & Associates Inc. (FAI, USA). The last official version (MAAP 4.04) has been released in fall 1999.

Because of the modular structure of MAAP, it is possible for users to adapt and run the code to model experiments for validation and benchmarking purposes. However it still requires a few modifications in the code to model specific geometry and physical phenomena and to define initial and boundary conditions.

MAAP: FRA

MAAP code is the reference scenario code in FRAMATOME ANP SAS. Numerous severe accident studies have been performed for French existing plants and for plants under development, such as the European Pressurized water Reactor (EPR).

Regarding existing reactors, Framatome used MAAP code in several studies for EDF. Regarding the EPR, severe accidents consequences were taken into account since the very beginning of the reactor design, and in particular to design mitigation equipment, such as recombiners and corium core-catcher. MAAP is the reference code for EPR in-vessel analysis. It has been used for several scenarios, including reflooding scenario, to define the source terms (water, steam, H_2, fission products, corium) for the reactor building.

MELCOR: IJS

At “Jožef Stefan Institute”, MELCOR code is primarily used for simulations of possible severe accidents in “Krško” PWR Nuclear Power Plant, in Slovenia, where MAAP code has been used for the same purposes. The results of the ISP-45 will help to estimate the reliability and accuracy of the MELCOR calculations of hydrogen production during the emergency cooling of the core with the safety injection systems, which will be important also in comparisons with the corresponding MAAP calculations.

An impact of ISP-45 may become important in future if the results of MELCOR simulations of severe accidents in the "Krsko" Nuclear Power Plant are compared with the corresponding results of MAAP simulations, maybe for some licensing purposes. The research institutions - Jožef Stefan Institute in Ljubljana and University of Maribor, and Slovenian Nuclear Safety Administration use MELCOR, whereas "Krsko" Nuclear Power Plant uses MAAP.

At this moment, we do not have any research or development projects for "Krsko" NPP, in which the use of MELCOR is requested or necessary, but there is a certain probability for such a project in a near future.

MELCOR: NK2

See NK3

MELCOR: REZ

The MELCOR code is very extensively used for the analysis of severe accident of nuclear reactors in Czech Republic. The code is used for analysis of both types of VVER reactors - VVER-440/213 (Dukovany NPP) and VVER-1000 (Temelin NPP) with the topics of the source term estimation and severe accident progress evaluation. The extended experience obtained from the work on the ISP-45 will significant improve, for example, the capability for the SAMG validation framework, which will include also the sequences with reflooding of overheated or partly damaged core.

MELCOR: SES

Studsvik EcoSafe has many years of experience in safety and severe accident analyses. Previously, the main code for severe accident was SCDAP/RELAP5 but from now on MELCOR will be the main code. One NPP accident analyses has been performed with MELCOR for a PWR on behalf of the Swedish authorities. A BWR study is under performance. The main purpose for EcoSafe to participate in the ISP-45 is mainly to get better knowledge about code behavior and better understanding of the modeling of the quench processes.

MELCOR: SNL

The MELCOR simulation code is being developed at Sandia National Laboratories for the U.S. Nuclear Regulatory Commission. It is available to United States citizens and to members of CSARP. MELCOR is a fully integrated, engineering-level computer code that has the ability to model a broad spectrum of severe accident phenomena in both boiling and pressurized water reactors in a unified framework. These phenomena include thermal-hydraulic response in the reactor coolant system, reactor cavity, containment, and confinement buildings; core heat up, degradation, and relocation; core-concrete attack; hydrogen production, transport, and combustion; fission product release and transport behavior.

MELCOR serves as a second-generation plant risk assessment tool, the successor to the Source Term Code Package. As such, it is used to model the progression of severe accidents in light water reactor nuclear power plants, including estimation of severe accident source terms and their sensitivities and uncertainties in a variety of applications. One current major application at Sandia National Laboratories involves characterizing the hydrogen source term.

Most of the modeling in MELCOR is quite general, and makes relatively few assumptions about the details of reactor design. Therefore, MELCOR has been used for analysis of reactors, including VVERs, with designs quite different from commercial United States power reactors. The generality also allows MELCOR to be used for non-reactor problems involving coupled fluid flow, heat transfer, and the transport of aerosols and trace gases. Such applications have included analysis of contamination accidents involving facilities and shipping containers.

Current regulatory policy in the United States does not include severe accident analysis or accident management as part of the licensing process. However, MELCOR has been used as a research tool to provide guidance when considering the impact of severe accidents or the consequences of proposed accident management strategies.

Until recently, MELCOR had no specialized models for reflooding and quenching of a reactor core, and calculations conducted for ISP-45 (including preliminary tests on QUENCH-01) represent the first real test of these new models. We anticipate that comparisons with data from various QUENCH experiments will allow us to determine and validate appropriate default values for the parameters in the model.

SCDAPSIM: CMX

Application of Severe Accident Codes in the Mexican Regulatory Authority (CNSNS)

Since about ten years ago the CNSNS has been working with severe accident codes in order to evaluate different topics related with accident analysis. The first experience was with the package STCP (Source Term Code Package) that was used to obtain the source term of the different accident sequences that have high contribution to the core damage frequency. These source terms were used in the development of the APS level 2.

According with the Mexican regulation, the Individual Plant Examination (IPE) for Laguna Verde Nuclear Power Plant (two units with BWR-5 reactors) was requested to the utility, Comisión Federal de Electricidad (CFE). One of the computer codes to develop the IPE was MAAP3-B to evaluate the behavior of the nuclear station under severe accident condition. As independent evaluation of the IPE the CNSNS used the codes MAAP and MELCOR.

The codes SCDAPSIM and MELCOR have been used by the CNSNS with the objective of carrying out studies related with the behavior of Laguna Verde Nuclear Power Plant during a severe accident and in a near future to evaluate the guides of accident administration for Laguna Verde Nuclear Power Station.

SCDAPSIM: DMM

The DIMNP of Pisa University has extensively utilized the SCDAP/RELAP5 code for AP-600, EP-1000, and EPP analyses in the frame of specific activities sponsored by ENEL, the main Italian Electric Utility. The DIMNP contribution was focused on the evaluation of Transient and

Severe Accident sequences. Typical other code applications concerned a lot of research projects developed in the frame of various EU Financed Programs on Nuclear Fission, as well in the frame of OECD Benchmarks and International Standard Problems. Finally, the code, at least for the thermal-hydraulic section, is being currently utilized for IRIS reactor, performed for the DBA and Transient design analyses

SCDAPSIM: ISS

RELAP/SCDAPSIM is being developed under the sponsorship of the SDTP software development and training program. Organizations contributing to the development include the International Atomic Energy Agency (IAEA), Comisión Nacional de Seguridad Nuclear y Salvaguardias (Mexico), Framatome-ANP (Germany), Institute of Nuclear Safety (Japan), Computer Software Development Co, Ltd (Japan), Hacettepe University (Turkey), University of Pisa, Texas A&M, University of Bochum, University of Michigan, Seoul National University, Carleton University (Canada), Hanyang University (Korea), Lappeenranta University (Finland), University of Catalunya (Spain), Shanghai Jiao Tong University (China), Idaho State University (USA), University of Florida (USA), University of Zagreb (Croatia), and the University of Mexico. Software configuration control and the administration of the program are handled by Innovative Systems Software LLC (ISS). ISS is located in Idaho Falls. Funding for the development of the software and the administration of the program comes from a combination of commercial sources and licensing fees for the use of the software.

RELAP/SCDAPSIM/MOD3.2(bd) uses models taken from the RELAP/MOD3.2 and SCDAP/RELAP/MOD3.2 codes publicly released by the US Nuclear Regulatory Commission, but with a number of improvements that allow the code to run significantly faster and more reliably. The code also includes a number of added user options and models. The improvements in speed and reliability are due to improvements in the code's numerical algorithms and programming as well as the correction of numerous coding errors in the original US NRC codes. The unique user features include the interactive 3D orthographic displays, Quick Plot options, integrated renodalization options, run display console, more automated time step control, and improved output. The unique modeling options include improved fuel rod simulator and shroud models.

The improved fuel rod simulator and shroud models were incorporated into the latest experimental version of RELAP/SCDAPSIM/MOD3.2(bd). Previously versions relied on the original INEEL model (which as noted below contained a serious error). The improved simulator model incorporated many of the features originally developed by FZK (Draft Report FZKA 6566, "Improvements of the SCDAP/RELAP5 Code with respect to the FZK QUENCH Facility") with a few added options. This new model allows the user to describe the simulator rod in much more detail including the use of Copper and/or Molybdenum portions of the electrode, electrode dimensions, contact resistances, and the type of pellets to be included (ZrO2 or UO2). The new model also accounts for the properties of the electrodes in the heat conduction solution. The improved shroud model allows the user to specify the properties of the shroud as a function of axial elevation so that the change in insulation in the upper portion of the bundle could be included.

SCDAPSIM: NEH

The computer code RELAP5 has been used at the Department of Nuclear Engineering, Hacettepe University, to model transients in PWR and CANDU reactors. Also post exercise analyses of ISP-33 and supporting calculations for ISP-42 have been performed. The analyses have ba-

sically focused on the thermal-hydraulics. ISP-45 exercise is the first SCDAP application performed.

SCDAPSIM: NK1

See NK3

SCDAPSIM: SIE

Framatome ANP GmbH uses SCDAPSIM mainly for the design and assessment of accident management measures for all kinds of LWRs (existing as well as future ones). In addition, it is used for the validation of the in-vessel results generated by simplified codes (e.g. MAAP) by benchmarking of key scenarios. Typical examples for the latter case are benchmark exercises mainly with respect to the mass- and energy release into the containment for the reference scenarios for the EPR hydrogen mitigation concept and the validation of training exercises for the plant operators and members of the Technical Support Center.

Our validation work for SCDAPSIM is strongly limited to the most risk relevant phenomena and the qualification of the user. Another related activity is the assessment of the potential of 'fast running'. By the improvements of the numerics performed in the last years by Innovative Systems Software LLC almost real time plant calculation (on PCs 2GHz) are already possible. Under these conditions we intend to replace simplified integral codes by coupled mechanistic codes for whole plant analyses in the near future.

SCDAPSIM: UZA

Most of the experience of the Nuclear Engineering Group at the Power Systems Department, founded in 1983, is related to NPP safety analysis, deterministic and probabilistic, particularly related to NPP Krsko. Regarding thermal-hydraulics we use RELAP codes since mid eighties and we already participated in several RELAP5 related ISPs. In the last few years, we have gained some experience in severe accident analysis using MELCOR and MAAP. In future we intend to use SCADAPSIM in performing benchmark calculations.

SCDAP-3D: INL

SCDAP-3D was developed to link the severe accident analysis capability, Developed for SCDAP/RELAP5 Mod3.3, with the three-dimensional hydrodynamic capability of RELAP5-3D. In addition, several models have been added to support the U.S. DOE Gen-IV Reactor Initiative, and lower head and debris coolability experiments performed for international customers. Current applications include a Large-break LOCA analysis using Thoria/Urania fuel, analyses to support experiments of debris-coolability and the investigation of the effects of a gap created between solidified corium and the lower head of the reactor vessel.

SCDAP/RELAP5mod3.2irs: FZK

S/R5irs is used for analyses within the CSARP agreement, for support of QUENCH experiments and analyses of safety features of existing and advanced nuclear power plants. Part of this work is done within the 5th Framework Program of the European Community, (COLOSS, EVITA, HPLWR), taking credit from the RELAP5 experience gained within the USNRC CAMP agreement.

Besides code improvements /4/ were performed and transmitted the customers of the QUENCH-program using SCDAP/RELAP5 based codes to take credit from our experience. Furthermore, model developments are under way to identify the basic mechanisms leading to increased hydrogen release during reflood situation, a major concern of hydrogen management measures in the containment.

11.5 Contributing Authors

Dr. Wolfgang Hering
Forschungszentrum Karlsruhe (FZK) GmbH
Institut für Reaktorsicherheit (IRS)
P.O. Box 3640
D-76021 Karlsruhe
Phone : +49 (7247) 82 2556
Fax : +49 (7247) 82 3718
E-mail : hering@irs.fzk.de

Dr. Christoph Homann
Forschungszentrum Karlsruhe (FZK) GmbH
Institut für Reaktorsicherheit (IRS)
P.O. Box 3640
D-76021 Karlsruhe
Phone : +49 (7247) 82 2958
Fax : +49 (7247) 82 3718
E-mail : homann@irs.fzk.de

Mr. Jean-Sylvestre Lamy
Electricité de France
c/o Forschungszentrum Karlsruhe (FZK) GmbH
Institut für Reaktorsicherheit (IRS)
P.O. Box 3640
D-76021 Karlsruhe
E-mail : lamy@edf.fr

Dr. Alex Miassoedov
Forschungszentrum Karlsruhe (FZK) GmbH
Institut für Materialforschung (IMF)
P.O. Box 3640
D-76021 Karlsruhe
Phone : +49 (7247) 82 2553
Fax : +49 (7247) 82 2095
E-mail : miassoedov@imf.fzk.de

Mr. Gerhard Schanz
Forschungszentrum Karlsruhe GmbH
Institut für Materialforschung (IMF)
P.O. Box 3640
D-76021 Karlsruhe
Phone : +49 (7247) 82 4642
Fax : +49 (7247) 82 3956
E-mail : schanz@imf.fzk.de

Mr. Leo Sepold
Forschunszentrum Karlsruhe GmbH
Institut für Materialforschung (IMF)

P.O. Box 3640
D-76021 Karlsruhe
Phone : +49 (7247) 82 3908
Fax : +49 (7247) 82 3956
E-mail : sepold@imf.fzk.de

Dr. Martin Steinbrück
Forschungszentrum Karlsruhe GmbH
Institut für Materialforschung (IMF)
P.O. Box 3640
D-76021 Karlsruhe
Phone : +49 (7247) 82 2517
Fax : +49 (7247) 82 3956
E-mail : steinbrueck@imf.fzk.de